

ตัวรับรู้ฟลูออเรสเซนซ์ฐานอิมิตาโซเลียมสำหรับไบโอเจนิคแอมีน



นายจตุรงค์ ก้องวุฒิเวช

จุฬาลงกรณ์มหาวิทยาลัย

CHULALONGKORN UNIVERSITY

บทคัดย่อและแฟ้มข้อมูลฉบับเต็มของวิทยานิพนธ์ตั้งแต่ปีการศึกษา 2554 ที่ให้บริการในคลังปัญญาจุฬาฯ (CUIR)

เป็นแฟ้มข้อมูลของนิสิตเจ้าของวิทยานิพนธ์ ที่ส่งผ่านทางบัณฑิตวิทยาลัย

The abstract and full text of theses from the academic year 2011 in Chulalongkorn University Intellectual Repository (CUIR)

are the thesis authors' files submitted through the University Graduate School.

วิทยานิพนธ์นี้เป็นส่วนหนึ่งของการศึกษาตามหลักสูตรปริญญาวิทยาศาสตรมหาบัณฑิต

สาขาวิชาเคมี ภาควิชาเคมี

คณะวิทยาศาสตร์ จุฬาลงกรณ์มหาวิทยาลัย

ปีการศึกษา 2559

ลิขสิทธิ์ของจุฬาลงกรณ์มหาวิทยาลัย

FLUORESCENCE SENSORS BASED ON IMIDAZOLIUM FOR BIOGENIC AMINES

Mr. Jaturong Kongwutthivech



A Thesis Submitted in Partial Fulfillment of the Requirements
for the Degree of Master of Science Program in Chemistry

Department of Chemistry

Faculty of Science

Chulalongkorn University

Academic Year 2016

Copyright of Chulalongkorn University

จตุรงค์ ก้องวุฒิเวช : ตัวรับรู้ฟลูออเรสเซนซ์ฐานอิมิดาโซเลียมสำหรับไบโอเจนิคเอมีน (FLUORESCENCE SENSORS BASED ON IMIDAZOLIUM FOR BIOGENIC AMINES) อ. ที่ปริกษาวิทยานิพนธ์หลัก: ผศ. ดร.บุษยรัตน์ ธรรมพัฒน์กิจ, 102 หน้า.

เป้าหมายของงานวิจัยนี้ คือ การพัฒนาระบบสำหรับการแยกตรวจวัดสารประกอบฮิสทีดิน (HD) และฮิสตามีน (HM) โดยใช้ตัวรับรู้ฟลูออเรสเซนซ์ ได้แก่ ฮิสตามีนบลู (HB) สารประกอบอิมิดาโซล (AN) และสารประกอบอิมิดาโซเลียม (ANI) ในขั้นตอนแรกการสังเคราะห์เซนเซอร์ HB AN และ ANI ได้ประสบความสำเร็จ โดยหลักการแรกได้ออกแบบการรวมตัวกันของ การใช้เซนเซอร์ HB และ ANI ในการแยกการตรวจวัด HD และ HM โดยใช้กระบวนการ FRET แต่เนื่องจาก ANI มีหมู่แทนพาลีไมด์เป็นองค์ประกอบซึ่งสามารถแข่งขันการเกิดสมบัติฟลูออเรสเซนซ์กับโมเลกุลเซนเซอร์ HB จึงทำให้ระบบนี้ไม่สามารถนำมาแยกการตรวจวัด HD และ HM ได้ สำหรับระบบที่สองคือ ความสามารถในการจับของ Cu^{2+} ไอออน กับสารประกอบเชิงซ้อน HBC₂H₂D และ HBC₂H₂M จะสามารถแยกการตรวจวัด HD และ HM โดยใช้เทคนิคฟลูออเรสเซนซ์ ซึ่ง Cu^{2+} ไอออน สามารถจับกับสารประกอบเชิงซ้อน HBC₂H₂D ได้อย่างมีความจำเพาะเจาะจง และ เกิดการดับสัญญาณฟลูออเรสเซนซ์ของ HBC₂H₂D เมื่อมี Cu^{2+} ไอออนมากเกินไป ดังนั้น ระบบที่ใช้ทั้งเซนเซอร์ HB และ Cu^{2+} จะสามารถแยกการตรวจวัด HD และ HM ได้ นอกจากนี้ ยังสามารถประยุกต์การตอบสนองทางฟลูออเรสเซนซ์ภายใต้สภาวะที่มีเกสท์แตกต่างกันเพื่อสร้างระบบลอจิกเกต นอกจากนี้ ได้ศึกษาการเลือกจำเพาะของ เซนเซอร์ AN และ ANI จากผลการทดลองแสดงให้เห็นว่า ฟลูออเรสเซนซ์สเปกตรัมของเซนเซอร์ AN ถูกดับสัญญาณเมื่อมี Cu^{2+} ไอออนอยู่ในระบบ เซนเซอร์ AN และ Cu^{2+} ไอออน มีค่า $\log K$ ในการเกิดสารประกอบเชิงซ้อน เท่ากับ 5.130 ด้วยอัตราส่วน 1:1 และ ในกรณีของเซนเซอร์ ANI การดับสัญญาณฟลูออเรสเซนซ์จะเกิดขึ้นเมื่อมี F^- ไอออนอยู่ในระบบ สำหรับการศึกษาความสามารถในการจับนั้น ขีดจำกัดในการตรวจพบ และขีดจำกัดในการตรวจวัดเชิงปริมาณ มีค่าเท่ากับ 0.18 mM และ 0.60 mM ตามลำดับ สุดท้ายนั้น เซนเซอร์ ANI ยังสามารถบ่งบอกความเลือกจำเพาะ และการหาปริมาณ F^- ไอออน โดยการเปลี่ยนแปลงสี และฟลูออเรสเซนซ์ ด้วยตาเปล่าได้อีกด้วย

ภาควิชา เคมี

ลายมือชื่อนิสิต

สาขาวิชา เคมี

ลายมือชื่อ อ.ที่ปรึกษาหลัก

ปีการศึกษา 2559

5671919423 : MAJOR CHEMISTRY

KEYWORDS: HISTIDINE / HISTAMINE / FLUORESCENCE SENSOR / IMIDAZOLIUM / DISCRIMINATION

JATURONG KONGWUTTHIVECH: FLUORESCENCE SENSORS BASED ON IMIDAZOLIUM FOR BIOGENIC AMINES. ADVISOR: ASST. PROF. BOOSAYARAT TOMAPATANAGET, Ph.D., 102 pp.

The aim of this work is to design the system for histidine (HD) and histamine (HM) discriminated detection by using the fluorescence sensors including Histamine Blue (HB), imidazole compound (AN) and imidazolium compound (ANI). Firstly, the synthesis of sensors HB, AN and ANI have been achieved. Our first concept was that the combination of sensors HB and ANI discriminated HD and HM by using FRET process. Unfortunately, sensor ANI consisting of a naphthalimide moiety cannot discriminate HD and HM due to a competitive fluorophore against sensor HB. For the second concept, the binding affinity of Cu^{2+} ion towards the $\text{HB} \rightleftharpoons \text{HD}$ and $\text{HB} \rightleftharpoons \text{HM}$ complexes could discriminate the HD and HM detection by using fluorescence technique. The Cu^{2+} ion bound selectively with $\text{HB} \rightleftharpoons \text{HD}$ complex and the fluorescent response of $\text{HB} \rightleftharpoons \text{HD}$ was quenched in the presence of excess Cu^{2+} ion. Therefore, we successfully discriminated HD and HM by using the combination of sensor HB and Cu^{2+} ion. Surprisingly, we enabled to apply the fluorescence responses under different guests to construct the logic gates system. Moreover, we have also studied the selectivity of sensors AN and ANI. The results showed that the fluorescence spectra of sensor AN was deeply quenched in the presence of Cu^{2+} ion. The complex of sensor AN and Cu^{2+} ion had the log K value for binding affinity of 5.130 with the stoichiometry 1:1. In case of sensor ANI, the fluorescence quenching of sensor ANI was observed in the presence of F^- ion. As the binding studies, the log K value of the complex was 3.05 with the binding mode of 1:1. Limit of detection and limit of quantification of F^- determination were 0.18 mM and 0.60 mM, respectively. Finally, sensor ANI gave a promising selectivity for F^- determination by colorimetric and fluorimetric naked-eye detection.

Department: Chemistry

Student's Signature

Field of Study: Chemistry

Advisor's Signature

Academic Year: 2016

ACKNOWLEDGEMENTS

First of all, I would like to express my grateful appreciation to my advisor, Assistant Professor Dr. Boosayarat Tomapatanaget for extremely endurance, honest kindness, valuable suggestions and constant encouragement both course work and research throughout my master degree level for 3.5 years. I also would like to thank Associated Professor Dr. Vudhichai Parasuk, Dr. Pannee Leeladee, and Assistant Professor Dr. Nantanit Wanichacheva for their useful comments, valuable supervision as thesis committee and thesis examiner.

Moreover, I would like to acknowledge the financial support for my study from the Graduate School, Chulalongkorn University to commemorate 72nd anniversary of his Majesty King Bhumibala Aduladeja. I would like to thank the Thailand Research Fund (RES5680015) for additional research grants.

Furthermore, this accomplishment could not occur without the support from Chulalongkorn University. Special thanks to Professor Dr. Thawatchai Tuntulani for beneficial suggestions and to all members of the Supramolecular Chemistry Research Unit at Department of Chemistry, Faculty of Science, Chulalongkorn University for their giving consultant, encouragement throughout my research.

Eventually, I wish to express my grateful gratitude to my parents for their deepest truly love, important moral support and comprehension throughout my life.

CONTENTS

	Page
THAI ABSTRACT	iv
ENGLISH ABSTRACT	v
ACKNOWLEDGEMENTS	vi
CONTENTS	vii
LIST OF TABLES	xii
LIST OF FIGURES	xiv
LIST OF SCHEMES	xxi
LIST OF ABBREVIATIONS AND SYMBOLS	xxii
CHAPTER I INTRODUCTION.....	1
1.1. Supramolecular chemistry concept.....	1
1.2. Molecular recognition	1
1.3. Chemical sensor.....	2
1.4. Phenomena of fluorescence	2
1.4.1. Photoinduced electron transfer (PET).....	3
1.4.2. Photoinduced charge transfer (PCT).....	4
1.4.3. Fluorescence resonance energy transfer (FRET).....	5
1.5. Logic gates.....	7
CHAPTER II LITERATURE REVIEWS	9
2.1 Literature reviews	9
2.1.1 Determination of biogenic amines by IDA assays	9
2.1.2 Determination of biogenic amines by Schiff base	13
2.1.3 Discrimination of biogenic amines by FRET	14

	Page
2.1.4 Determination of biogenic amines by mesoionic acid.....	16
2.1.5 Literature of naphthalimide sensors	18
2.1.6 Literature of imidazolium derivatives sensors.....	21
2.2 Objectives and scope of this research	24
CHAPTER III EXPERIMENTAL.....	26
3.1 General procedures.....	26
3.1.1 Analytical instruments.....	26
3.1.2 Materials.....	26
3.2 Synthesis.....	27
3.2.1 Synthesis of histamine blue sensor.....	27
3.2.1.1 Synthesis of 3-(Fluorocarbonyl)-1-(2-methoxy-2-oxoethyl)-2-oxo-2,3-dihydro-1H-imidazo[2,1-a]isoquinolin-4-ium-3-ide (histamine blue, HB)	27
3.2.2 Synthesis of imidazole derivatives sensors	28
3.2.2.1 Synthesis of 6-Bromo-2-phenyl-1H-benzo[de]isoquinoline-1,3(2H)-dione (1).....	28
3.2.2.2 Synthesis of 6-((2-Aminoethyl)amino)-2-phenyl-1H-benzo[de]isoquinoline -1,3(2H)-dione (2).....	29
3.2.2.3 Synthesis of 2-Chloro-N-(2-((1,3-dioxo-2-phenyl-2,3-dihydro-1H-benzo[de] isoquinolin-6-yl)amino)ethyl)acetamide (3)	30
3.2.2.4 Synthesis of N-(2-((1,3-dioxo-2-phenyl-2,3-dihydro-1H-benzo[de] isoquinolin-6-yl)amino)ethyl)-2-(1H-imidazol-1-yl)acetamide (AN).....	31

	Page
3.2.2.5 Synthesis of 1-(2-((2-((1,3-dioxo-2-phenyl-2,3-dihydro-1H-benzo[de] isoquinolin-6-yl)amino)ethyl)amino)-2-oxoethyl)-3-methyl-1H-imidazol-3-ium (ANI).....	32
3.3 Qualitative discrimination of biogenic amines by using sensor HB	33
3.3.1 Fluorescence studies of sensor HB and biogenic amines.....	33
3.3.1.1 Time effect for complexation studies of sensor HB and biogenic amines.....	33
3.3.1.2 Concentration of biogenic amines effect for complexation study of sensor HB and biogenic amines.....	33
3.3.1.3 Kinetic study of sensor HB and biogenic amines.....	34
3.3.1.4 Discrimination by using sensor ANI compound.....	35
3.3.1.5 Discrimination by using Cu ²⁺ ion	35
3.3.2 Complex simulation of sensor HB and histidine.....	36
3.3.3 Naked-eye fluorescence discrimination of sensor HB against biogenic amines	37
3.4 Fluorescence studies of imidazole compound.....	37
3.4.1 Selectivity of sensor AN against various metal ions.....	37
3.4.2 Job's plot analysis between sensor AN and Cu ²⁺ ion	39
3.4.3 Binding constant determination of sensor AN and Cu ²⁺ ion	40
3.5 Fluorescence studies of imidazolium compound	42
3.5.1 Selectivity of sensor ANI against various amino acids.....	42
3.5.2 Selectivity of sensor ANI against various nucleotides.....	43
3.5.3 Selectivity of sensor ANI against various anions	45
3.5.4 Job's plot analysis between sensor ANI and F ⁻ ion	46

	Page
3.5.5 Binding constant studies of sensor ANI and F ⁻ ion	47
3.5.6 LOD/LOQ determination of sensor ANI.....	48
3.6 NMR titration of sensor ANI against F ⁻ ion.....	49
3.7 Naked-eye detection.....	49
3.7.1 Colorimetric detection of sensor ANI against various anions	49
3.7.2 Fluorometric detection of sensor ANI against various anions	50
CHAPTER IV RESULTS AND DISCUSSION	51
4.1 Conceptual design.....	51
4.1.1 Discrimination of biogenic amines by using FRET mechanism.....	51
4.1.2 Discrimination of biogenic amines by metal ion via PET process	53
4.2 Synthesis.....	55
4.2.1 Synthesis and characterization of histamine blue (HB)	55
4.2.2 Synthesis and characterization of 6-Bromo-2-phenyl-1H-benzo[de] isoquinoline-1,3(2H)-dione (1).....	57
4.2.3 Synthesis and characterization of 6-((2-Aminoethyl)amino)-2-phenyl- 1H-benzo[de]isoquinoline-1,3(2H)-dione (2)	57
4.2.4 Synthesis and characterization of 2-Chloro-N-(2-((1,3-dioxo-2-phenyl- 2,3-dihydro-1H-benzo[de]isoquinolin-6-yl)amino)ethyl)acetamide (3).....	58
4.2.5 Synthesis and characterization of N-(2-((1,3-dioxo-2-phenyl-2,3- dihydro-1H-benzo[de]isoquinolin-6-yl)amino)ethyl)-2-(1H-imidazol-1- yl)acetamide (AN)	59
4.2.6 Synthesis and characterization of 1-(2-((2-((1,3-dioxo-2-phenyl-2,3- dihydro -1H-benzo[de]isoquinolin-6-yl)amino)ethyl)amino)-2- oxoethyl)-3-methyl-1H-imidazol-3-ium (ANI)	59
4.3 Qualitative discrimination of biogenic amines by using sensor HB	60

	Page
4.3.1 Complexation studies of sensor HB and biogenic amines.....	60
4.3.2 Kinetic study of sensor HB and biogenic amines.....	62
4.3.3 Discrimination of biogenic amines by using imidazolium sensor	63
4.3.4 Discrimination of biogenic amines by using sensor HB with Cu ²⁺ ion.....	66
4.3.1.5 Naked-eye fluorescence discrimination of sensor HB against biogenic amines.....	73
4.4 Fluorescence studies of imidazole derivatives.....	74
4.4.1 Fluorescence studies of sensor AN.....	74
4.4.1.1 Selectivity of sensor AN against various metal ions.....	74
4.4.1.2 Job's plot analysis between sensor AN and Cu ²⁺ ion.....	75
4.4.1.3 Binding constant determination of sensor AN and Cu ²⁺ ion.....	76
4.4.2 Fluorescence studies of sensor ANI.....	78
4.4.2.1 Selectivity of sensor ANI against various amino acids	78
4.4.2.2 Selectivity of sensor ANI against various nucleotides.....	79
4.4.2.3 Selectivity of sensor ANI against various anions	80
CHAPTER V CONCLUSION	89
5.1 Conclusion	89
REFERENCES	91
APPENDIX.....	96
VITA.....	102

LIST OF TABLES

	Page
Table 3.1 Amounts of guests used for studies of fluorescence spectrophotometry technique	38
Table 3.2 Amounts of guests used for studies of fluorescence spectrophotometry technique	38
Table 3.3 Mole fraction and volume of sensor AN (1×10^{-5} M) and Cu^{2+} ion guest (1×10^{-5} M) for Job's plot experiment	39
Table 3.4 The concentration of Cu^{2+} used for complexation studies with sensor AN and the ratio of AN : Cu^{2+}	40
Table 3.5 Amounts of guests used for studies of fluorescence spectrophotometry	42
Table 3.6 Amounts of guests used for studies of fluorescence spectrophotometry	43
Table 3.7 Amounts of guests used for studies of fluorescence spectrophotometry	44
Table 3.8 Amounts of guests used for studies of fluorescence spectrophotometry	44
Table 3.9 Amounts of guests used for studies of fluorescence spectrophotometry	45
Table 3.10 Amounts of guests used for studies of fluorescence spectrophotometry	46
Table 3.11 Mole fraction and volume of sensor ANI (1×10^{-5} M) and F^- anion guest (1×10^{-5} M) for Job's plot experiment	47
Table 3.12 The concentration of F^- used for complexation studies with sensor ANI and the ratio of ANI : F^-	48

	Page
Table 4.1 Complexation energies for copper complexes with ligand (L) and relative energies for CuL₂(1) and CuL₂(2) isomers	69
Table 4.2 The logic gates truth table for Output ($\lambda = 421 \text{ nm}$).....	72
Table 4.3 Naked-eye fluorescence of sensor HB with HD and HM with Cu^{2+} ion.....	73



LIST OF FIGURES

	Page
Figure 1.1	The schematic presentation of response of a chemosensor with a guest analyte 2
Figure 1.2	The schematic Jablonski diagram and the mechanism for absorption, fluorescence and phosphorescence phenomena 3
Figure 1.3	The energy level of an OFF-ON chemosensor (upper) and the schematic mechanism of the PET process (lower) 4
Figure 1.4	The schematic of PCT process of a donor group (a) and an acceptor group (b)..... 5
Figure 1.5	The integral overlap between the emission spectrum of donor and the absorption spectrum of acceptor 6
Figure 1.6	The schematic diagram of the fluorescence resonance energy transfer process (FRET)..... 6
Figure 1.7	The truth table data for one inputs logic gate operation 7
Figure 1.8	The truth table data for two inputs logic gate operation 8
Figure 2.1	The fluorescence results at $\lambda = 670$ nm of IDA-Ni probe against various biogenic amines..... 10
Figure 2.2	The reaction of IDA-Ni complex with histamine 10
Figure 2.3	Summary of spectrofluorometric titration (I/I_0 at 640 nm) of Ru₂Eu-1 (1.0×10^{-4} M) to putrescine, histamine, spermidine, aniline, ammonia, H ₂ S, CO, CH ₄ , H ₂ , N ₂ , and atmospheric air monitored as a function of the increase in their concentration. All titrations were carried out in ethanol at 298 K 11

Figure 2.4	Photographs of the luminometric responses of the Ru₂Eu-1 (1.0×10^{-4} M) in EtOH at 298 K: (1) Ru₂Eu-1 + histamine; (2) Ru₂Eu-1 + putrescine; (3) Ru₂Eu-1 + spermidine; (4) Ru₂Eu-1 + NH ₃ ; (5) Ru₂Eu-1 only; (6) Ru₂Eu-1 + aniline; (7-12) Ru₂Eu-1 + H ₂ S, CO, N ₂ , CH ₄ , H ₂ , and air, respectively. (1) Excitation $\lambda_{\text{ex}} = 365$ nm 12	12
Figure 2.5	Proposed molecular recognition and luminescence signaling mechanism 12	12
Figure 2.6	Proposed mechanism of histidine sensing with TARDHD sensor 13	13
Figure 2.7	Changes of absorbance of TARDHD (10 μ M) upon addition of histidine (0 - 5000 μ M) in HEPES buffered (0.1 M) solution (ethanol/water = 1:9, v/v, pH 7.3) 13	13
Figure 2.8	Conceptual design of an intermolecular assembled complex for catecholamine sensing by FRET-on process..... 15	15
Figure 2.9	Fluorescence spectra of the mixed sensors of PBA (1 μ M) and CA (30 μ M) in buffer solution (100 mM Na ₂ S ₂ O ₃ , 50 mM HEPES, 20 mM NaCl, pH 7.4) with various biogenic amines and inset: relative fluorescence intensity of the mixed sensors of PBA and CA ($\lambda_{\text{ex}} = 340$ nm) in the presence of various biogenic amines 16	16
Figure 2.10	Synthesis pathway of Histamine Blue (HB)..... 16	16
Figure 2.11	Reaction of 4a with histamine in PBS. Fluorescence spectra of 4a before (black) and after (blue) reacts with histamine; exc: 340 nm. Fluorescent images of PBS solutions of 4a and 5i under a 365 nm lamp..... 17	17
Figure 2.12	The mechanism between the HB and histamine..... 17	17

Figure 2.13	Fluorescent response of HB (10 μ M) after incubation with different signaling molecules (5 mM) for 30 min in PBS (pH: 7.3). Inset: Kinetic analysis of the reactions of HB with histamine (blue), GABA (red), adenosine (green), glutamate (orange), inositol (purple), and other (grey); exc: 370 nm. Values are represented as means (n = 4) and errors bars as standard deviations 18	18
Figure 2.14	Syntheses of fluorescence sensors 1 and 2 19	19
Figure 2.15	(a) Fluorescence spectra of 1 ($\lambda_{\text{ex}} = 426$ nm, 0.15 μ M) with addition of perchlorate salts of Hg^{2+} , Co^{2+} , Ag^+ , Cd^{2+} , Mn^{2+} , K^+ , Pb^{2+} , Na^+ , Fe^{2+} , Ca^{2+} , Mg^{2+} , and Cu^{2+} , (123 μ M). (b) The luminescence under UV of 1 (23 μ M) in the presence and absence of Hg^{2+} , Cu^{2+} , Co^{2+} , Ag^+ , Cd^{2+} , Mn^{2+} , K^+ , Pb^{2+} , Na^+ , Fe^{2+} , Ca^{2+} , and Mg^{2+} (3.0 μ M) 20	20
Figure 2.16	Schematic presentation of the synthesis of sensors 1 and 2 21	21
Figure 2.17	Fluorescence intensity vs analyte concentration plot of sensor 1 titrated upon gradual addition of PA. Inset: visual color change due to the formation [1 ⊂PA] complex 22	22
Figure 2.18	Fluorescence quenching efficiencies of sensors 1 and 2 toward different analytes. PA = picric acid; DDQ = 2,3-dichloro-5,6-dicyano-1,4-benzoquinone; 4-NP = 4-nitrophenol; TNT = trinitrotoluene; TNB = trinitrobenzene; 4-NT = 4-nitrotoluene; 3,4-DNT = 3,4-dinitrotoluene; 2,4-DNT = 2,4-dinitrotoluene; NB = nitrobenzene; NM = nitromethane; BA = benzoic acid 23	23
Figure 2.19	Structure of fluorescence chemosensors HB and ANI 24	24
Figure 4.1	Reaction of histamine blue (HB) with histamine compound 51	51
Figure 4.2	The fluorescence spectra of sensor HB (10 μ M) in 10% DMSO:phosphate buffer (5×10^{-4} M, pH 7.4) against histidine (HD) and histamine (HM) $\lambda_{\text{ex}} = 320$ nm 52	52

	Page
Figure 4.3	The conceptual mechanism for sensors HB and ANI for HM (top) and HD (bottom) discrimination..... 53
Figure 4.4	The mechanism of HB complex with HM..... 54
Figure 4.5	The conceptual design of discrimination mechanism of HD (left) and HM (right) by using the combination of sensor HB and Cu^{2+} ion.. 55
Figure 4.6	The $^1\text{H-NMR}$ spectrum of sensor HB in CDCl_3 at 400 MHz..... 56
Figure 4.7	The competitive reaction pathway of sensor HB (5d) and 6a..... 56
Figure 4.8	The $^1\text{H-NMR}$ spectrum of compound 1 in $d_6\text{-DMSO}$ at 400 MHz..... 57
Figure 4.9	The $^1\text{H-NMR}$ spectrum of compound 2 in $d_6\text{-DMSO}$ at 400 MHz..... 58
Figure 4.10	The $^1\text{H-NMR}$ spectrum of compound 3 in $d_6\text{-DMSO}$ at 400 MHz..... 58
Figure 4.11	The $^1\text{H-NMR}$ spectrum of sensor AN in $d_6\text{-DMSO}$ at 400 MHz..... 59
Figure 4.12	The $^1\text{H-NMR}$ spectrum of sensor ANI in $d_6\text{-DMSO}$ at 400 MHz..... 60
Figure 4.13	The fluorescence spectra of sensor HB (1×10^{-5} M) and the HB complex with excess HD in 10% DMSO:phosphate buffer (5×10^{-4} M, pH 7.4) with vary time ($\lambda_{\text{ex}} = 320$ nm)..... 61
Figure 4.14	The fluorescence spectra of sensor HB (1×10^{-5} M) in 10% DMSO:phosphate buffer (5×10^{-4} M, pH 7.4) with varying amount of HD ($\lambda_{\text{ex}} = 320$ nm)..... 62
Figure 4.15	The kinetic profiles of complexation of sensor HB (1×10^{-5} M) and HD or HM in 10% DMSO:phosphate buffer (5×10^{-4} M, pH 7.4) with varying time ($\lambda_{\text{ex}} = 320$ nm)..... 63
Figure 4.16	The fluorescence spectra of HB ⊂HD complex (1×10^{-5} M) in 10% DMSO:phosphate buffer (5×10^{-4} M, pH 7.4) with varying amount of sensor ANI ($\lambda_{\text{ex}} = 320$ nm)..... 64
Figure 4.17	The structure of HB ⊂HM (left) and HB ⊂HD (right) 64

	Page
Figure 4.18	The UV-visible spectra of sensors HB and ANI (1×10^{-5} M) in 10% DMSO:phosphate buffer (5×10^{-4} M, pH 7.4)..... 65
Figure 4.19	The fluorescence spectra of sensor HB (1×10^{-5} M) in 10% DMSO:phosphate buffer (5×10^{-4} M, pH 7.4) with varying amount of sensor ANI ($\lambda_{\text{ex}} = 320$ nm)..... 65
Figure 4.20	The fluorescence spectra of sensor HB (1×10^{-5} M) in 10% DMSO:phosphate buffer (5×10^{-4} M, pH 7.4) with various metals ($\lambda_{\text{ex}} = 320$ nm)..... 66
Figure 4.21	The fluorescence spectra of HB ⊂HD complex (1×10^{-5} M) in 10% DMSO:phosphate buffer (5×10^{-4} M, pH 7.4) with various metal cations ($\lambda_{\text{ex}} = 320$ nm)..... 67
Figure 4.22	The fluorescence spectra of HB ⊂HM complex (1×10^{-5} M) in 10% DMSO:phosphate buffer (5×10^{-4} M, pH 7.4) with various metal cations ($\lambda_{\text{ex}} = 320$ nm)..... 67
Figure 4.23	The CPCM(DMSO)/CAMB3LYP/6-31G(d,p) optimized structures of (a) CuL₂(1) and (b) CuL₂(2) isomers. Top and bottom are top and side views of molecules, respectively 68
Figure 4.24	The fluorescence spectra of HB (1×10^{-5} M) complexes with 5 equiv HD, 5 equiv HM and 5 equiv Cu^{2+} ion in 10% DMSO:phosphate buffer (5×10^{-4} M, pH 7.4, $\lambda_{\text{ex}} = 320$ nm). 70
Figure 4.25	The structure of imidazole derivatives including sensor AN (left) and sensor ANI (right)..... 74
Figure 4.26	Fluorescence spectra of sensor AN (10 μM) upon addition of Cr^{3+} , Mn^{2+} , Co^{2+} , Ni^{2+} , Cu^{2+} , Zn^{2+} , Cd^{2+} , Ag^{+} , and Au^{3+} solutions (10 equiv) in 10% DMSO/HEPES buffer pH 7.4 ($\lambda_{\text{ex}} = 448$ nm) 75
Figure 4.27	Job's plot for sensor AN and Cu^{2+} complex with the total concentration of 10 μM 76

Figure 4.28	a) Fluorescence spectral titration of sensor AN (10 μM) in the presence of different amounts of Cu^{2+} ion (0 – 3.5 equiv) in 10% DMSO/HEPES buffer pH 7.4. b) Fluorescence titration curves in the presence of Cu^{2+} ion.....	77
Figure 4.29	Fluorescence spectra of sensor ANI (10 μM) upon addition of various amino acids including Phe, His, Leu, Gly, Lys, Glu, Ala, Cys, Met and Thr solutions (10 equiv) in 10% DMSO/phosphate buffer pH 7.4 ($\lambda_{\text{ex}} = 448 \text{ nm}$).....	78
Figure 4.30	Fluorescence spectra of sensor ANI (10 μM) upon the addition of various nucleotides including UMP, UDP, UTP, AMP, ADP, ATP, GMP, GDP and CMP solutions (10 equiv) in 10% DMSO/HEPES buffer pH 7.4 ($\lambda_{\text{ex}} = 448 \text{ nm}$)	79
Figure 4.31	Fluorescence spectra of sensor ANI (10 μM) upon the addition of various anions including F^- , Cl^- , Br^- , I^- , CN^- , OH^- , PO_4^{3-} , AcO^- and BzO^- solutions (10 equiv) in 100% DMSO solution ($\lambda_{\text{ex}} = 448 \text{ nm}$)	80
Figure 4.32	Fluorescence spectra of sensor AN (10 μM) upon the addition of various anions including F^- , Cl^- , Br^- , I^- , CN^- , OH^- , PO_4^{3-} , AcO^- and BzO^- solutions (10 equiv) in 100% DMSO solution ($\lambda_{\text{ex}} = 448 \text{ nm}$)	81
Figure 4.33	Comparison of the selectivity between sensors ANI (10 μM) and AN (10 μM) with various anions including F^- , Cl^- , Br^- , I^- , CN^- , OH^- , PO_4^{3-} , AcO^- and BzO^- solutions (10 equiv) in 100% DMSO solution ($\lambda_{\text{ex}} = 448 \text{ nm}$).....	82
Figure 4.34	Job's plot for sensor ANI and F^- complex with the total concentration of 10 μM	83
Figure 4.35	a) Fluorescence spectral titration of sensor ANI (10 μM) in the presence of different amounts of F^- ion (0 – 1000 equiv) in 100% DMSO solution. b) Fluorescent titration curves of sensor ANI in the presence of F^- ion	84

Figure 4.36	Calibration curve of the intensity of sensor ANI and various concentration of F ⁻ anion	85
Figure 4.37	NMR titration spectra of sensor ANI (100 mM) upon addition of various concentration of F ⁻ anion including 0 equiv, 0.5 equiv, 1.0 equiv, 2.0 equiv and 4.0 equiv	86
Figure 4.38	Colorimetric assay of sensor ANI (1×10 ⁻⁵ M) responses upon addition of vary concentration (0-900 equiv) of various anions including F ⁻ , Cl ⁻ , Br ⁻ , I ⁻ , CN ⁻ , OH ⁻ , PO ₄ ³⁻ , AcO ⁻ and BzO ⁻	87
Figure 4.39	Fluorometric assay of sensor ANI (1×10 ⁻⁵ M) responses upon addition of vary concentration (0-900 equiv) of various anions including F ⁻ , Cl ⁻ , Br ⁻ , I ⁻ , CN ⁻ , OH ⁻ , PO ₄ ³⁻ , AcO ⁻ and BzO ⁻ (λ _{exc} = 265 nm)	88
Figure A1	The ¹³ C-NMR spectrum of 1 in d ₆ -DMSO at 100 MHz	97
Figure A2	The ¹³ C-NMR spectrum of 2 in d ₆ -DMSO at 100 MHz	97
Figure A3	The ¹³ C-NMR spectrum of 3 in d ₆ -DMSO at 100 MHz	98
Figure A4	The ¹³ C-NMR spectrum of sensor AN in d ₆ -DMSO at 100 MHz	98
Figure A5	MALDI-TOF mass spectrum of sensor AN shown at 439.678 m/z	99
Figure A6	The ESI-High Resolution Mass spectrum of sensor AN	99
Figure A7	The ¹³ C-NMR spectrum of sensor ANI in d ₆ -DMSO at 100 MHz	100
Figure A8	MALDI-TOF mass spectrum of sensor ANI shown at 453.742 m/z	100
Figure A9	The ESI-High Resolution Mass spectrum of sensor ANI	101

LIST OF SCHEMES

	Page
Scheme 3.1 Synthesis pathway of sensors AN and ANI	28
Scheme 4.1 Schematic logic gate system for the complexes of sensor HB with HD, HM, Cu ²⁺ ion including Input 1 (HD), Input 2 (HM), Input 3 (Cu ²⁺) and Output ($\lambda = 421$ nm).....	71



LIST OF ABBREVIATIONS AND SYMBOLS

ADP	Adenosine diphosphate
AMP	Adenosine monophosphate
ATP	Adenosine triphosphate
Ala	Alanine
Anal. Calcd	Analysis calculated
¹³ C-NMR	Carbon-13 Nuclear Magnetic Resonance
cm	Centimeter
δ	Chemical shift
CA	Coumarin aldehyde
<i>J</i>	Coupling constant
Cys	Cysteine
CMP	Cytidine monophosphate
°C	Degree Celsius (centigrade)
DA	Dopamine
DMSO	Dimethyl sulfoxide
ESI-HRMS	Electrospray Ionization High-Resolution Mass Spectroscopy
EPI	Epinephrine
equiv	Equivalence
EtOH	Ethanol
λ_{ex}	Excitation wavelength
FRET	Fluorescence Resonance Energy Transfer
g	Gram

Glu	Glutamic acid
Gly	Glycine
GDP	Guanosine diphosphate
GMP	Guanosine monophosphate
Hz	Hertz
HM	Histamine
HB	Histamine blue
HBCHM	Histamine blue-histamine complex
HBCHD	Histamine blue-histidine complex
HD, His	Histidine
h	Hour
K	Kelvin
Leu	Leucine
Lys	Lysine
m/z	Mass per charge ratio
MALDI-TOF	Matrix Assisted Laser Desorption/Ionization – Time of Flight
MHz	Mega Hertz
MeOH	Methanol
Met	Methionine
μL	Microliter
μM	Micromolar
min	Minute
mm	Millimeter
mM	Millimolar

mL	Milliliter
mmol	Millimole
M	Molar
nm	Nanometer
NE	Norepinephrine
NMR	Nuclear Magnetic Resonance
ppm	Parts per million
Phe	Phenylalanine
¹ H-NMR	Proton Nuclear Magnetic Resonance
PBA	Pyrene boronic acid
RT	Room temperature
s, d, t, m	Splitting patterns of ¹ H-NMR (singlet, doublet, triplet, multiplet)
Thr	Threonine
UDP	Uridine diphosphate
UMP	Uridine monophosphate
UTP	Uridine triphosphate
λ	Wavelength

CHAPTER I

INTRODUCTION

1.1. Supramolecular chemistry concept

In 1978, Prof. Dr. Jean Marie Lehn created the word “Supramolecular chemistry” or “Host-guest chemistry” in his work [1]. Supramolecular chemistry was defined that a supramolecule is the organization of complex which is the association of two or more chemical species. All of them could react together by intermolecular interaction forces including hydrogen bonding, ion-dipole interaction, π - π interaction and hydrophobic interaction. The intermolecular interactions can induce many small molecules to form the supramolecular structures.

In the present, supramolecular chemistry is widely used in the multidisciplinary field of chemistry such as the organic chemistry and inorganic chemistry research areas, need to synthesize the substances for supramolecular systems and to study the behavior of the supramolecular complex system, and to be applied to the daily life [2]. In the present, Ariga *et al.* [3] classified the supramolecular chemistry into three types: (i) molecular recognition; (ii) translocation and (iii) transformation. Moreover, we will describe the most fundamental of supramolecular chemistry by initially explaining the molecular recognition.

1.2. Molecular recognition

Molecular recognition is a recognition process which involves in the interaction between hosts and guests. This process does not define only binding behavior but indicated the selectivity between hosts and guests. In physiological system, the perfect recognition of the receptor depended on many factors such as electronic geometry and polarity of hosts and guests [1, 4, 5]. In addition, the signaling unit is the unit that could be changed the optical responses when the recognition unit interacts with the target analytes. Optical signal based on the change of absorbance or fluorescence properties are usually employed because these techniques give the benefits of the

inexpensive instruments and easy operation. Moreover, the signaling response in term of the fluorescence changing is increase of interest in high sensitivity for sensory molecules [6, 7].

1.3. Chemical sensor

A chemosensor is the modified molecule which is selectively binding and reversibility against analyte with a simultaneous change in one or more properties of the system such as a colorimetric change, redox potential, and fluorescence response [8-12]. Thus, the chemosensor is generally composed of two molecular units including recognition unit and signaling unit. A recognition unit is a binding part which is designed a high selectivity with analytes including cations, anions, or neutral molecules. A signaling unit is a response part which can change their properties after complexation between sensor and analyte [13] as shown in Figure 1.1.

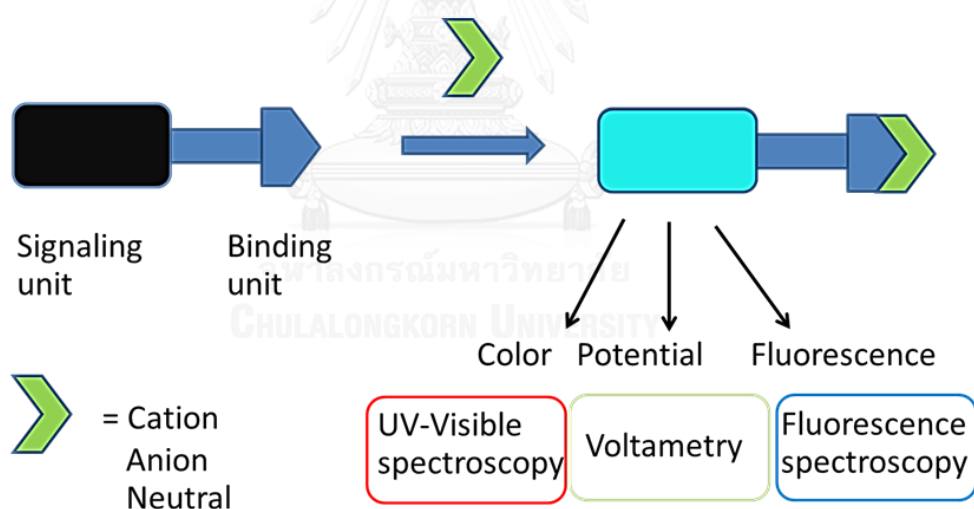


Figure 1.1 The schematic presentation of response of a chemosensor with a guest analyte

1.4. Phenomena of fluorescence

In 1888, Wiedmann explained the emission of light of any molecules which occurs from electronic transition phenomena in the term “luminescence” [7].

Considerably, luminescence is divided into two types including fluorescence and phosphorescence according to the electronic transition pathway.

Fluorescence is an emission light when the electron in the electronic transition of singlet excited state (S_1) relaxed to singlet ground state (S_0). Thus, the fluorescence lifetime is shorter than phosphorescence approximately in nanosecond [14].

Phosphorescence is a light emission when the transition of electron from triplet excited state (T_1) to the ground state (S_0) is forbidden. Hence, the lifetime of phosphorescence is quite long in the range of milliseconds to seconds.

The process of fluorescence and phosphorescence would be explained by using the Jablonski diagrams as shown in Figure 1.2.

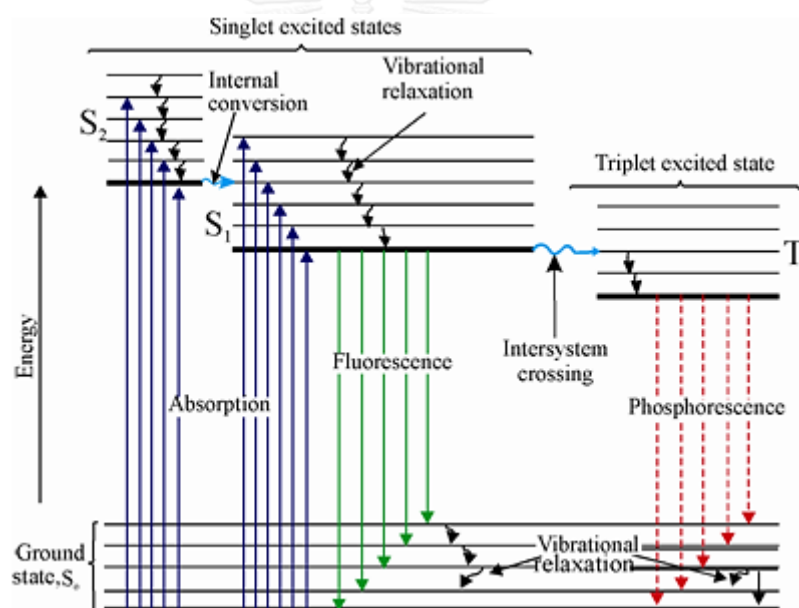


Figure 1.2 The schematic Jablonski diagram and the mechanism for absorption, fluorescence and phosphorescence phenomena [15]

1.4.1. Photoinduced electron transfer (PET)

The chemosensors which are consisted of a fluorophore and the recognition unit, can induce the photoinduced electron transfer (PET) phenomenon. Generally, the chemosensor can emit the weak fluorescence signal when the electron from

HOMO of the recognition unit relaxes to the HOMO energy level of fluorophore. This phenomenon is called PET process [16].

After the complexation between chemosensor and guest, the stabilized binding energy of recognition units is lower than the HOMO of fluorophore. Then, the excited electron on the lowest unoccupied molecular orbital (LUMO) of fluorophore was relaxed to the highest occupied molecular orbital (HOMO) or ground state of fluorophore and the strong fluorescence signal will be observed. Therefore, the PET process will disrupt the electron transferring to ground state and it leads to a decrease of fluorescence intensity or fluorescence quenching [16-20] as shown in Figure 1.3

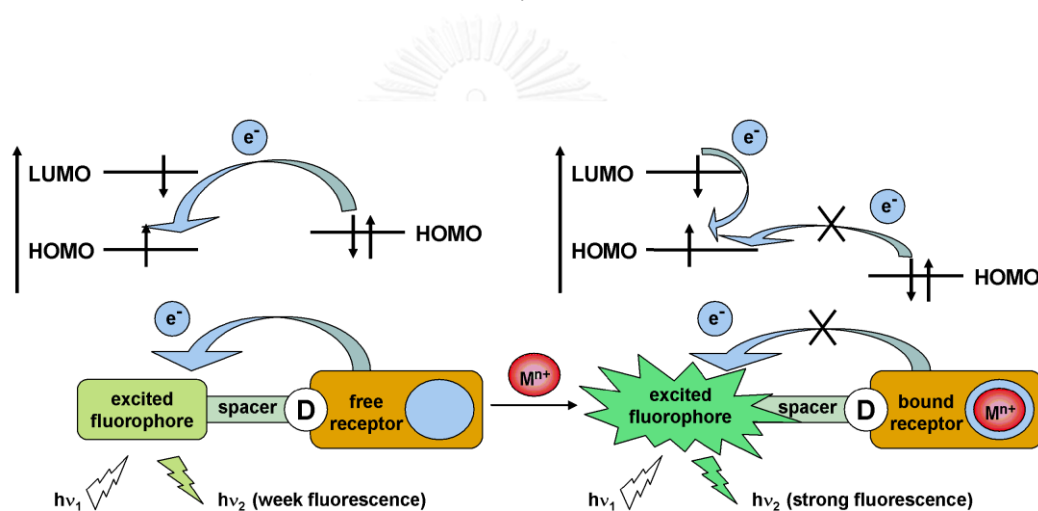


Figure 1.3 The energy level of an OFF-ON chemosensor (upper) and the schematic mechanism of the PET process (lower) [21]

1.4.2. Photoinduced charge transfer (PCT)

The photoinduced charge transfer phenomenon is the intramolecular charge transfer process from the electron donating group to electron withdrawing group upon excitation by light. This phenomenon involved in the change of dipole moment. Thus, it can give a response when the analytes including cations and anions closely interact with donor or acceptor group resulting in the change of photophysical properties of the fluorophore [22-24].

For instance, the electron donating group associated with a fluorophore interacts with a cation. The electron donating property of a donor moiety is reduced and the excited state of the complex is less stable than the ground state. The effect of reducing of the stability of molecule results in a blue shift of absorption and emission spectra as shown in Figure 1.4a. On the other hand, the cation was bound with the electron withdrawing group. Then, the complex is more stable than the free molecule which causes the red shift of the absorption and emission spectra as shown in Figure 1.4b [7, 25].

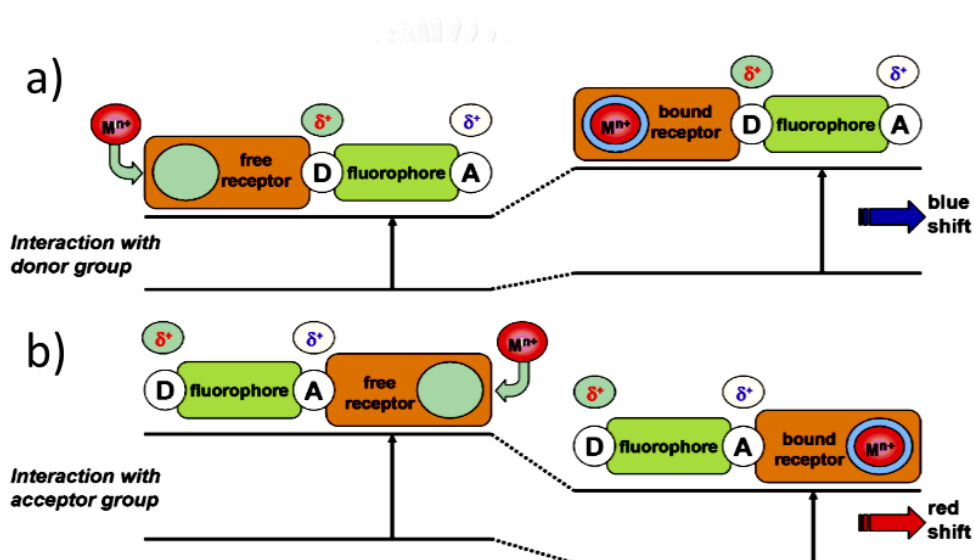


Figure 1.4 The schematic of PCT process of a donor group (a) and an acceptor group (b) [21]

1.4.3. Fluorescence resonance energy transfer (FRET)

The fluorescence resonance energy transfer (FRET) is the non-radiative mechanism for transfer the energy from an excited donor molecule to an acceptor molecule [7]. There are the significant three factors to induce on the FRET process including the distance between the donor and acceptor group of 10-100 Å, the overlapped spectrum of emission band of donor and absorption band of acceptor as shown in Figure 1.5, and the direction of dipole moment between donor and acceptor [25, 26].

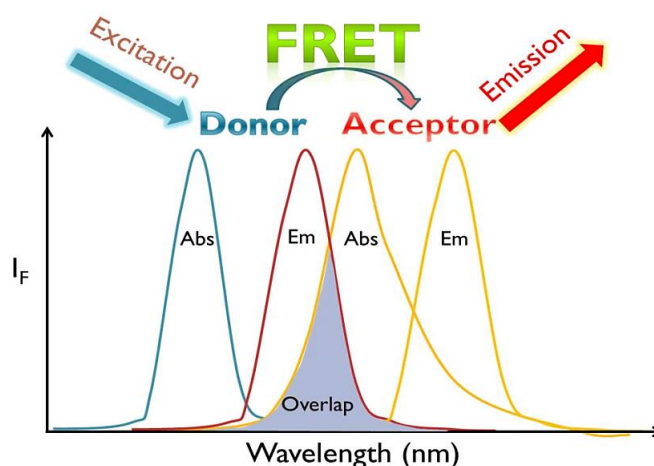


Figure 1.5 The integral overlap between the emission spectrum of donor and the absorption spectrum of acceptor

The non-radiative energy transfer mechanism is shown in Figure 1.6. Firstly, the electron from donor molecule is excited by the light or a photon. Then, the electron relaxes to the lowest singlet state (S_1). Next, the electron is released the energy and returned to the ground state (S_0) and released the energy which further excited electron of the acceptor molecule. This non-radiative mechanism is called as “resonance”. Finally, the fluorescence emission of the acceptor was turned on after the excitation at proximate absorption of acceptor.

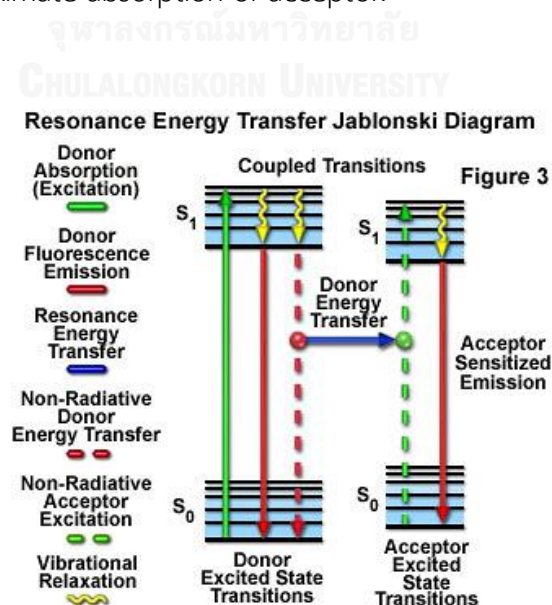


Figure 1.6 The schematic diagram of the fluorescence resonance energy transfer process (FRET) [27]

1.5. Logic gates

Molecular level information processing is a numerous number of information which performs an interaction or a general feature of the chemical systems. Generally, the information processing was easily operated based on the Boolean algebra or Boolean logic rules. The Boolean algebra is a binary logic operation which encoded the signals into the logic code level assigned as 0 and 1 for low and high level, respectively. Interestingly, many of the chemical systems can be miniaturized by using the Boolean algebra to easily understand the whole concept as called as molecular logic gates systems. In the supramolecular chemistry, the most of molecular devices performed changing optical or electrical output signals in the presence of target analytes. Interestingly, De Silva constructed the first molecular logic gates system by using the YES logic gate operation from fluorescence molecular device [28]. This system sets up the input and output as the concentration of H^+ species and fluorescence signal of the molecular device, respectively. Considerably, the presence and absence of H^+ species in the system were assigned as 1 and 0, respectively. Following to the YES logic operation, the results showed that the fluorescence output was turned on that assigned as 1 in the presence of H^+ species. On the contrary, the fluorescence output was turned off that assigned as 0 in the absence of H^+ species. Moreover, the invert operation of YES gate is the NOT logic gate operation which explained the opposite results against YES logic operation as shown in Figure 1.7.

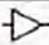
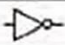
output input	YES	NOT
		
0	0	1
1	1	0

Figure 1.7 The truth table data for one inputs logic gate operation [29]

After that, the development of the molecular logics gates was expanded into multiple inputs, thus, many new logic gate operation including OR, AND, XOR, INH, NOR, NAND, and XNOR gates were used to explain the systems. Briefly, Each of logic gate

operation was differently explained as a following; (i) OR is an operation which is activated in the presence of stimuli at least one input, (ii) AND is an operation which is displayed in the presence of all stimuli, (iii) XOR (exclusive-OR) is an operation which is activated in the presence of only one input, (iv) INH is an operation which is utilized in the presence of the dominated input, (v) NOR is a combination of NOT and OR operation which can converted the result of OR operation, (vi) NAND is a combination of NOT and AND operation which can converted the result of AND operation, and (vii) XNOR (exclusive-NOR) is an operation which is showed the output when all stimuli presented or absented in the system. Finally, the truth table for all of the multiple inputs gate operation which explained the outputs response was shown in Figure 1.8.


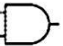



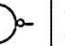
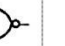
input \ output		OR	AND	XOR	INH	NOR	NAND	XNOR
								
0	0	0	0	0	0	1	1	1
0	1	1	0	1	1	0	1	0
1	0	1	0	1	0	0	1	0
1	1	1	1	0	0	0	0	1

Figure 1.8 The truth table data for two inputs logic gate operation [29]

CHAPTER II

LITERATURE REVIEWS

2.1 Literature reviews

Biogenic amines were classified by core structure into three groups including catecholamines, indolamines and histamines which have important roles in biological systems [30]. Biogenic amines based histamine group are including histamine and histidine which are differed by the additional of carboxyl group. However, histamine is a major source of food poisoning agents because it is widely spread in many kinds of foods such as fish, meat, and dairy products by degradation of histidine [30]. Especially, the high concentration of histamine causes the allergy and cancers. In the recent years, there are many techniques for histamine detection such as high performance liquid chromatography and liquid chromatography-mass spectrometry but they are consuming time, expensive and no selectivity [31-33]. Therefore, many scientists focused on the development of the determination of histamine with fast, easy and highly selective detection.

2.1.1 Determination of biogenic amines by IDA assays

In 2010, Seto *et al.* reported the novel fluorescence probe which is composed of two moieties including Nile red and iminodiacetic acid-Ni complex (IDA-Ni) for histamine determination by using Indicator Displacement Assays [34]. They hypothesized that the biogenic amines which contain two amine functional groups can be removed the metal ion and turned on fluorescence of IDA complex. The results showed that the IDA-Ni probe has high selectivity with histamine as shown in Figure 2.1. The probe was turned on the fluorescence signal at $\lambda = 670$ nm when histamine was added into the solution because of the proper length between imidazole and amino groups of histamine.

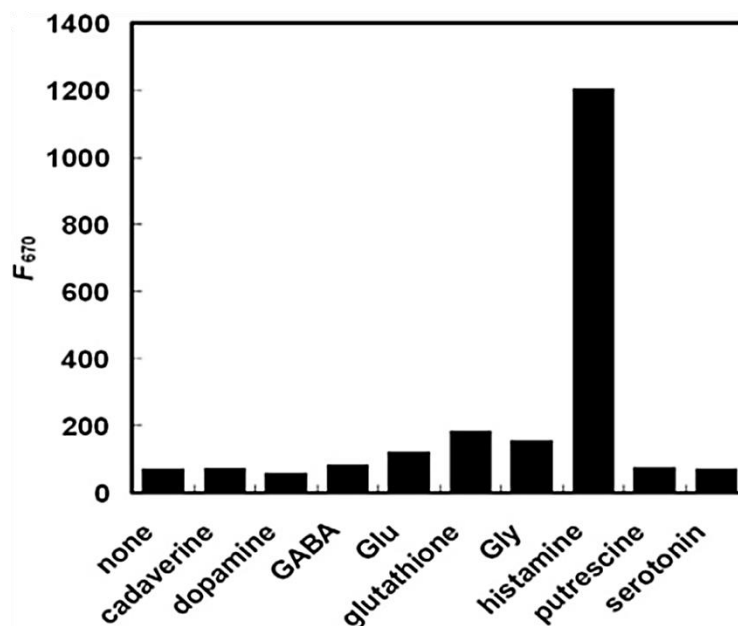


Figure 2.1 The fluorescence results at $\lambda = 670$ nm of IDA-Ni probe against various biogenic amines [34]

Moreover, they proposed the reaction between IDA-Ni complex and histamine as shown in Figure 2.2. Firstly, the fluorescence signal of IDA complex was quenched when it bound with the metal ion such as Cu^{2+} and Ni^{2+} ions. Upon the addition of histamine into the solution, histamine removed the Ni^{2+} ion from IDA-Ni complex and fluorescence signal of IDA complex was turned on. In addition, histamine-Ni complex was formed with 3:1 stoichiometric ratio by using imidazole and aliphatic amines groups. Therefore, the novel IDA-Ni fluorescence probe is highly selective with histamine.

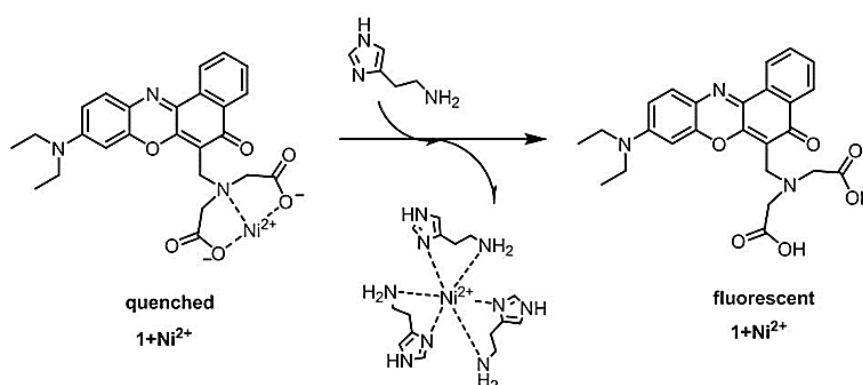


Figure 2.2 The reaction of IDA-Ni complex with histamine [34]

In 2011, Chow *et al.* reported the heterobimetallic nuclear complex can be used as chemodosimetric sensor for biogenic amines determination [35]. They synthesized the complex $K\{[Eu(H_2O)_4][Ru(^tBubpy)(CN)_4]_2\} \cdot 8H_2O$ (**Ru₂Eu-1**) which has a specific binding with biogenic amines. The results showed that the **Ru₂Eu-1** solution was turned on fluorescence signal at $\lambda = 640$ nm in the presence of biogenic amines vapour in the solution including ammonia, histamine, spermidine and putrescine. Moreover, the fluorescence ratio (I/I_0) at 640 nm was largely increased upon the addition of biogenic amines between 0 to 2 molar equiv (2×10^{-4} M) as shown in Figure 2.3.

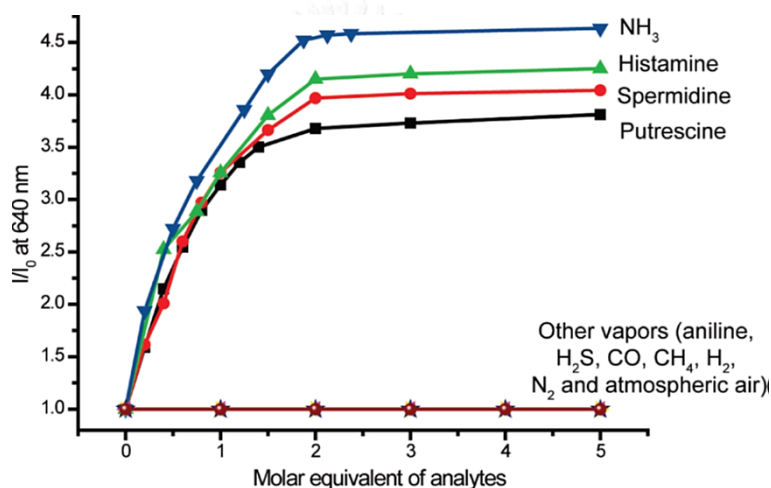


Figure 2.3 Summary of spectrofluorometric titration (I/I_0 at 640 nm) of **Ru₂Eu-1** (1.0×10^{-4} M) to putrescine, histamine, spermidine, aniline, ammonia, H_2S , CO, CH_4 , H_2 , N_2 , and atmospheric air monitored as a function of the increase in their concentration. All titrations were carried out in ethanol at 298 K [35]

Moreover, they studied the naked-eye luminometric response of **Ru₂Eu-1** solution by using excitation wavelength at 365 nm as shown in Figure 2.4. The results showed that the solution emitted the red luminescence in a presence of biogenic amines. On the other hand, the luminescence response cannot change in the presence of other analytes including aniline, H_2S , CO, N_2 , CH_4 , H_2 and air, respectively.



Figure 2.4 Photographs of the luminometric responses of the $\text{Ru}_2\text{Eu-1}$ (1.0×10^{-4} M) in EtOH at 298 K: (1) $\text{Ru}_2\text{Eu-1}$ + histamine; (2) $\text{Ru}_2\text{Eu-1}$ + putrescine; (3) $\text{Ru}_2\text{Eu-1}$ + spermidine; (4) $\text{Ru}_2\text{Eu-1}$ + NH_3 ; (5) $\text{Ru}_2\text{Eu-1}$ only; (6) $\text{Ru}_2\text{Eu-1}$ + aniline; (7-12) $\text{Ru}_2\text{Eu-1}$ + H_2S , CO, N_2 , CH_4 , H_2 , and air, respectively. (1) Excitation $\lambda_{\text{ex}} = 365$ nm [35]

According to the results, they proposed the possibility mechanism as shown in Figure 2.5 that the $\text{Ru}_2\text{Eu-1}$ complex was initially quenched the luminescence response because the electron-withdrawing effect of Eu(III) caused the energy transfer from Ru(II) complex ligand to Eu(III) center. After adding of biogenic amines, biogenic amines removed the lanthanide metal center from $\text{Ru}_2\text{Eu-1}$ complex because they have two amino groups coordinated with Eu(III) under 2:1 stoichiometric ratio to form Eu(III)-amine adduct. Therefore, the heterobimetallic complex can be used to determine of biogenic amines by IDA assays.

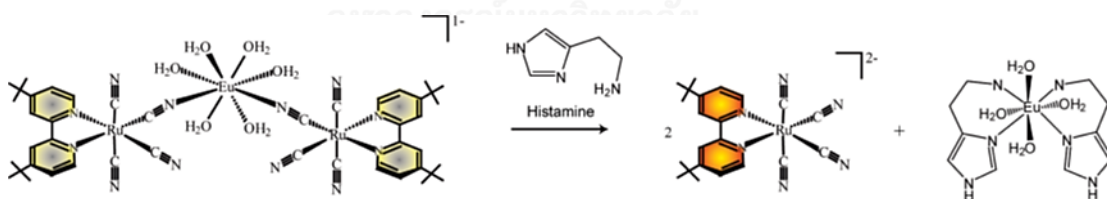


Figure 2.5 Proposed molecular recognition and luminescence signaling mechanism [35]

Moreover, the Indicator Displacement Assays was also used for histidine determination by using fluorescent coumarin-based chemosensor [36]. Therefore, the Indicator Displacement Assays is widely used for the biogenic amines determination because chemosensors were specifically designed for each analytes and their signaling has been easily monitored by spectroscopic instruments.

2.1.2 Determination of biogenic amines by Schiff base

In 2014, Lohar *et al.* published the naked-eye fluorescence sensor for histidine detection by using Schiff base condensation [37]. They synthesized the imine based rhodamine B derivatives (**TARDHD**) naked-eye sensor for histidine sensing against various amino acids. They proposed the mechanism for histidine sensing with **TARDHD** sensor as shown in Figure 2.6. **TARDHD** sensor is composed of aldehyde moiety which formed imine compound by coupling with amino group of amino acids. Moreover, the imidazole group of histidine forms hydrogen bonding with carbonyl based spiro lactam ring resulting in turns on fluorescence detection due to the spiro lactam ring opening.

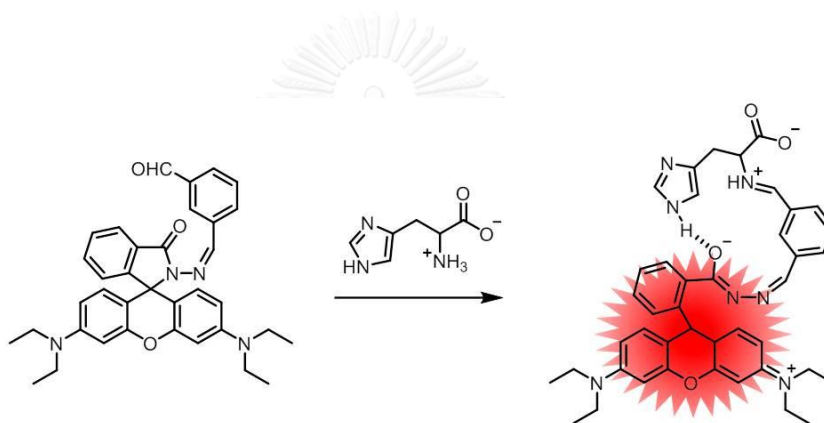


Figure 2.6 Proposed mechanism of histidine sensing with **TARDHD** sensor [37]

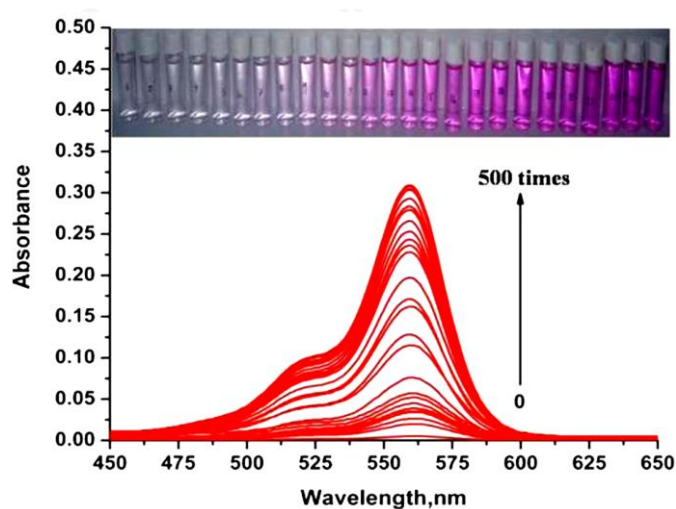


Figure 2.7 Changes of absorbance of **TARDHD** (10 μM) upon addition of histidine (0 - 5000 μM) in HEPES buffered (0.1 M) solution (ethanol/water = 1:9, v/v, pH 7.3) [37]

From the UV-visible spectra results showed that the new absorption peak appeared at 560 nm in the presence of histidine as shown in Figure 2.7. The absorption spectra of **TARDHD**-histidine were largely increased when the addition of histidine from 0 to 500 equivalences. Moreover, histidine can be detected with **TARDHD** sensor by naked-eye detection as shown in Figure 2.7. The color of free **TARDHD** solution was changed from colorless to purple solution depended on the additional concentration of histidine in the solution. Therefore, they successfully synthesized a highly selective naked-eye fluorescence sensor for histidine detection.

However, the detection limit of **TARDHD** sensor for naked-eye detection of histidine compound is using the high concentration of histidine. Thus, we would like to develop the techniques to increase sensitivity, selectivity and low limit of detection for biogenic amine detection.

2.1.3 Discrimination of biogenic amines by FRET

In 2013, Chaicham *et al.* reported the novel fluorescence system for discrimination of catecholamines by using FRET on/off process [38]. Their conceptual design is using catecholamines as a linkage of two fluorophores which act as donor and acceptor resulting in the FRET on process as shown in Figure 2.8. They hypothesized that the dual fluorescence sensors can discriminate the biogenic amines which contain the similar structure based on catechol and amine group.

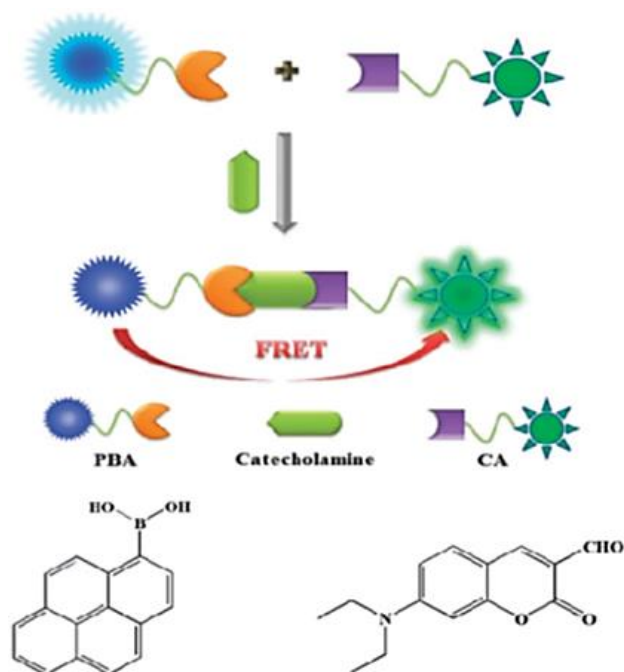


Figure 2.8 Conceptual design of an intermolecular assembled complex for catecholamine sensing by FRET-on process [38]

According to the conceptual design, they chose the combination of 1-pyreneboronic acid (PBA) and coumarin aldehyde (CA) as a donor and acceptor fluorophores, respectively. The results showed that fluorescence spectra of catecholamines including dopamine (DA), epinephrine (EPI), and norepinephrine (NE) showed by the excimer of PBA at 450 nm. After the addition of CA, the fluorescence spectra of DA and NE at 450 nm were shifted to 487 nm corresponding of emission band of CA. This signified the FRET-on emission band obtained by DA and NE as a good guest linker of PBA and CA. Meanwhile, the excimer of PBA-EPI complex is still remained at 450 nm because the secondary amine chain of EPI cannot react with CA as shown in Figure 2.9. Therefore, they successfully discriminate the EPI from the other biogenic amines by using FRET process.

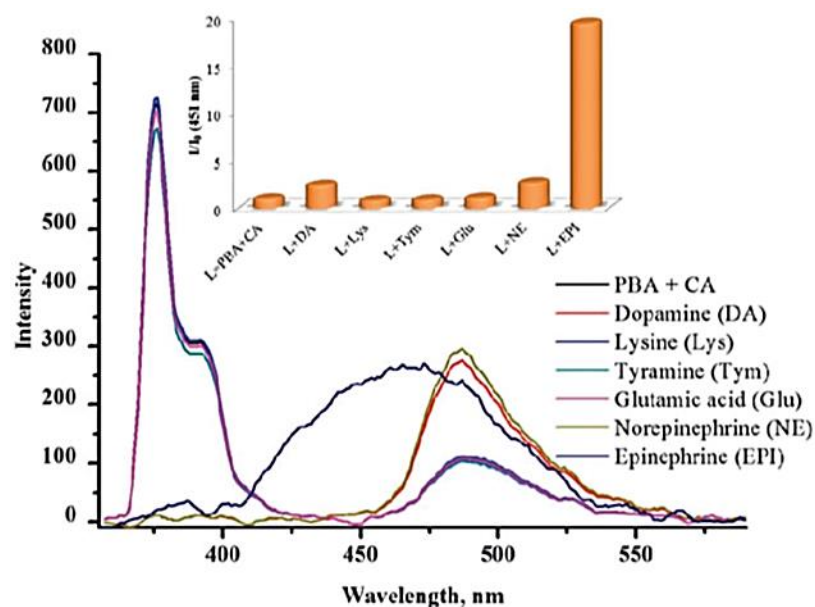


Figure 2.9 Fluorescence spectra of the mixed sensors of PBA (1 μM) and CA (30 μM) in buffer solution (100 mM $\text{Na}_2\text{S}_2\text{O}_3$, 50 mM HEPES, 20 mM NaCl, pH 7.4) with various biogenic amines and inset: relative fluorescence intensity of the mixed sensors of PBA and CA ($\lambda_{\text{ex}} = 340 \text{ nm}$) in the presence of various biogenic amines [38]

2.1.4 Determination of biogenic amines by mesoionic acid

In 2012, Kielland *et al.* reported highly selective fluorescence sensor for histamine sensing [39]. They synthesized the mesoionic acid fluoride derivative which is called Histamine Blue (HB) by using multicomponent reaction (MCR) [40] as shown in Figure 2.10.

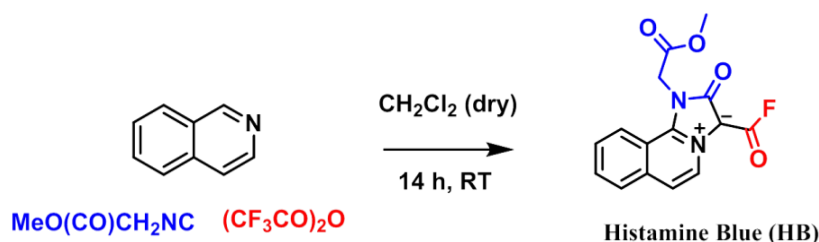


Figure 2.10 Synthesis pathway of Histamine Blue (HB)

Interesting, HB turned on the light blue fluorescence in the presence of histamine. They proposed that the HB reacts with histamine by using amide condensation and forms the adduct **5i** as shown in Figure 2.11. The fluorescence

spectrum was shifted from 393 nm to 421 nm and the naked-eye detection of **HB** toward histamine was carried out under UV lamp. Moreover, Imidazole group of histamine is the key for the reaction because the imidazole performed a self-catalyst to form the stable intermediate compound as shown in Figure 2.12.

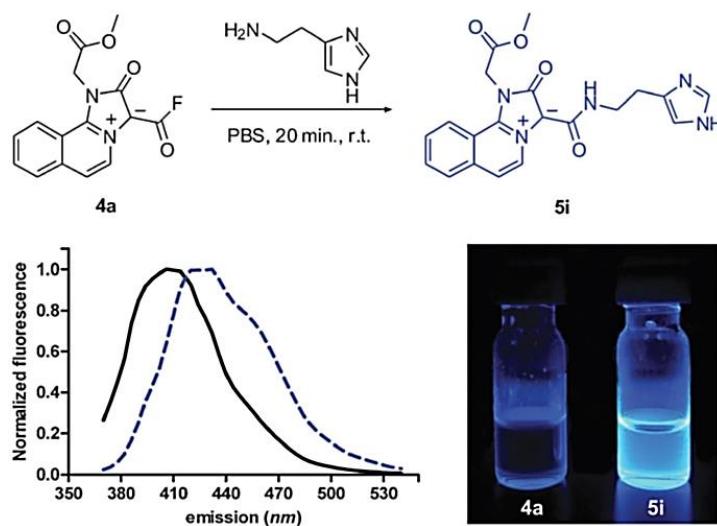


Figure 2.11 Reaction of 4a with histamine in PBS. Fluorescence spectra of 4a before (black) and after (blue) reacts with histamine; exc: 340 nm. Fluorescent images of PBS solutions of 4a and **5i** under a 365 nm lamp [39]

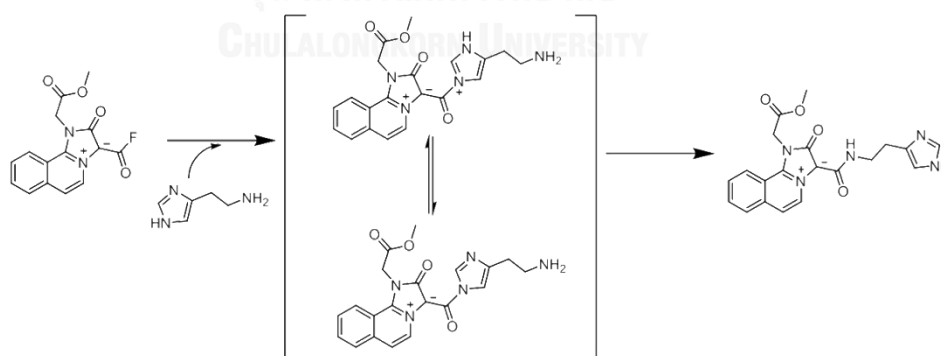


Figure 2.12 The mechanism between the **HB** and histamine [39]

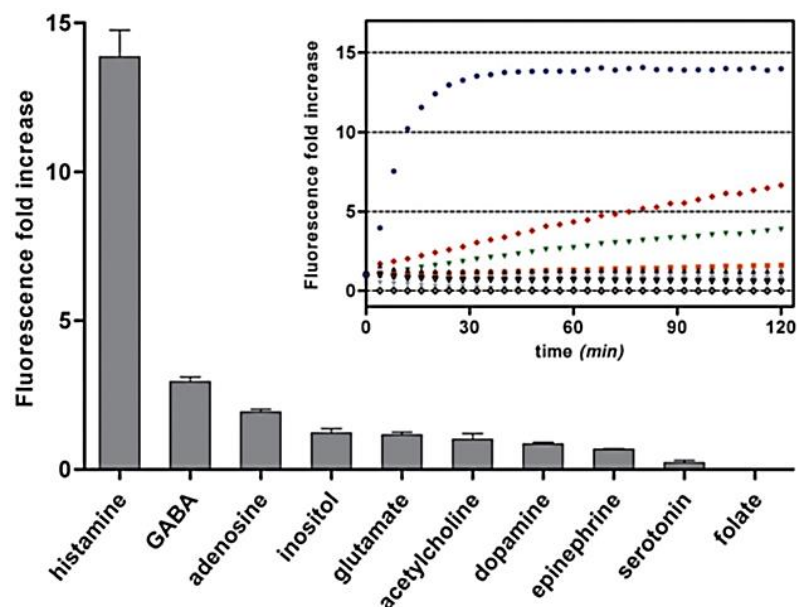


Figure 2.13 Fluorescent response of **HB** (10 μ M) after incubation with different signaling molecules (5 mM) for 30 min in PBS (pH: 7.3). Inset: Kinetic analysis of the reactions of **HB** with histamine (blue), GABA (red), adenosine (green), glutamate (orange), inositol (purple), and other (grey); exc: 370 nm. Values are represented as means ($n = 4$) and errors bars as standard deviations [39]

According to the preliminary results, they studied the selectivity of **HB** with various biogenic amines such as histamine, GABA, adenosine, glutamate, dopamine, and folate. Moreover, they also studied the kinetic between **HB** and various biogenic amines. The results showed that the fluorescence intensity of **HB** and histamine was higher around 10 folded than the other and the **5i** adduct was completely formed in 30 minute as shown in Figure 2.13. Therefore, they successfully discriminated histamine from the other biogenic amines by using Histamine blue compound.

2.1.5 Literature of naphthalimide sensors

In 2015, Tachapermpon *et al.* published two novel fluorescence sensors based on naphthalimide derivatives for Hg^{2+} sensing [41]. They synthesized the naphthalimide derivatives sensors **1** and **2** as shown in Figure 2.14. Both of them were modified with S and N atoms for cation binding unit.

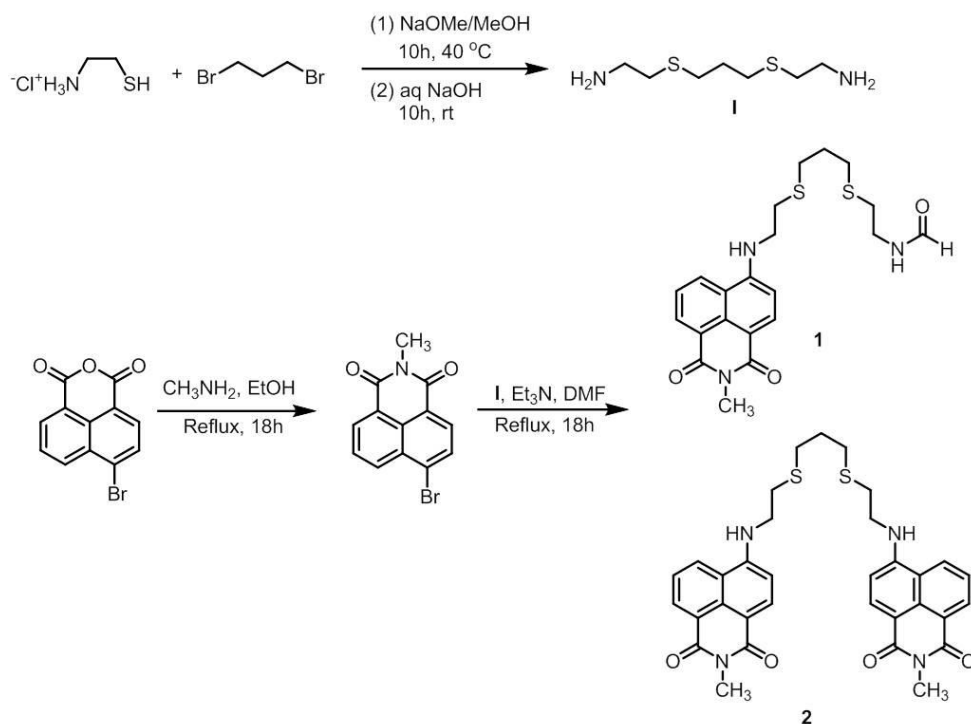
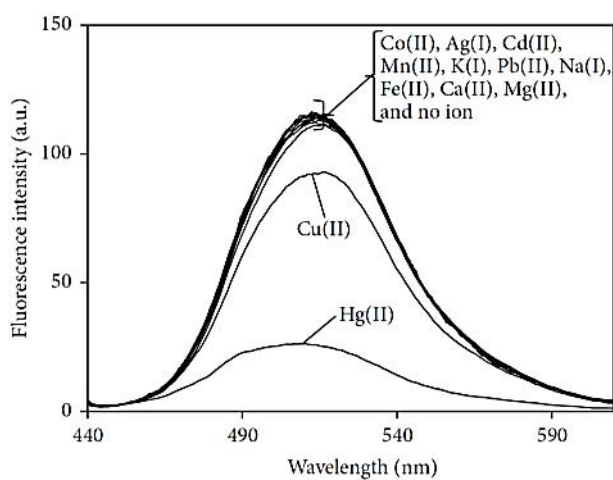
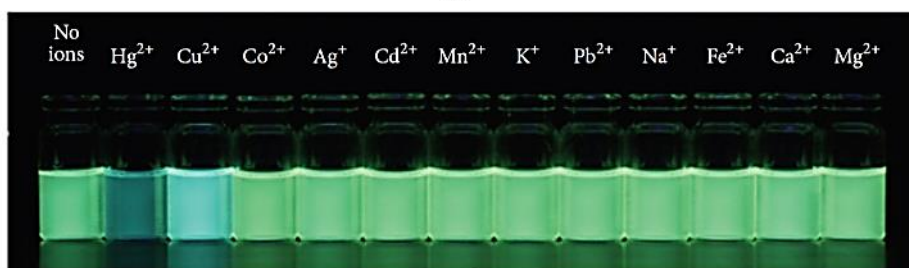


Figure 2.14 Syntheses of fluorescence sensors **1** and **2** [41]

They studied the selectivity of **1** and **2** sensors against various cations including Hg²⁺, Cu²⁺, Ag⁺, Cd²⁺, Mn²⁺, K⁺, Pb²⁺, Na⁺, Fe²⁺, Ca²⁺, Mg²⁺, and Co²⁺. From the results showed that, the fluorescence spectra of **1** was deeply quenched in the presence of Hg²⁺ ion while the fluorescence spectra of **1** were slightly quenched in the presence of Cu²⁺ ion. Moreover, they also studied the fluorescence changing by using the naked-eye detection as shown in Figure 2.15. The fluorescence response of **1** was changed from green to dark blue and light blue upon the addition of Hg²⁺ and Cu²⁺, respectively. The fluorescence quenching of sensor **1** is occurred because the N and S atoms can coordinate with some cations according to hard soft acid base (HSAB) theory. Thus, the fluorescence signal was quenched by PET process.



(a)



(b)

Figure 2.15 (a) Fluorescence spectra of **1** ($\lambda_{\text{ex}} = 426 \text{ nm}$, $0.15 \mu\text{M}$) with addition of perchlorate salts of Hg^{2+} , Co^{2+} , Ag^+ , Cd^{2+} , Mn^{2+} , K^+ , Pb^{2+} , Na^+ , Fe^{2+} , Ca^{2+} , Mg^{2+} , and Cu^{2+} , ($123 \mu\text{M}$). (b) The luminescence under UV of **1** ($23 \mu\text{M}$) in the presence and absence of Hg^{2+} , Cu^{2+} , Co^{2+} , Ag^+ , Cd^{2+} , Mn^{2+} , K^+ , Pb^{2+} , Na^+ , Fe^{2+} , Ca^{2+} , and Mg^{2+} ($3.0 \mu\text{M}$) [41]

On the other hand, the selectivity of **2** was interfered with some cations such as Ag^+ and Cu^{2+} because the steric effect between two naphthalimide fluorophores. Therefore, they successfully synthesized two novel fluorescence sensors based on naphthalimide derivatives for Hg^{2+} sensing.

In addition, the sensors based naphthalimide derivatives were also used for detection of anions and biochemical species because the naphthalimide dye is easily modified and can be useful for cell imaging [42, 43].

2.1.6 Literature of imidazolium derivatives sensors

In 2013, Roy *et al.* reported two novel fluorescence sensors based on imidazolium for picric acid sensing [44]. They designed the sensor **1** and **2** by using tris-imidazolium moiety as shown in Figure 2.16. Both of them have three anthracene rings as fluorophore. Sensor **1** and **2** contain the different core to study the effect of the distance between imidazolium unit with binding ability. They hypothesized that the sensor based tris-imidazolium could be attracted to picric acid by using the positive-negative ion attraction. Binding affinity can be carried out by spectroscopic method.

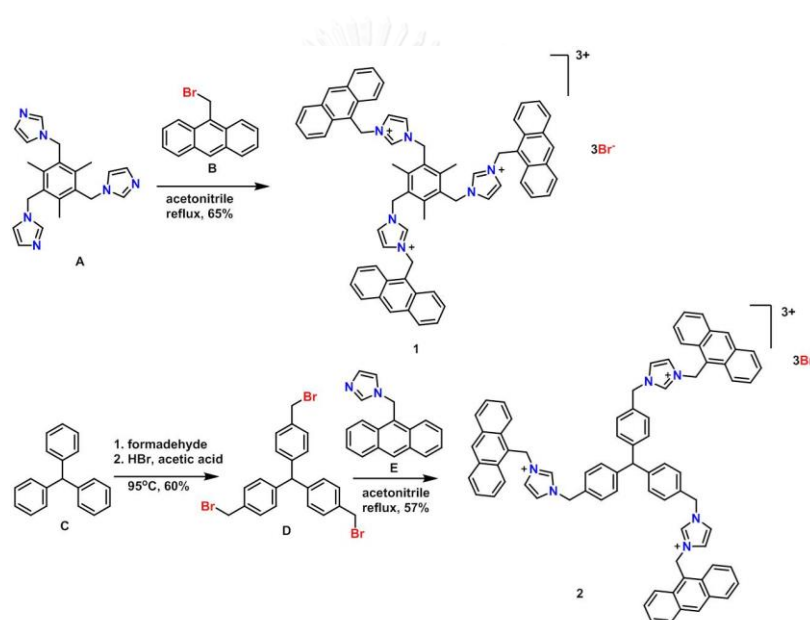


Figure 2.16 Schematic presentation of the synthesis of sensors **1** and **2** [44]

The results showed that the emission band of sensor **1** and **2** were significantly decreased in the presence of picric acid (PA) from 0 to 250 equivalences as shown in Figure 2.17. Moreover, the inset showed that the color solution of **1**⊂PA was changed from colorless to yellow solution. This is indicative of complex **1**⊂PA.

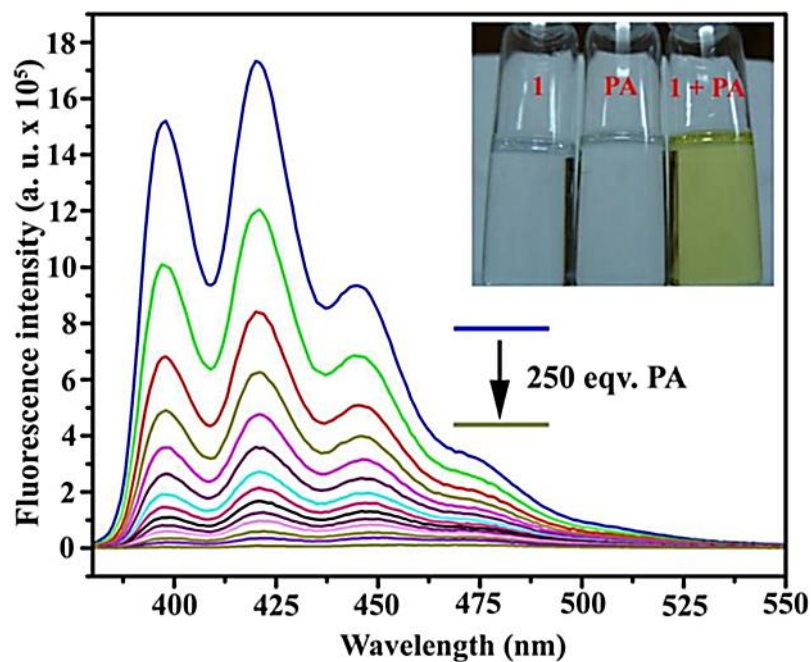


Figure 2.17 Fluorescence intensity vs analyte concentration plot of sensor **1** titrated upon gradual addition of PA. Inset: visual color change due to the formation [1+PA] complex

After that, they studied the selectivity of sensor **1** and **2** against the various aromatic compounds. The result showed that the fluorescence quenching efficiency of sensor **1** and **2** in the presence of PA is 92% and 91%, respectively. Thus, both of sensors are highly effective for PA sensing in water and organic solvent.

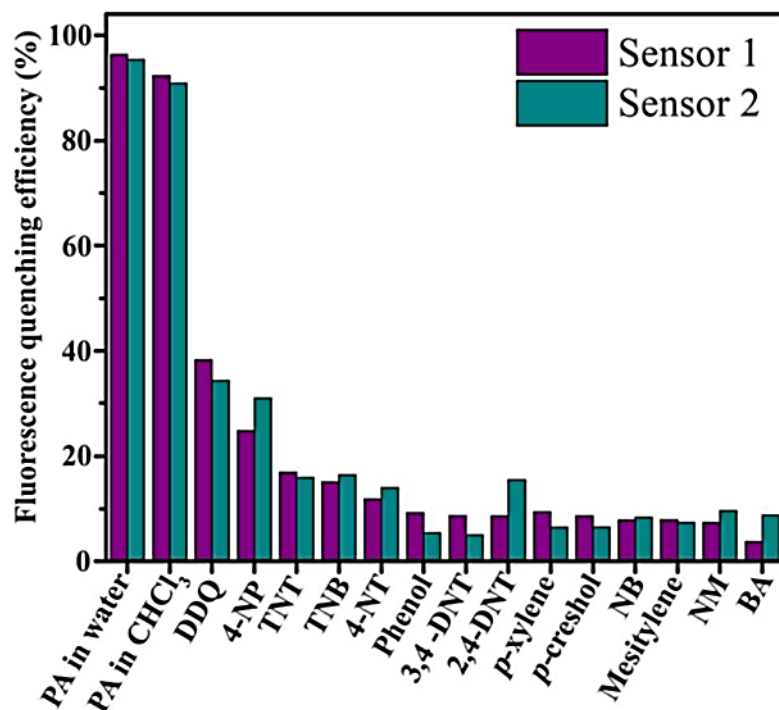


Figure 2.18 Fluorescence quenching efficiencies of sensors 1 and 2 toward different analytes. PA = picric acid; DDQ = 2,3-dichloro-5,6-dicyano-1,4-benzoquinone; 4-NP = 4-nitrophenol; TNT = trinitrotoluene; TNB = trinitrobenzene; 4-NT = 4-nitrotoluene; 3,4-DNT = 3,4-dinitrotoluene; 2,4-DNT = 2,4-dinitrotoluene; NB = nitrobenzene; NM = nitromethane; BA = benzoic acid [44]

Moreover, imidazolium based sensor was used to detect the nucleoside polyphosphate species [44, 45]. Considerably, the positive imidazolium cation preferred to bind with anions and phosphate group. Therefore, the imidazolium cations are used to detect various anions.

2.2 Objectives and scope of this research

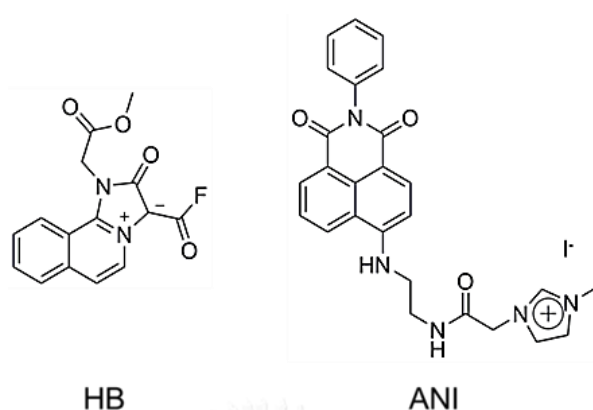


Figure 2.19 Structure of fluorescence chemosensors **HB** and **ANI**

Following on the literature reviews, many researches have paid attention to design the sensor for detection of the biogenic amines compounds such as catecholamines, histamine, and amino acids. As a previous work, there are a few reports about the discrimination of histidine and histamine by fluorescence methods because histidine and histamine consists of the same core structure base on imidazole unit which give a similar reactivity. Therefore, the aim of our research is to develop the fluorescence sensors and method for discriminating the same structure of biogenic amines including histidine and histamine. This research is beneficial for preliminary test for histamine contamination [39, 46]. Therefore, two fluorescence chemosensors **HB** and **ANI** were chosen in this research. As shown in Figure 2.19, The **HB** sensor is a mesoionic acid compound which has high selectivity with histamine group because histamine is consisted of imidazole moiety [39]. The sensor **ANI** has been designed and synthesized. It comprised imidazolium unit and naphthalimide acting as recognition unit and fluorophore moiety, respectively.

The spectroscopy properties of these sensors for biogenic amines discrimination were measured in 10% DMSO in phosphate buffer pH 7.4 by fluorescence spectrophotometry technique. Conceptually, the histidine, contains primary amine and carboxyl group which enable to bind with **HB** and **ANI**, respectively,

was proposed to be a good linkage. Consequently, the fluorescence resonance energy transfer emission band will be observed under energy transfer from FRET donor of **HB** to FRET acceptor of **ANI**. Meanwhile, this approach cannot be observed in the case of histamine because histamine has no carboxylate anion to form complex with **ANI**.



CHAPTER III

EXPERIMENTAL

3.1 General procedures

3.1.1 Analytical instruments

Nuclear magnetic resonance (NMR) spectra were measured by a Varian Mercury Plus 400 NMR spectrometer and Bruker Avance 400 NMR spectrometer. Samples were dissolved in *d*-CDCl₃ and *d*₆-DMSO. The chemical shift was recorded in part per million (ppm) and using a residue proton solvents as internal reference. MALDI-TOF mass spectra were recorded on Bruker Doltonic using doubly crystallized 2-cyano-4-hydroxy cinnamic acid (CCA) as a matrix. Absorption spectra were recorded on a Varian Cary 50 UV-Vis spectrophotometer. All fluorescence spectra were measured by Cary Eclipse Varian fluorescence spectrophotometer. The light source is the Cary Eclipse a pulsed xenon lamp and a detector is a photomultiplier tube. All naked-eye fluorescence photos were recorded by Samsung galaxy S5. All naked-eye colorimetric photos were recorded by Nikon D5500.

3.1.2 Materials

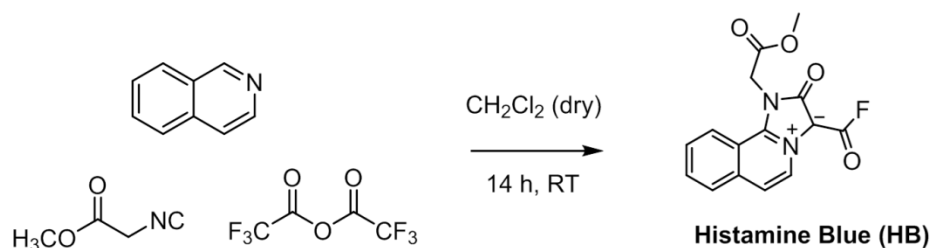
All reagents were purchased from Aldrich, Merck, BDH, Carlo Erba, Fluka and TCI. They were used without further purification. All commercial grade solvents were purified by distillation before used. Tetrahydrofuran (THF) was dried up with Na metal and benzophenone as a drying reagent. Dimethylformamide (DMF) was dried up with CaH₂ as a drying reagent. Thin-layer chromatography (TLC) was performed on silica gel plates (Kieselgel 60 F₂₅₄, 1 mm, Merck). Dimethylsulfoxide (DMSO), spectrophotometric grade used in UV-Visible and fluorescence measurement was provided form Merck.

In this research, we synthesized 3 sensors including sensors **HB**, **AN** and **ANI** for complexation study toward biogenic amines, metal ions and various anions.

3.2 Synthesis

3.2.1 Synthesis of histamine blue sensor

3.2.1.1 Synthesis of 3-(Fluorocarbonyl)-1-(2-methoxy-2-oxoethyl)-2-oxo-2,3-dihydro-1H-imidazo[2,1-a]isoquinolin-4-ium-3-ide (histamine blue, HB)



HB was synthesized by using one-pot reaction [40]. Isoquinoline (1.085g, 8.4 mmol) was dissolved in CH_2Cl_2 at 0 °C. Trifluoroacetic anhydride (TFAA) (1.416g, 10.025 mmol) and methyl isocyanacetate (0.759 mL, 8.349 mmol) were added to the solution. The reaction was stirred overnight under N_2 atmosphere. The crude product was treated by Na_2CO_3 and it was separated with $\text{CH}_2\text{Cl}_2/\text{H}_2\text{O}$. Na_2SO_4 and silica were added into the organic extraction and then stirred for 1 h. The mixture was filtrated through Celite and the solution was collected. The solvent was removed under vacuum and recrystallized with diethyl ether. The brown solid was obtained (10% yield).

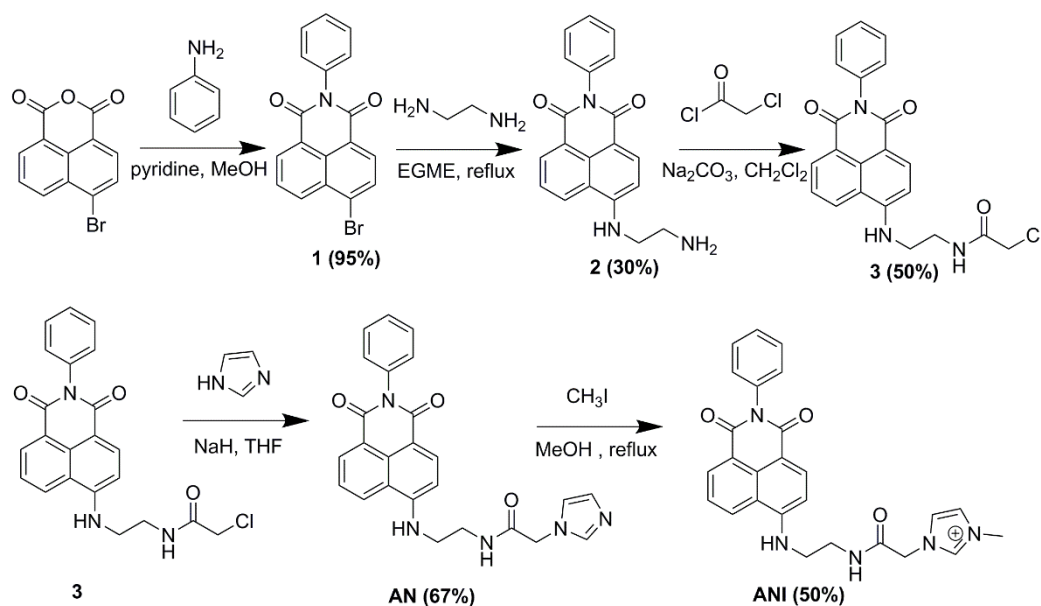
Characterization data for **HB**

$^1\text{H-NMR}$ (400 MHz, CDCl_3): δ (in ppm) = 9.28 (d, J = 6.8 Hz, 1 H, ArH), 8.04 (d, J = 8.4 Hz, 1 H, ArH), 7.96 (d, J = 8.0 Hz, 1 H, ArH), 7.83 (m, J = 7.2, 8.0 Hz, 1 H, ArH), 7.76 (m, J = 8.4, 7.2 Hz, 1 H, ArH), 7.56 (d, J = 7.2 Hz, 1 H, ArH), 5.31 (s, 2 H, CH_2), 3.80 (s, 3 H, CH_3)

$^{13}\text{C-NMR}$ (100 MHz, CDCl_3): δ (in ppm) = 167.8, 157.1, 152.9, 135.0, 133.3, 131.6, 129.8, 128.9, 124.1, 122.3, 116.6, 116.4, 90.7, 53.5, 43.4

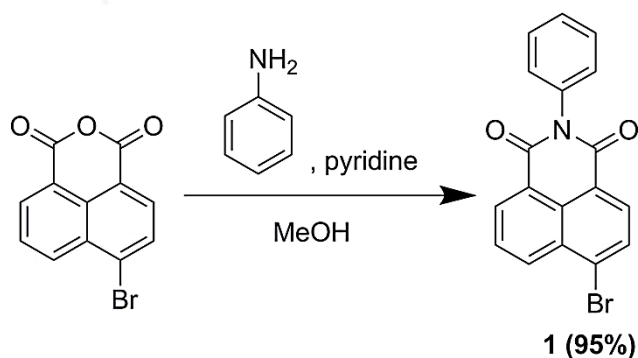
3.2.2 Synthesis of imidazole derivatives sensors

The imidazole derivatives sensors including **AN** and **ANI** were synthesized as shown in scheme 3.1. Both of them employed with 4-bromo-1,8-naphthalic anhydride as a starting material.



Scheme 3.1 Synthesis pathway of sensors AN and ANI

3.2.2.1 Synthesis of 6-Bromo-2-phenyl-1H-benzo[de]isoquinoline-1,3(2H)-dione (1)



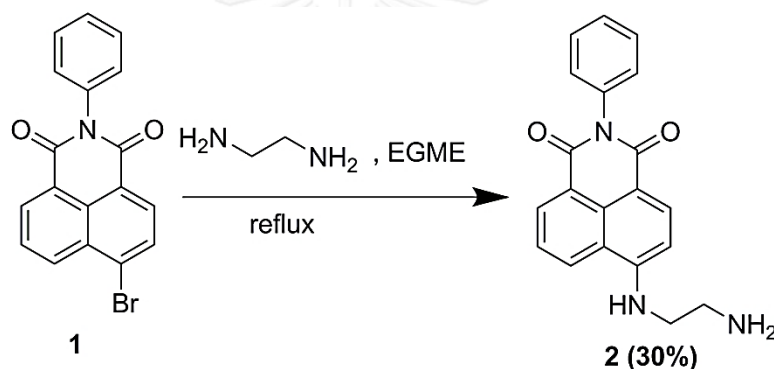
4-Bromo-1,8-naphthalic anhydride (5 g, 18 mmol) and aniline (2 mL, 21.9 mmol) were dissolved in dried methanol. The mixture was stirred for 5 min. The catalytic amount of pyridine was added into the mixture and it was refluxed overnight under nitrogen atmosphere. After that, the crude product was purified with methanol to obtain compound **1** as white solid (95% yield).

Characterization data for Compound **1**

$^1\text{H-NMR}$ (400 MHz, d_6 -DMSO): δ (in ppm) = 8.57 (t, J = 7.4 Hz, 2 H, ArH), 8.32 (d, J = 8.0 Hz, 1 H, ArH), 8.23 (d, J = 8.0 Hz, 1 H, ArH), 8.01 (t, J = 7.8 Hz, 1 H, ArH), 7.51 (d, J = 7.4 Hz, 2 H, ArH), 7.45 (d, J = 7.2 Hz, 1 H, ArH), 7.37 (d, J = 6.8 Hz, 2 H, ArH)

$^{13}\text{C-NMR}$ (100 MHz, d_6 -DMSO): δ (in ppm) = 163.14, 163.08, 135.75, 132.69, 131.57, 131.36, 130.93, 129.92, 129.15, 129.01, 128.85, 128.81, 128.75, 128.26, 123.34, 122.57

3.2.2.2 Synthesis of 6-((2-Aminoethyl)amino)-2-phenyl-1H-benzo[de]isoquinoline-1,3(2H)-dione (**2**)



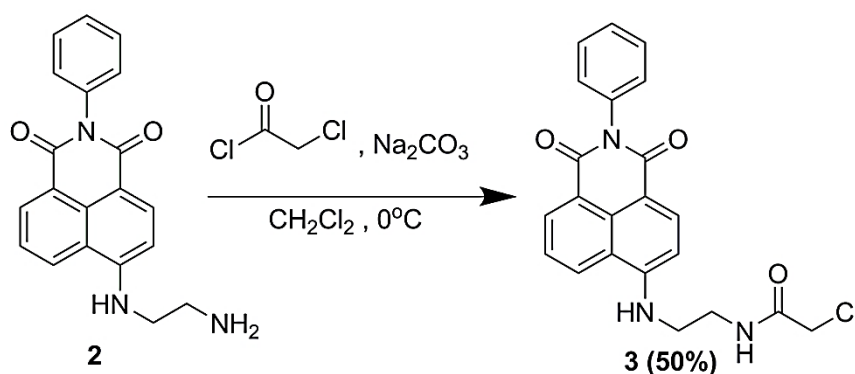
Compound **1** (2.00 g, 5.68 mmol) was dissolved in ethylene glycol monomethyl ether (EGME) and ethylenediamine (1 mL, 14.9 mmol) was added into the solution. The mixture was refluxed for 4 h under nitrogen atmosphere. After the reaction was completed, the product was precipitated by adding ice into the mixture solution. The sediment was collected and recrystallized with methanol to obtain compound **2** as yellow solid (30% yield).

Characterization data for compound **2**

$^1\text{H-NMR}$ (400 MHz, d_6 -DMSO): δ (in ppm) = 8.75 (d, J = 8.8 Hz, 1 H, ArH), 8.41 (d, J = 7.2 Hz, 1 H, ArH), 8.24 (d, J = 8.4 Hz, 1 H, ArH), 7.70 (t, J = 8.0 Hz, 1 H, ArH), 7.49 (d, J = 3.6 Hz, 2 H, ArH), 7.41 (d, J = 7.2 Hz, 1 H, ArH), 7.28 (d, J = 6.8 Hz, 2 H, ArH), 3.14 (s, 2 H, CH_2), 2.86 (t, J = 6.6 Hz, 2 H, CH_2)

$^{13}\text{C-NMR}$ (100 MHz, d_6 -DMSO): δ (in ppm) = 163.99, 163.14, 150.97, 136.81, 134.25, 130.74, 129.86, 128.99, 128.86, 128.75, 128.70, 127.79, 124.19, 122.19, 120.21, 107.79, 103.88, 46.35

3.2.2.3 Synthesis of 2-Chloro-N-(2-((1,3-dioxo-2-phenyl-2,3-dihydro-1H-benzo[de]isoquinolin-6-yl)amino)ethyl)acetamide (3)



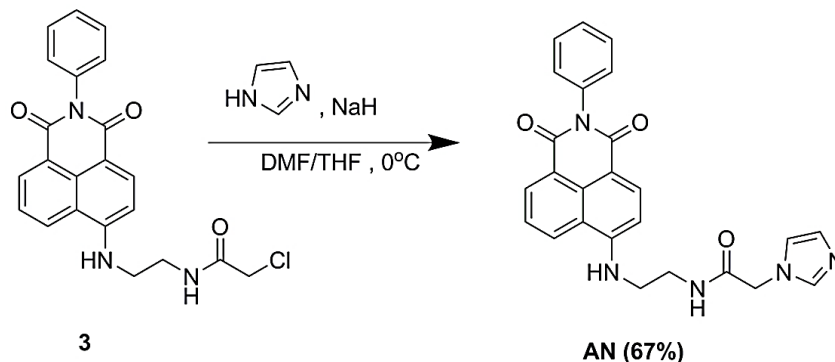
The compound **2** (1.00 g, 3.02 mmol) and Na_2CO_3 (1.06 g, 10 mmol) was dissolved in CH_2Cl_2 and stirred at 0°C for 5 min under nitrogen atmosphere. Chloroacetyl chloride (0.5 mL, 6.28 mmol) was added to the mixture solution by using the syringe and then the mixture solution was stirred overnight under nitrogen atmosphere. The reaction mixture was extracted with DI water and the organic phase was collected. The solvent was evaporated to give a crude product. The product was crystallized with methanol to obtain the orange powder (50% yield).

Characterization data for compound **3**

$^1\text{H-NMR}$ (400 MHz, d_6 -DMSO): δ (in ppm) = 8.65 (d, $J = 8.4$ Hz, 1 H, ArH), 8.50 (s, 1 H, ArH), 8.42 (d, $J = 7.2$ Hz, 1 H, ArH), 8.24 (d, $J = 8.4$ Hz, 1 H, ArH), 7.87 (s, 1 H, ArH), 7.71 (t, $J = 7.6$ Hz, 1 H, ArH), 7.48 (d, $J = 7.2$ Hz, 2 H, ArH), 7.42 (d, $J = 7.2$ Hz, 1 H, ArH), 7.29 (d, $J = 7.6$ Hz, 2 H, ArH), 6.88 (d, $J = 8.4$ Hz, 1 H, ArH), 4.10 (s, 2 H, CH_2), 3.47 (t, $J = 5.6$ Hz, 2 H, CH_2), 3.45 (t, $J = 6.0$ Hz, 2 H, CH_2)

$^{13}\text{C-NMR}$ (100 MHz, d_6 -DMSO): δ (in ppm) = 163.12, 150.62, 136.50, 134.15, 131.37, 131.06, 130.77, 130.32, 129.84, 129.18, 128.80, 128.69, 128.59, 128.48, 128.10, 127.80, 127.15, 126.54, 124.38, 119.37, 103.78, 53.71, 43.70, 42.61

3.2.2.4 Synthesis of N-(2-((1,3-dioxo-2-phenyl-2,3-dihydro-1H-benzo[de]isoquinolin-6-yl)amino)ethyl)-2-(1H-imidazol-1-yl)acetamide (AN)



Imidazole (0.20 g, 2.94 mmol) and NaH powder in catalytic amount were dissolved in THF at 0°C and stirred for 15 min. The compound **3** (0.50 g, 1.22 mmol) in 15 mL of DMF/THF (1:99) mixing solvent was slightly added into the mixture solution. The reaction was stirred overnight under nitrogen atmosphere. The solvent was removed by rotary evaporator to give a crude product. Then, the crude mixture was extracted with CH₂Cl₂/H₂O 3 times. The organic phase was collected and evaporated under vacuum providing the yellow solid (67% yield).

Characterization data for **AN**

¹H-NMR (400 MHz, *d*₆-DMSO): δ (in ppm) = 8.65 (d, *J* = 8.4 Hz, 1 H, ArH), 8.42 (d, *J* = 7.2 Hz, 1 H, ArH), 8.38 (s, 1 H, NH), 8.25 (d, *J* = 8.4 Hz, 1 H, ArH), 7.88 (s, 1 H, CONH), 7.71 (t, *J* = 8.0 Hz, 1 H, ArH), 7.56 (s, 1H, ArH), 7.47 (t, *J* = 3.6 Hz, 2 H, ArH), 7.42 (t, *J* = 7.2 Hz, 1 H, ArH), 7.28 (d, *J* = 6.8 Hz, 2 H, ArH), 7.07 (s, 1 H, ArH), 6.87 (d, *J* = 8.4 Hz, 1 H, ArH), 6.85 (s, 2 H, ArH), 4.67 (s, 2 H, CH₂), 3.48 (t, *J* = 2.6 Hz, 2 H, CH₂), 3.43 (t, *J* = 5.4 Hz, 2 H, CH₂)

¹³C-NMR (100 MHz, *d*₆-DMSO): δ (in ppm) = 167.55, 163.12, 150.65, 138.10, 136.50, 134.18, 130.81, 129.88, 129.18, 128.69, 128.06, 127.80, 124.40, 122.35, 120.41, 120.31, 103.77, 48.70, 42.36, 37.50

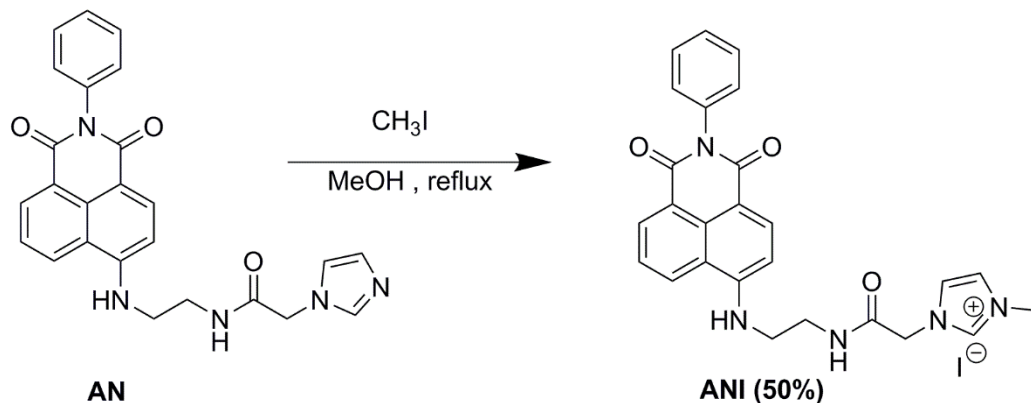
MALDI-TOF mass: Anal. calcd. For [C₂₅H₂₁N₅O₃]⁺ *m/z* = 439.16

Found *m/z* = 439.678

ESI-HRMS: Anal. Calcd for [C₂₅H₂₁N₅O₃+H]⁺ *m/z* = 440.18

Found *m/z* = 440.1364

3.2.2.5 Synthesis of 1-(2-((2-((1,3-dioxo-2-phenyl-2,3-dihydro-1H-benzo[de]isoquinolin-6-yl)amino)ethyl)amino)-2-oxoethyl)-3-methyl-1H-imidazol-3-ium (ANI)



AN (0.581 g, 1.0 mmol) was dissolved in methanol. Next, methyl iodide (0.1 mL, 1.60 mmol) was slightly added into the methanol solution and then refluxed overnight at 60°C under nitrogen atmosphere. The solution was evaporated by rotary evaporator to give a crude product. The crude product was washed with methanol 2-3 times. The orange powder was obtained (50% yield).

Characterization data for ANI

¹H-NMR (400 MHz, *d*₆-DMSO): δ (in ppm) = 9.05 (s, 1 H, ArH), 8.65 (d, *J* = 7.2 Hz, 1 H, ArH), 8.44 (d, *J* = 6.8 Hz, 1 H, ArH), 8.26 (d, *J* = 8.4 Hz, 1 H, ArH), 7.84 (s, 1 H, CONH), 7.72 (t, *J* = 8.0 Hz, 1 H, ArH), 7.68 (s, 1H, ArH), 7.65 (s, 1H, ArH), 7.48 (t, *J* = 3.6 Hz, 2 H, ArH), 7.41 (t, *J* = 7.2 Hz, 1 H, ArH), 7.28 (d, *J* = 6.8 Hz, 2 H, ArH), 6.87 (d, *J* = 8.4 Hz, 1 H, ArH), 4.98 (s, 1 H, CH₂), 3.87 (s, 3 H, CH₃), 3.49 (t, *J* = 5.2 Hz, 2 H, CH₂), 3.47 (t, *J* = 4.4 Hz, 2 H, CH₂)

¹³C-NMR (100 MHz, *d*₆-DMSO): δ (in ppm) = 166.22, 164.45, 163.63, 151.10, 138.19, 136.97, 134.71, 131.37, 130.38, 129.68, 129.23, 128.36, 124.96, 124.23, 123.71, 122.89, 120.84, 108.90, 104.28, 50.75, 42.75, 38.19, 36.34

MALDI-TOF mass: Anal. calcd. For [C₂₆H₂₃N₅O₃]⁺ *m/z* = 454.19

Found *m/z* = 453.742

ESI-HRMS: Anal. Calcd for [C₂₆H₂₄N₅O₃ + K]⁺ *m/z* = 620.06

Found *m/z* = 619.5627

3.3 Qualitative discrimination of biogenic amines by using sensor HB

3.3.1 Fluorescence studies of sensor HB and biogenic amines

3.3.1.1 Time effect for complexation studies of sensor HB and biogenic amines

Typically, the stock solution of sensor **HB** was prepared in a spectrophotometric grade DMSO at concentration of 1×10^{-3} M. Stock solution 1×10^{-2} M of biogenic amines (histamine and histidine) in 5×10^{-4} M phosphate buffer solution pH 7.4 was prepared in the volumetric flask.

Complexation between sensor **HB** and biogenic amines was prepared in 1-cm quartz cuvette by micropipette. The stock solution of sensor **HB** and biogenic amines was added 20 μ L and 10 μ L, respectively. The solution was stirred with vary time. After that, the solution was adjusted into 2 mL into 10% DMSO:phosphate buffer pH 7.4 condition. Fluorescence spectra were measured under the following condition:

Start: 330 nm

End: 700 nm

Excitation: 320 nm

Excitation slit: 5.0

Emission slit: 5.0

3.3.1.2 Concentration of biogenic amines effect for complexation study of sensor HB and biogenic amines

Typically, the stock solution of sensor **HB** was prepared in a spectrophotometric grade DMSO at concentration of 1×10^{-3} M. Stock solution of 1×10^{-2} M biogenic amines (histamine and histidine) in 5×10^{-4} M phosphate buffer solution pH 7.4 were prepared in the volumetric flask.

Complexation between sensor **HB** and biogenic amines were prepared in 1-cm quartz cuvette by micropipette. Firstly, the 20 μ L of **HB** stock solution was pipetted into the quartz cell. Next, the various concentration of histidine stock solution was

added into the quartz cell. The solution was stirred for 30 min. After that, the solution was adjusted to be 2 mL by 10% DMSO:phosphate buffer pH 7.4 condition. Fluorescence spectra were measured under the following condition:

Start: 330 nm

End: 700 nm

Excitation: 320 nm

Excitation slit: 5.0

Emission slit: 5.0

3.3.1.3 Kinetic study of sensor **HB** and biogenic amines

Typically, the stock solution of sensor **HB** was prepared in a spectrophotometric grade DMSO at concentration of 1×10^{-3} M. Stock solution of 1×10^{-2} M biogenic amines (histamine and histidine) in 5×10^{-4} M phosphate buffer solution pH 7.4 were prepared in the volumetric flask.

Complexation between sensor **HB** and biogenic amines was prepared in 1-cm quartz cuvette by micropipette. The stock solution of sensor **HB** and biogenic amines was added 20 μ L and 10 μ L into the cuvette, respectively. The solution was stirred with vary time. After that, the solution was adjusted into 2 mL into 10% DMSO:phosphate buffer pH 7.4 condition. Fluorescence spectra were measured under the following condition:

Start: 330 nm

End: 700 nm

Excitation: 320 nm

Excitation slit: 5.0

Emission slit: 5.0

3.3.1.4 Discrimination by using sensor ANI compound

The stock solution of sensors **HB** and **ANI** was prepared in a spectrophotometric grade DMSO at concentration of 1×10^{-3} M. Stock solution 1×10^{-2} M of biogenic amines (histamine and histidine) in 5×10^{-4} M phosphate buffer solution pH 7.4 was prepared in the volumetric flask.

Complexation between sensor **HB** and biogenic amines (histidine and histamine) was prepared in a 1-cm quartz cell. The 20 μ L of **HB** stock solution was pipetted into a cell. Next, the 10 μ L of biogenic amines stock solution was added by micropipette. The reaction was stirred for 30 min. After that, the various amount of **ANI** stock solution was added and the reaction was stirred for 5 min. Finally, the solution was adjusted to be 2 mL by 10% DMSO:phosphate buffer pH 7.4. Fluorescence spectra were measured under the following condition:

Start: 330 nm

End: 700 nm

Excitation: 320 nm

Excitation slit: 5.0

Emission slit: 5.0

On the other hand, the 20 μ L of **HB** stock solution was added into the 1-cm quartz cell. Next, the various amount **ANI** solution was added in the cuvette and the reaction was stirred for 5 min. Finally, the solution was adjusted to be 2 mL by 10% DMSO:phosphate buffer pH 7.4. Fluorescence spectra were measured under the previous condition.

3.3.1.5 Discrimination by using Cu^{2+} ion

The stock solution of sensor **HB** was prepared in a spectrophotometric grade DMSO at concentration of 1×10^{-3} M. Stock solution of 1×10^{-2} M biogenic amines (histamine and histidine) in 5×10^{-4} M phosphate buffer solution pH 7.4 was prepared

in the volumetric flask. The stock solution of Cu^{2+} ion was prepared in MilliQ water at concentration of 1×10^{-3} M.

Typically, the 20 μL of **HB** stock solution was pipetted into a 1-cm quartz cell. Next, the 10 μL of biogenic amines stock solution was added by micropipette. The reaction was stirred in 30 min. the 100 μL of Cu^{2+} ion stock solution was added into the cell. The reaction was stirred for 10 min. Finally, the solution was adjusted to be 2 mL by 10% DMSO:phosphate buffer pH 7.4. Fluorescence spectra were measured under the following condition:

Start: 330 nm

End: 700 nm

Excitation: 320 nm

Excitation slit: 5.0

Emission slit: 5.0

3.3.2 Complex simulation of sensor HB and histidine

The complex simulation between HD complex and Cu^{2+} ion was carried out by using density functional theory (DFT) calculation. Following computer simulation, we purposed two possible structures of Cu^{2+} complex via complexation energies ($\Delta E_{\text{complex}}$) calculation. The complexation energies ($\Delta E_{\text{complex}}$) are computed by equation 3.1

$$\Delta E_{\text{complex}} = E_{\text{complex}} - (nE_L + E_{\text{Cu}}) \quad 3.1$$

E_{complex} = total energies of complex

E_L = total energies of HD complex (L)

E_{Cu} = total energies of Cu^{2+} ion

n = number of ligand molecule (L) in $\text{CuL}_n^{(2-n)}$ complex of which the charge is (2-n).

3.3.3 Naked-eye fluorescence discrimination of sensor HB against biogenic amines

The stock solution of sensor **HB** was prepared in a spectrophotometric grade DMSO at concentration of 1×10^{-3} M. Stock solution of 1×10^{-2} M biogenic amines (histamine and histidine) in 5×10^{-4} M phosphate buffer solution pH 7.4 were prepared in the volumetric flask. The 1×10^{-3} M stock solution of Cu^{2+} ion was prepared in MilliQ water.

Typically, the 20 μL of **HB** stock solution was pipetted into a vial. Next, the 10 μL of biogenic amines stock solution was added by micropipette. The reaction was stirred in 30 min. the 100 μL of Cu^{2+} ion stock solution was added into the vial. The reaction was stirred for 10 min. Finally, the solution was adjusted to be 2 mL by 10% DMSO:phosphate buffer pH 7.4 condition. The solution was excited under UV lamp at 265 nm and taken a photo with Samsung Galaxy S5 smartphone.

3.4 Fluorescence studies of imidazole compound

3.4.1 Selectivity of sensor AN against various metal ions

The stock solution of **AN** was prepared in a spectrophotometric grade DMSO at concentration of 1×10^{-3} M. The 1×10^{-2} M stock solutions of metal ions including Cr^{3+} , Mn^{2+} , Co^{2+} , Ni^{2+} , Cu^{2+} , Zn^{2+} , Cd^{2+} , Ag^+ , and Au^{3+} were prepared in MilliQ water.

Typically, the 20 μL of **AN** stock solution was pipetted into a 1-cm quartz cell. Next, the 20 μL of various metal ion stock solution was added by micropipette. The reaction was stirred for 10 min. Finally, the solution was adjusted to be 2 mL by 10% DMSO:HEPES buffer pH 7.4 condition. Fluorescence spectra were measured under the following condition:

Start: 458 nm

End: 700 nm

Excitation: 448 nm

Excitation slit: 5.0

Emission slit: 5.0

Table 3.1 Amounts of guests used for studies of fluorescence spectrophotometry technique

Guests	Molecular weight (g/mol)	Weight (mg)	Volume (mL)
Cr ³⁺	400.15	8.00	2
Mn ²⁺	361.93	7.24	2
Co ²⁺	365.93	7.32	2
Ni ²⁺	290.79	5.82	2
Cu ²⁺	370.54	7.41	2
Zn ²⁺	372.38	7.45	2
Cd ²⁺	308.48	6.17	2
Ag ⁺	169.87	3.40	2
Au ³⁺	393.83	7.88	2

Table 3.2 Amounts of guests used for studies of fluorescence spectrophotometry technique

Guests	[Guest] (M)	Guest added (μ L)	Guest:AN ratio
Cr ³⁺	1×10^{-2}	20	10:1
Mn ²⁺	1×10^{-2}	20	10:1
Co ²⁺	1×10^{-2}	20	10:1
Ni ²⁺	1×10^{-2}	20	10:1
Cu ²⁺	1×10^{-2}	20	10:1
Zn ²⁺	1×10^{-2}	20	10:1
Cd ²⁺	1×10^{-2}	20	10:1
Ag ⁺	1×10^{-2}	20	10:1
Au ³⁺	1×10^{-2}	20	10:1

3.4.2 Job's plot analysis between sensor AN and Cu²⁺ ion

The stock solution of sensor **AN** was prepared in a spectrophotometric grade DMSO at concentration of 1×10^{-3} M. The 1×10^{-3} M stock solution of Cu²⁺ metal ions was prepared in MilliQ water.

Typically, the 20 μ L of **AN** stock solution was pipetted into a 1-cm quartz cell. Next, the various amounts of Cu²⁺ ion was added by micropipette depended on the mole fraction of Cu²⁺ ion. The reaction was stirred for 10 min. Finally, the solution was adjusted into 2 mL into 10% DMSO:HEPES buffer pH 7.4 condition. Fluorescence spectra were measured under the following condition:

Start: 458 nm

End: 700 nm

Excitation: 448 nm

Excitation slit: 5.0

Emission slit: 5.0

Table 3.3 Mole fraction and volume of sensor **AN** (1×10^{-5} M) and Cu²⁺ ion guest (1×10^{-5} M) for Job's plot experiment

Sample	Mole fraction of sensor AN	Mole fraction of guest	V of sensor AN (mL)	V of guest (mL)
1	1.0	0.0	2.00	0.00
2	0.9	0.1	1.80	0.20
3	0.8	0.2	1.60	0.40
4	0.7	0.3	1.40	0.60
5	0.6	0.4	1.20	0.80
6	0.5	0.5	1.00	1.00
7	0.4	0.6	0.80	1.20
8	0.3	0.7	0.60	1.40
9	0.2	0.8	0.40	1.60
10	0.1	0.9	0.20	1.80
11	0.0	1.0	0.00	2.00

3.4.3 Binding constant determination of sensor AN and Cu²⁺ ion

The stock solution of sensor **AN** was prepared in a spectrophotometric grade DMSO at concentration of 1×10^{-3} M. The 1×10^{-3} M stock solution of Cu²⁺ metal ions was prepared in MilliQ water.

Typically, the 20 μ L of **AN** stock solution was pipetted into a 1-cm quartz cell and the solution was adjusted to be 2 mL by 10% DMSO:HEPES buffer pH 7.4 condition. Next, the various amounts of Cu²⁺ ion was added by micropipette from 0 – 3.5 equivalent into the quartz cell and the mixed solution was stirred for 10 min. Fluorescence spectra were measured under the following condition:

Start: 458 nm

End: 700 nm

Excitation: 448 nm

Excitation slit: 5.0

Emission slit: 5.0

Table 3.4 The concentration of Cu²⁺ used for complexation studies with sensor **AN** and the ratio of **AN**:Cu²⁺

Entry	Cu ²⁺ /AN	[AN] (M)	[Cu ²⁺] (M)	V of Cu ²⁺ (mL)	V total (mL)
1	0	1.0×10^{-5}	0	0	2
2	0.1	9.99×10^{-6}	9.99×10^{-7}	0.002	2.002
3	0.2	9.98×10^{-6}	2.0×10^{-6}	0.004	2.004
4	0.3	9.97×10^{-6}	2.99×10^{-6}	0.006	2.006
5	0.4	9.96×10^{-6}	3.98×10^{-6}	0.008	2.008
6	0.5	9.95×10^{-6}	4.98×10^{-6}	0.01	2.01
7	0.6	9.94×10^{-6}	5.96×10^{-6}	0.012	2.012
8	0.7	9.93×10^{-6}	6.95×10^{-6}	0.014	2.014
9	0.8	9.92×10^{-6}	7.94×10^{-6}	0.016	2.016
10	0.9	9.91×10^{-6}	8.92×10^{-6}	0.018	2.018

Entry	Cu ²⁺ /AN	[AN] (M)	[Cu ²⁺] (M)	V of Cu ²⁺ (mL)	V total (mL)
11	1	9.9×10 ⁻⁶	9.9×10 ⁻⁶	0.02	2.02
12	1.1	9.89×10 ⁻⁶	1.09×10 ⁻⁵	0.022	2.022
13	1.2	9.88×10 ⁻⁶	1.19×10 ⁻⁵	0.024	2.024
14	1.3	9.87×10 ⁻⁶	1.28×10 ⁻⁵	0.026	2.026
15	1.4	9.86×10 ⁻⁶	1.38×10 ⁻⁵	0.028	2.028
16	1.5	9.85×10 ⁻⁶	1.48×10 ⁻⁵	0.03	2.03
17	1.6	9.84×10 ⁻⁶	1.57×10 ⁻⁵	0.032	2.032
18	1.7	9.83×10 ⁻⁶	1.67×10 ⁻⁵	0.034	2.034
19	1.8	9.82×10 ⁻⁶	1.77×10 ⁻⁵	0.036	2.036
20	1.9	9.81×10 ⁻⁶	1.86×10 ⁻⁵	0.038	2.038
21	2	9.8×10 ⁻⁶	1.96×10 ⁻⁵	0.04	2.04
22	2.1	9.79×10 ⁻⁶	2.06×10 ⁻⁵	0.042	2.042
23	2.2	9.78×10 ⁻⁶	2.15×10 ⁻⁵	0.044	2.044
24	2.3	9.78×10 ⁻⁶	2.25×10 ⁻⁵	0.046	2.046
25	2.4	9.77×10 ⁻⁶	2.34×10 ⁻⁵	0.048	2.048
26	2.5	9.76×10 ⁻⁶	2.44×10 ⁻⁵	0.05	2.05
27	2.6	9.75×10 ⁻⁶	2.53×10 ⁻⁵	0.052	2.052
28	2.7	9.74×10 ⁻⁶	2.63×10 ⁻⁵	0.054	2.054
29	2.8	9.73×10 ⁻⁶	2.72×10 ⁻⁵	0.056	2.056
30	2.9	9.72×10 ⁻⁶	2.82×10 ⁻⁵	0.058	2.058
31	3.0	9.71×10 ⁻⁶	2.91×10 ⁻⁵	0.06	2.06
32	3.1	9.7×10 ⁻⁶	3.01×10 ⁻⁵	0.062	2.062
33	3.2	9.69×10 ⁻⁶	3.1×10 ⁻⁵	0.064	2.064
34	3.3	9.68×10 ⁻⁶	3.19×10 ⁻⁵	0.066	2.066
35	3.4	9.67×10 ⁻⁶	3.29×10 ⁻⁵	0.068	2.068
36	3.5	9.66×10 ⁻⁶	3.38×10 ⁻⁵	0.07	2.07

3.5 Fluorescence studies of imidazolium compound

3.5.1 Selectivity of sensor ANI against various amino acids

The stock solution of sensor **ANI** was prepared in a spectrophotometric grade DMSO at concentration of 1×10^{-3} M. 1×10^{-2} M stock solutions of various amino acids including Phe, His, Leu, Gly, Lys, Glu, Ala, Cys, Met and Thr in 5×10^{-4} M phosphate buffer solution pH 7.4 were prepared in the volumetric flask.

Typically, the 20 μ L of **ANI** stock solution was pipetted into a 1-cm quartz cell. Next, the 20 μ L of various amino acids stock solution were added by micropipette. The reaction was stirred for 10 min. Finally, the solution was adjusted to be 2 mL by 10% DMSO:phosphate buffer pH 7.4 condition. Fluorescence spectra were measured under the following condition:

Start: 458 nm

End: 700 nm

Excitation: 448 nm

Excitation slit: 5.0

Emission slit: 5.0

Table 3.5 Amounts of guests used for studies of fluorescence spectrophotometry

Guests	Molecular weight (g/mol)	Weight (mg)	Volume (mL)
Phe	165.19	3.30	2
His	155.16	3.10	2
Leu	131.17	2.62	2
Gly	75.067	1.50	2
Lys	149.19	2.98	2
Glu	147.13	2.94	2
Ala	89.09	1.78	2
Cys	121.16	2.42	2
Met	149.21	2.98	2
Thr	119.12	2.38	2

Table 3.6 Amounts of guests used for studies of fluorescence spectrophotometry

Guests	[Guest] (M)	Guest added (μ L)	Guest:ANI ratios
Phe	1×10^{-2}	20	10:1
His	1×10^{-2}	20	10:1
Leu	1×10^{-2}	20	10:1
Gly	1×10^{-2}	20	10:1
Lys	1×10^{-2}	20	10:1
Glu	1×10^{-2}	20	10:1
Ala	1×10^{-2}	20	10:1
Cys	1×10^{-2}	20	10:1
Met	1×10^{-2}	20	10:1
Thr	1×10^{-2}	20	10:1

3.5.2 Selectivity of sensor ANI against various nucleotides

The stock solution of sensor **ANI** was prepared in a spectrophotometric grade DMSO at concentration of 1×10^{-3} M. 1×10^{-2} M stock solutions of various nucleotides including UMP, UDP, UTP, AMP, ADP, ATP, GMP, GDP and CMP in 5×10^{-4} M HEPES buffer solution pH 7.4 were prepared in the volumetric flask.

Typically, the 20 μ L of **ANI** stock solution was pipetted into a 1-cm quartz cell. Next, the 20 μ L of various nucleotides stock solution was added by micropipette. The reaction was stirred for 10 min. Finally, the solution was adjusted to be 2 mL by 10% DMSO:HEPES buffer pH 7.4 condition. Fluorescence spectra were measured under the following condition:

Start: 458 nm

End: 700 nm

Excitation: 448 nm

Excitation slit: 5.0

Emission slit: 5.0

Table 3.7 Amounts of guests used for studies of fluorescence spectrophotometry

Guests	Molecular weight (g/mol)	Weight (mg)	Volume (mL)
UMP	368.15	7.36	2
UDP	448.12	8.96	2
UTP	586.12	11.72	2
AMP	365.24	7.30	2
ADP	449.2	8.98	2
ATP	551.1	11.02	2
GMP	407.19	8.14	2
GDP	443.2	8.86	2
CMP	367.16	7.34	2

Table 3.8 Amounts of guests used for studies of fluorescence spectrophotometry

Guests	[Guest] (M)	Guest added (μ L)	Guest: ANI ratios
UMP	1×10^{-2}	20	10:1
UDP	1×10^{-2}	20	10:1
UTP	1×10^{-2}	20	10:1
AMP	1×10^{-2}	20	10:1
ADP	1×10^{-2}	20	10:1
ATP	1×10^{-2}	20	10:1
GMP	1×10^{-2}	20	10:1
GDP	1×10^{-2}	20	10:1
CMP	1×10^{-2}	20	10:1

3.5.3 Selectivity of sensor ANI against various anions

The stock solution of sensor **ANI** was prepared in a spectrophotometric grade DMSO at concentration of 1×10^{-3} M. 1×10^{-2} M stock solutions of various anions including F^- , Cl^- , Br^- , I^- , CN^- , OH^- , PO_4^{3-} , AcO^- and BzO^- in a spectrophotometric grade DMSO were prepared in the volumetric flask.

Typically, the 20 μ L of **ANI** stock solution was pipetted into a 1-cm quartz cell. Next, the 20 μ L of various anions in stock solution were added by micropipette. The reaction was stirred for 5 min. Finally, the solution was adjusted to be 2 mL by DMSO. Fluorescence spectra were measured under the following condition:

Start: 458 nm

End: 700 nm

Excitation: 448 nm

Excitation slit: 5.0

Emission slit: 5.0

Table 3.9 Amounts of guests used for studies of fluorescence spectrophotometry

Guests	Molecular weight (g/mol)	Weight (mg)	Volume (mL)
F^-	315.51	6.31	2
Cl^-	227.92	4.56	2
Br^-	546.8	10.94	2
I^-	369.37	7.39	2
CN^-	156.27	3.12	2
OH^-	259.479	5.19	2
PO_4^{3-}	339.49	6.79	2
AcO^-	301.51	6.03	2
BzO^-	363.58	7.27	2

Table 3.10 Amounts of guests used for studies of fluorescence spectrophotometry

Guests	[Guest] (M)	Guest added (μL)	Guest:ANI ratios
F ⁻	1×10^{-2}	20	10:1
Cl ⁻	1×10^{-2}	20	10:1
Br ⁻	1×10^{-2}	20	10:1
I ⁻	1×10^{-2}	20	10:1
CN ⁻	1×10^{-2}	20	10:1
OH ⁻	1×10^{-2}	20	10:1
PO ₄ ³⁻	1×10^{-2}	20	10:1
AcO ⁻	1×10^{-2}	20	10:1
BzO ⁻	1×10^{-2}	20	10:1

3.5.4 Job's plot analysis between sensor ANI and F⁻ ion

The stock solution of sensor ANI was prepared in a spectrophotometric grade DMSO at concentration of 1×10^{-3} M. The 1×10^{-2} M stock solution of F⁻ anion was prepared in a spectrophotometric grade DMSO.

Typically, the 20 μL of ANI stock solution was pipetted into a 1-cm quartz cell. Next, the various amounts of F⁻ stock solution were added by micropipette regarding to the mole fraction of F⁻ ion. The reaction was stirred for 5 min. Finally, the solution was adjusted to be 2 mL by DMSO. Fluorescence spectra were measured under the following condition:

Start: 458 nm

End: 700 nm

Excitation: 448 nm

Excitation slit: 5.0

Emission slit: 5.0

Table 3.11 Mole fraction and volume of sensor **ANI** (1×10^{-5} M) and F^- anion guest (1×10^{-5} M) for Job's plot experiment

Samples	Mole fraction of sensor ANI	Mole fraction of guest	V of sensor ANI (mL)	V of guest (mL)
1	1.0	0.0	2.00	0.00
2	0.9	0.1	1.80	0.20
3	0.8	0.2	1.60	0.40
4	0.7	0.3	1.40	0.60
5	0.6	0.4	1.20	0.80
6	0.5	0.5	1.00	1.00
7	0.4	0.6	0.80	1.20
8	0.3	0.7	0.60	1.40
9	0.2	0.8	0.40	1.60
10	0.1	0.9	0.20	1.80
11	0.0	1.0	0.00	2.00

3.5.5 Binding constant studies of sensor ANI and F^- ion

The stock solution of sensor **ANI** was prepared in a spectrophotometric grade DMSO at concentration of 1×10^{-3} M. The stock solution of F^- anions was prepared in a spectrophotometric grade DMSO at concentration of 1×10^{-1} M in volumetric flask.

Typically, the 20 μ L of **ANI** stock solution was pipetted into a 1-cm quartz cell and the solution was adjusted to be 2 mL by 100% DMSO. Next, the various amount of F^- stock solution was added by micropipette from 0 – 1000 equivalent into the quartz cell and the mixed solution was stirred for 5 min. Fluorescence spectra were measured under the following condition:

Start: 458 nm

End: 700 nm

Excitation: 448 nm

Excitation slit: 5.0

Emission slit: 5.0

Table 3.12 The concentration of F^- used for complexation studies with sensor **ANI** and the ratio of **ANI**: F^-

Entry	F^-/ANI	[ANI] (M)	[F^-] (M)	V of F^- (mL)	V total (mL)
1	0	1×10^{-5}	0	0	2
2	10	9.99×10^{-6}	9.99×10^{-5}	0.002	2.002
3	20	9.98×10^{-6}	2.00×10^{-4}	0.004	2.004
4	30	9.97×10^{-6}	2.99×10^{-4}	0.006	2.006
5	50	9.95×10^{-6}	4.98×10^{-4}	0.01	2.01
6	100	9.9×10^{-6}	9.90×10^{-4}	0.02	2.02
7	250	9.76×10^{-6}	2.44×10^{-3}	0.05	2.05
8	500	9.52×10^{-6}	4.76×10^{-3}	0.1	2.1
9	750	9.3×10^{-6}	6.98×10^{-3}	0.15	2.15
10	1000	9.09×10^{-6}	9.09×10^{-3}	0.2	2.2
11	1500	8.7×10^{-6}	1.30×10^{-2}	0.3	2.3
12	2000	8.33×10^{-6}	1.67×10^{-2}	0.4	2.4
13	3000	7.69×10^{-6}	2.31×10^{-2}	0.6	2.6
14	4000	7.14×10^{-6}	2.86×10^{-2}	0.8	2.8
15	5000	6.67×10^{-6}	3.33×10^{-2}	1	3
16	6000	6.25×10^{-6}	3.75×10^{-2}	1.2	3.2
17	7000	5.88×10^{-6}	4.12×10^{-2}	1.4	3.4
18	8000	5.56×10^{-6}	4.44×10^{-2}	1.6	3.6
19	9000	5.26×10^{-6}	4.74×10^{-2}	1.8	3.8

3.5.6 LOD/LOQ determination of sensor ANI

The stock solution of sensor **ANI** was prepared in a spectrophotometric grade DMSO at concentration of 1×10^{-3} M. The stock solution of F^- anions was prepared in a spectrophotometric grade DMSO at concentration of 1×10^{-2} M in volumetric flask.

Typically, the 20 μ L of **ANI** stock solution was pipetted into a 1-cm quartz cell and the solution was adjusted to be 2 mL by 100% DMSO. This solution was set as a

blank solution with fluorescence measurement which was repeated 10 times. Next, the various amount of F^- stock solution was added into the cell and the mixed solution was stirred for 5min. Fluorescence spectra were measured under the following condition:

Start: 458 nm

End: 700 nm

Excitation: 448 nm

Excitation slit: 5.0

Emission slit: 5.0

3.6 NMR titration of sensor ANI against F^- ion

The stock solution of sensor **ANI** was prepared in a d_6 -DMSO at concentration of 1×10^{-2} M. The stock solution of F^- anions was prepared in a d_6 -DMSO at concentration of 2.5 M in volumetric flask.

The 0.01 M **ANI** solution was added in NMR tube and measured by the NMR technique. Next, the various amounts of F^- stock solution was added into the NMR tube by micro syringe from 0 - 4 equivalent and NMR spectra were collected after each of addition of F^- anion.

3.7 Naked-eye detection

3.7.1 Colorimetric detection of sensor ANI against various anions

The stock solution of **ANI** was prepared in a spectrophotometric grade DMSO at concentration of 1×10^{-3} M. Stock solutions of 1×10^{-2} M various anions including F^- , Cl^- , Br^- , I^- , CN^- , OH^- , PO_4^{3-} , AcO^- and BzO^- in a spectrophotometric grade DMSO were prepared in the volumetric flask.

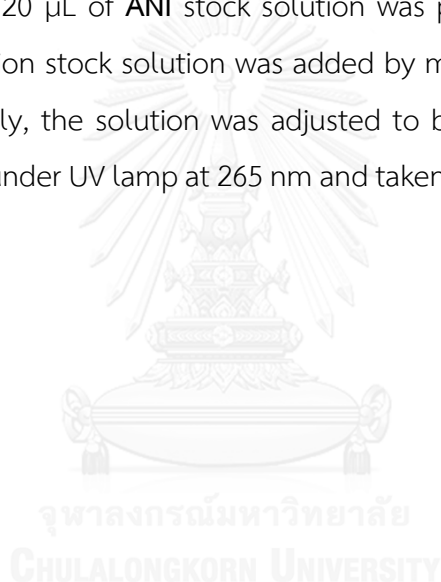
Typically, the 20 μ L of **ANI** stock solution was pipetted into a vial. Next, the various amount of anion stock solution was added by micropipette. The solution was

stirred in 5 min. Finally, the solution was adjusted to be 2 mL by 100% DMSO. The solution was taken a photo with Nikon D550 camera.

3.7.2 Fluorometric detection of sensor ANI against various anions

The stock solution of sensor **ANI** was prepared in a spectrophotometric grade DMSO at concentration of 1×10^{-3} M. Stock solutions of 1×10^{-2} M of anions including F^- , Cl^- , Br^- , I^- , CN^- , OH^- , PO_4^{3-} , AcO^- and BzO^- in a spectrophotometric grade DMSO were prepared in the volumetric flask.

Typically, the 20 μ L of **ANI** stock solution was pipetted into a vial. Next, the various amount of anion stock solution was added by micropipette. The solution was stirred in 5 min. Finally, the solution was adjusted to be 2 mL by 100% DMSO. The solution was excited under UV lamp at 265 nm and taken a photo with Samsung Galaxy S5 smartphone.



CHAPTER IV

RESULTS AND DISCUSSION

4.1 Conceptual design

4.1.1 Discrimination of biogenic amines by using FRET mechanism

This research has focused on the discrimination of biogenic amines because they can be used as the indication for the biological symptoms such as Parkinson's disease and allergy. Unfortunately, most biogenic amines have a similar core structure containing catechol, indole and histamine groups. Therefore, the discrimination of the same core structure of biogenic amines is challenging. Most of reports demonstrated the histamine-based detection by using displacement of metal complex [34, 35]. Interesting work of Kielland reported the fluorescence chemosensor for detection of histamine group. They were the pioneer to prepare Histamine blue (HB) containing mesoionic acid which is capable of specific reaction with amine moiety in the histamine base as shown in Figure 4.1 [39]. However, sensor HB cannot discriminate histamine group including histidine and histamine due to the similar fluorescence responses as shown in Figure 4.2.

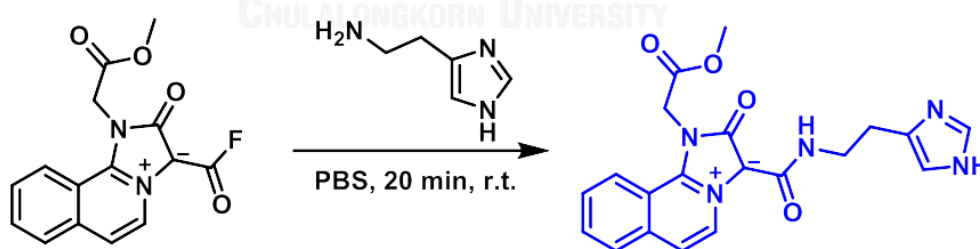


Figure 4.1 Reaction of histamine blue (HB) with histamine compound [39]

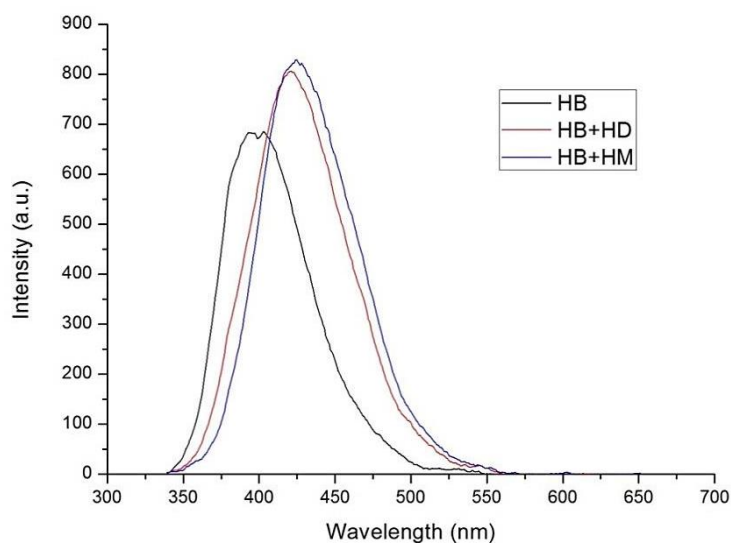


Figure 4.2 The fluorescence spectra of sensor **HB** (10 μM) in 10% DMSO:phosphate buffer (5×10^{-4} M, pH 7.4) against histidine (HD) and histamine (HM) $\lambda_{\text{ex}} = 320$ nm

Our research has focused on design and development of molecular sensors for detection of biogenic amines in pseudo biological system. Molecular sensors were designed and synthesized for sensitive and selective discrimination between histidine and histamine via fluorescence resonance energy transfer (FRET) process. Considerably, the difference between histamine and histidine structure is the carboxylic functional group on the side chain. Thus, the second fluorescence sensor has been designed for carboxylic acid binding site. Our concept is to discriminate the biogenic amines including histamine and histidine via FRET process by using two fluorescence sensors. As anticipated, the complete complexation of both fluorescence sensors and the proper analyte gives the shift of the fluorescence spectra due to energy transfers from donor to acceptor fluorophore. This phenomenon is called FRET mechanism as shown in Figure 4.3.

From this approach, we designed and synthesized sensor **ANI** which is composed of the imidazolium moiety for binding with carboxylate group in histidine base by hydrogen bonding interaction. Therefore, we proposed to discriminate histidine and histamine by using two fluorescence sensors including sensors histamine blue (**HB**) and **ANI**.

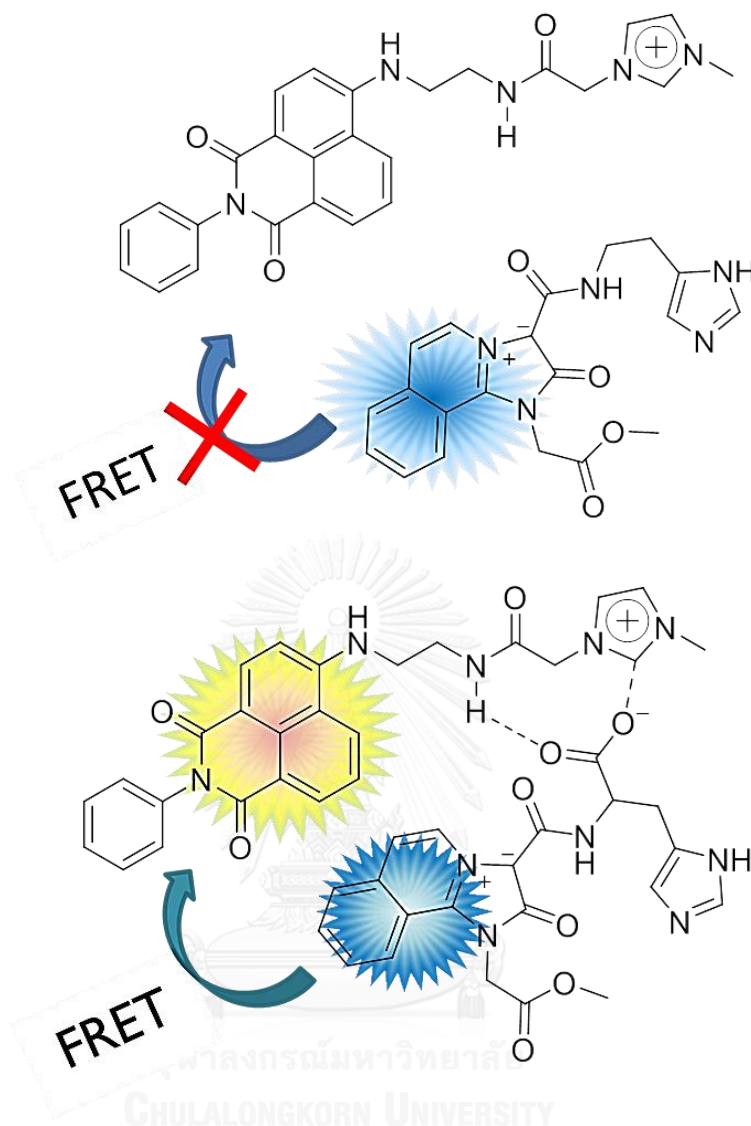


Figure 4.3 The conceptual mechanism for sensors **HB** and **ANI** for **HM** (top) and **HD** (bottom) discrimination

4.1.2 Discrimination of biogenic amines by metal ion via PET process

According to the Kielland's work, sensor **HB** was used to discriminate histamine from the other biogenic amines by fluorescence technique [39]. However, sensor **HB** cannot discriminate the imidazole based biogenic amines of histidine and histamine because the imidazole group is a self-catalyst for covalent bonding with sensor **HB** as shown in the Figure 4.4.

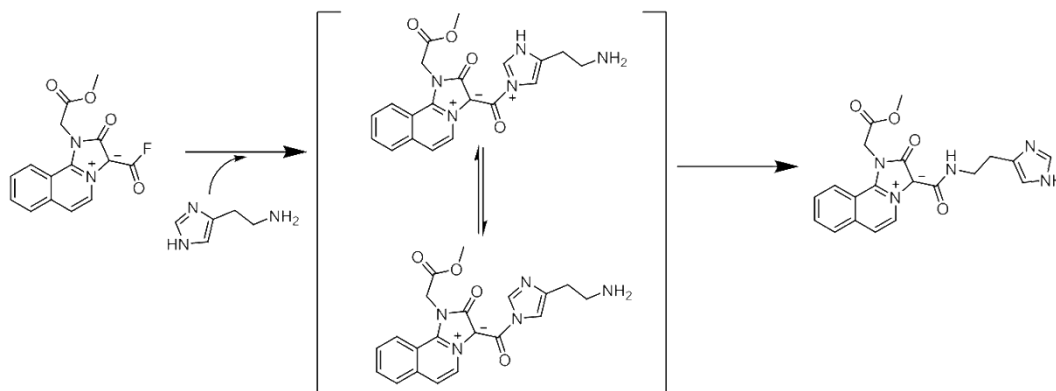


Figure 4.4 The mechanism of **HB** complex with HM [39]

Based on the different binding affinity of metal complex, most of researches utilized the various metal ions for the discrimination of biogenic amines compounds [34, 35]. Many biogenic amines are composed of amino groups which bound with metal ions. Meanwhile, the binding affinity of the metal ion depended on the number of the coordinating group. In 2010, Seto *et al.* reported that the histamine enabled to remove Cu^{2+} and Ni^{2+} ions from the metal-Nile red dye complexes [34]. The results showed that histamine bound to metal ions with 3:1 stoichiometric ratio of histamine and metal ions resulting in the recovery of fluorescence signal belonging to free Nile red dye.

Herein, we designed the concept of biogenic amines discrimination by using sensor **HB** and Cu^{2+} ion. Following to the **HB** complex with HD and HM which are assigned as **HB**⊂HD and **HD**⊂HM, respectively, both of them have the same fluorescence response because of the similarity of the core structure. However, the difference of two complex structures is only carboxylic acid group of **HB**⊂HD. We expected that the remaining carboxylate and imidazole groups of **HB**⊂HD enabled to give a different binding affinity with transition metal resulting in the discriminated detection of HM and HD. Firstly, the complexation between sensor **HB** and HD or HM was performed resulting in the strong fluorescent responses. After that, the use of metal ion possibly induced the discrimination of these complexes because the **HB**⊂HD prefers to bind with metal ion by the imidazole and carboxylic groups but the **HB**⊂HM cannot bind with metal ion due to the insufficient binding site as shown in Figure 4.5.

Therefore, we attempted to use the combination of sensor **HB** and Cu^{2+} ion for discrimination of histidine and histamine.

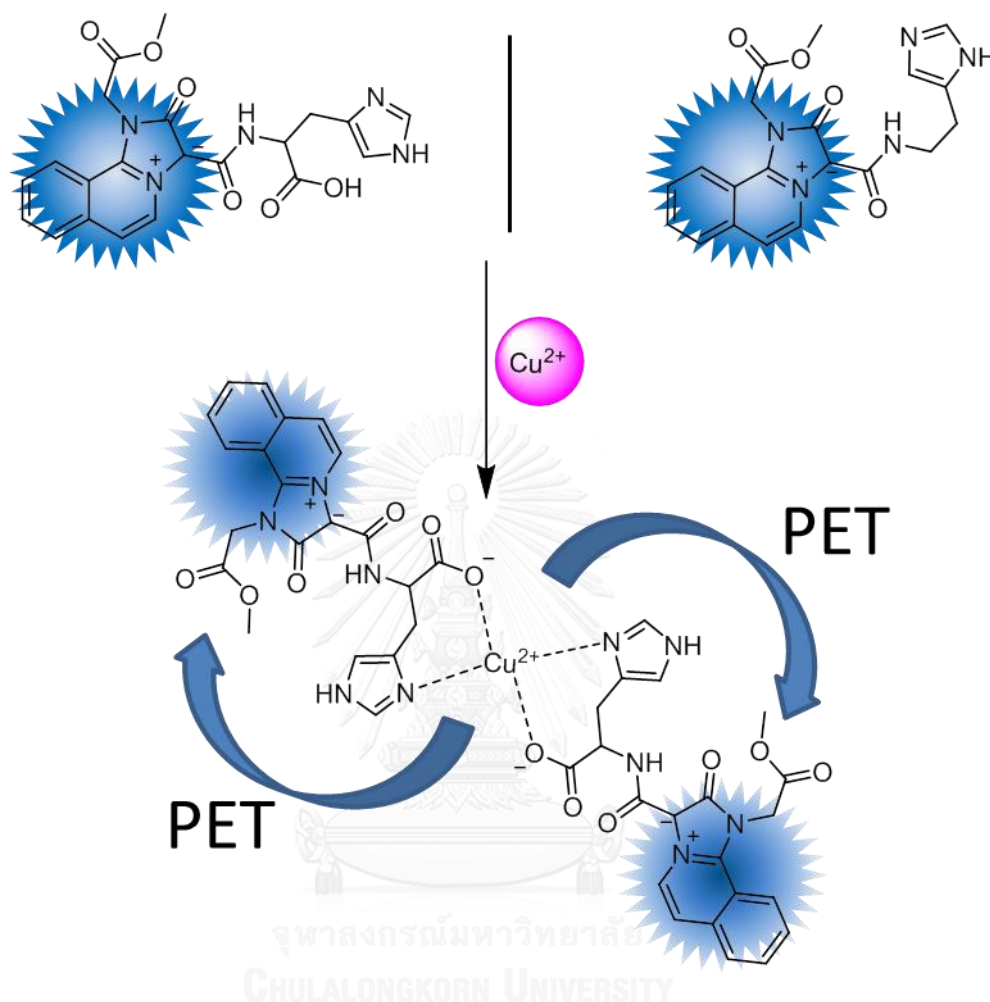


Figure 4.5 The conceptual design of discrimination mechanism of HD (left) and HM (right) by using the combination of sensor **HB** and Cu^{2+} ion

4.2 Synthesis

4.2.1 Synthesis and characterization of histamine blue (HB)

Sensor **HB** was synthesized following by multicomponent reaction [40]. Firstly, methyl isocyanoacetate was obtained by trifluoroacetic anhydride (TFAA) to form an intermediate species as shown in Figure 4.7. After that, isoquinoline attacked the intermediate by using a lone pair electron of the nitrogen. Next, sensor **HB** was formed by heteroaromatic cyclization and the brown solid was obtained in 10% yield.

The $^1\text{H-NMR}$ spectrum showed two singlet characteristic peaks of methylene and methyl groups at 5.31 and 3.80 ppm defined as b and a in the spectrum of Figure 4.6, which supported the structure of sensor **HB**.

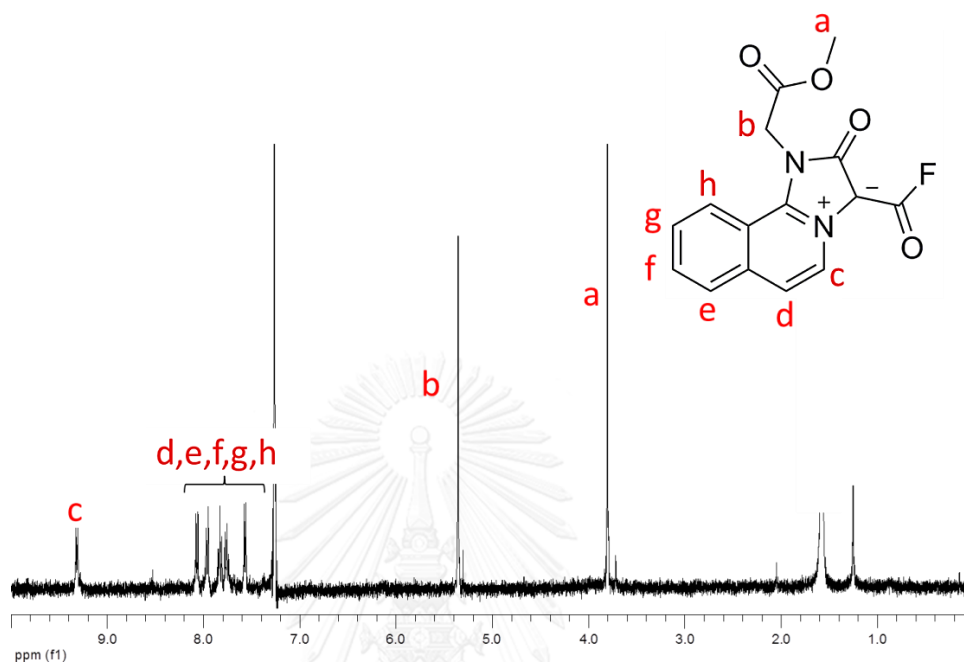


Figure 4.6 The $^1\text{H-NMR}$ spectrum of sensor **HB** in CDCl_3 at 400 MHz

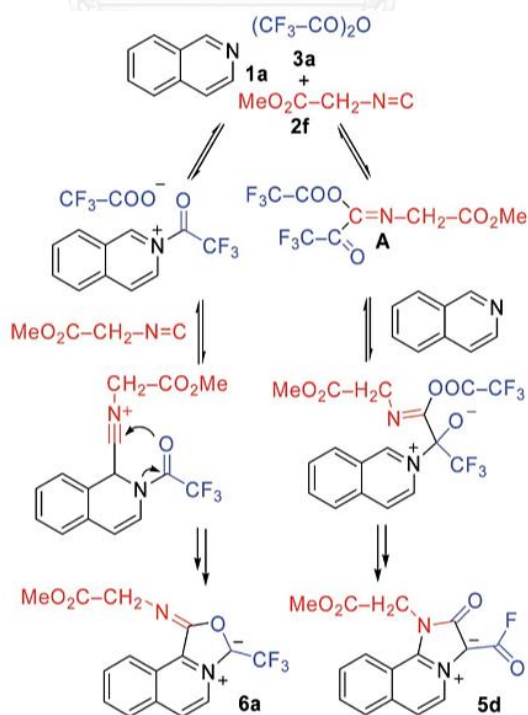


Figure 4.7 The competitive reaction pathway of sensor **HB** (5d) and **6a** [40]

4.2.2 Synthesis and characterization of 6-Bromo-2-phenyl-1H-benzo[de]isoquinoline-1,3(2H)-dione (1)

The compound **1** was synthesized by amide condensation reaction between 4-bromo-1,8-naphthalic anhydride and primary amine of aniline. In this reaction, pyridine was used as catalyst for acid amide prevention. Moreover, the reaction must be heated for dehydration to give the white solid of compound **1** in 95% yield. $^1\text{H-NMR}$ spectrum showed the characteristic peaks in the aromatic region around 7.00 – 9.00 ppm. Signals in the range 7.20 – 7.50 ppm are assigned as aromatic protons of aniline ring and those in the range 8.00 – 8.60 ppm are assigned as aromatic protons of naphthalimide ring.

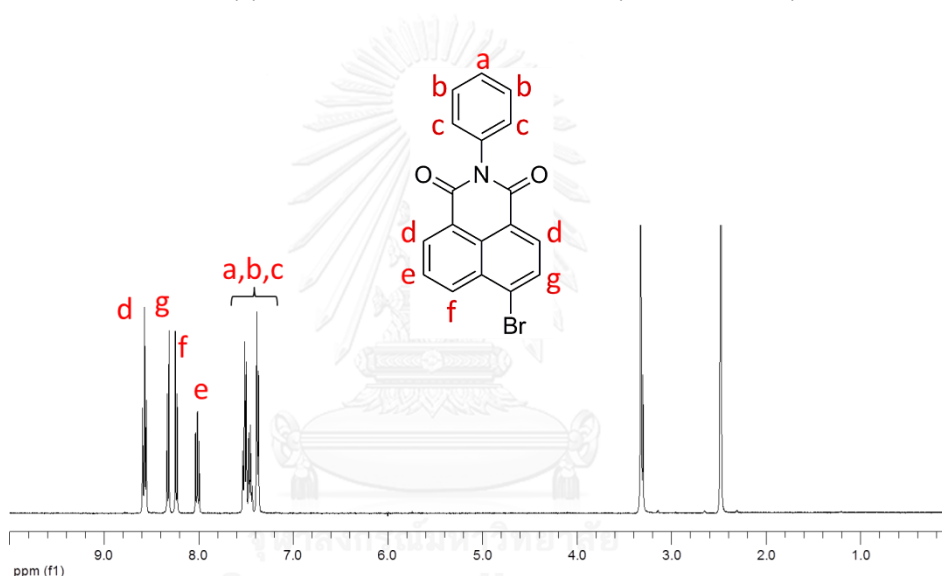


Figure 4.8 The $^1\text{H-NMR}$ spectrum of compound **1** in d_6 -DMSO at 400 MHz

4.2.3 Synthesis and characterization of 6-((2-Aminoethyl)amino)-2-phenyl-1H-benzo[de]isoquinoline-1,3(2H)-dione (2)

The compound **2** was synthesized using nucleophilic aromatic substitution reaction [47]. Ethylenediamine acts as a nucleophile species due to a lone pair electron of nitrogen atom. Especially, ethylene glycol monomethyl ether (EGME) as a magical solvent in strong condition was used in this reaction. The yellow solid was obtained in 30% yield. $^1\text{H-NMR}$ spectrum showed the upfield shift of naphthalimide proton from 8.57 to 7.28 ppm due to the donating group of amine moiety. Moreover, the ethylene protons were observed at 3.14 and 2.86 ppm which confirmed the structure of compound **2**.

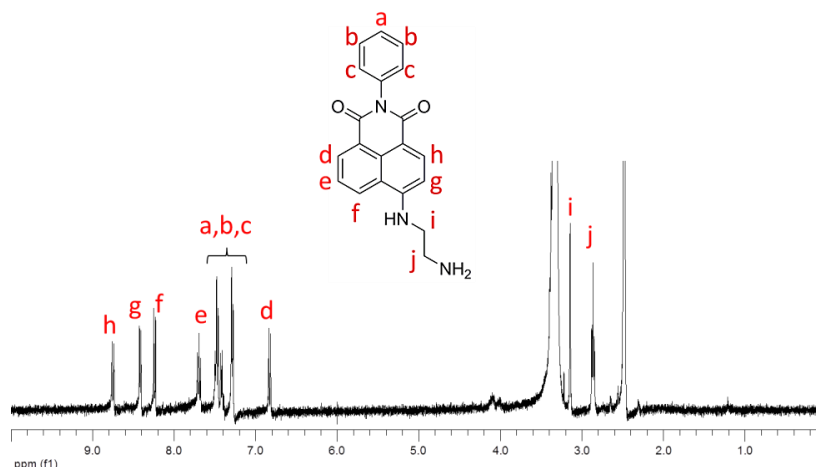


Figure 4.9 The $^1\text{H-NMR}$ spectrum of compound **2** in d_6 -DMSO at 400 MHz

4.2.4 Synthesis and characterization of 2-Chloro-N-(2-((1,3-dioxo-2-phenyl-2,3-dihydro-1H-benzo[de]isoquinolin-6-yl)amino)ethyl)acetamide (**3**)

The compound **3** was synthesized by amide condensation reaction [48]. Chloroacetyl chloride is a strong coupling reagent. Therefore, the reaction was cooled down to reduce the acidic gases. The orange powder of compound **3** was obtained in 50% yield. $^1\text{H-NMR}$ spectrum showed the characteristic peaks of amide proton and aliphatic proton at 7.80 ppm and 4.10 ppm, respectively. Moreover, aliphatic protons showed downfield shift from the amide functional group effect. These assignments supported the structure of compound **3**.

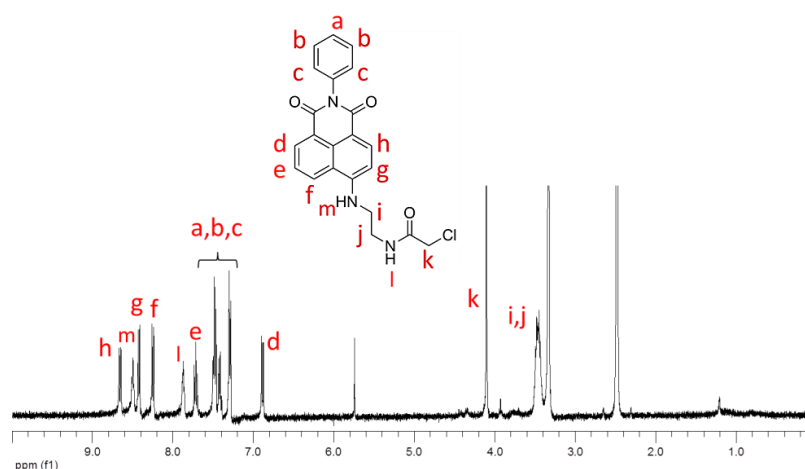


Figure 4.10 The $^1\text{H-NMR}$ spectrum of compound **3** in d_6 -DMSO at 400 MHz

4.2.5 Synthesis and characterization of N-(2-((1,3-dioxo-2-phenyl-2,3-dihydro-1H-benzo[de]isoquinolin-6-yl)amino)ethyl)-2-(1H-imidazol-1-yl)acetamide (AN)

The sensor **AN** was synthesized by nucleophilic substitution [49]. Firstly, imidazole was activated by NaH to deprotonate the hydrogen from N-H based imidazole ring. Imidazole anion acts as nucleophile to substitute chloride ion. The yellow solid of sensor **AN** was obtained in 67% yield. $^1\text{H-NMR}$ spectrum showed the new peaks of imidazole moiety in the range of aromatic proton and the downfield shift of H_k was obtained by the effect of electron withdrawing group of nitrogen based imidazole.

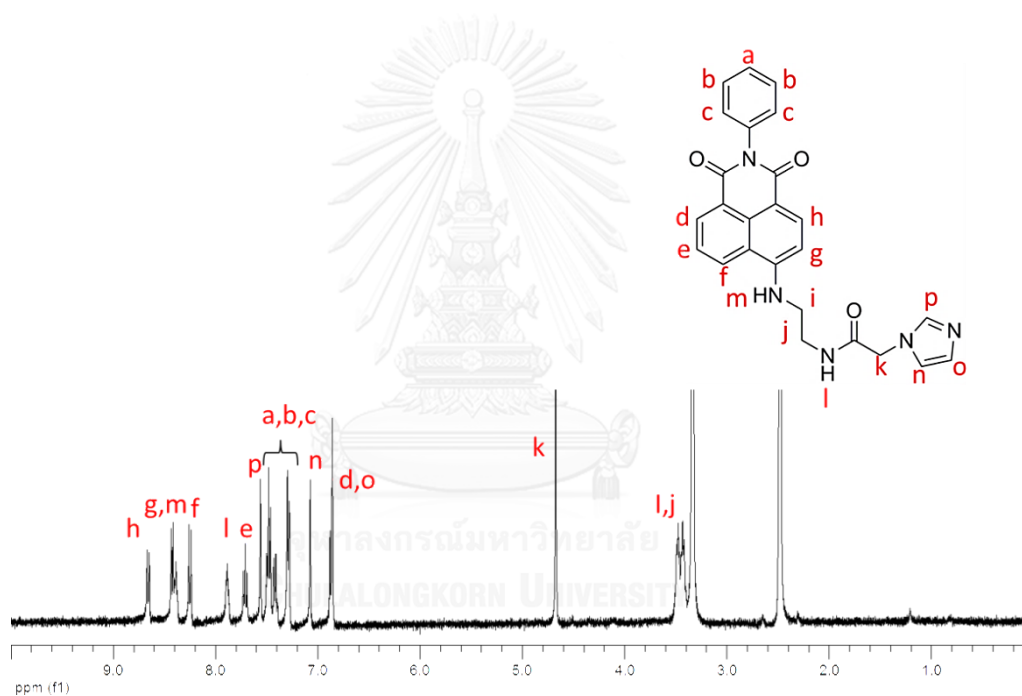


Figure 4.11 The $^1\text{H-NMR}$ spectrum of sensor **AN** in d_6 -DMSO at 400 MHz

4.2.6 Synthesis and characterization of 1-(2-((2-((1,3-dioxo-2-phenyl-2,3-dihydro-1H-benzo[de]isoquinolin-6-yl)amino)ethyl)amino)-2-oxoethyl)-3-methyl-1H-imidazol-3-ium (ANI)

The sensor **ANI** was synthesized by the methylation of methyl iodide [50]. The nitrogen atom based imidazole unit acts as nucleophile and reacts with iodide position to yield the imidazolium compound. The red solid of product was obtained in 60%

yield. $^1\text{H-NMR}$ spectrum showed the downfield shift of the acidic proton at C2 position from 7.56 to 9.00 ppm.

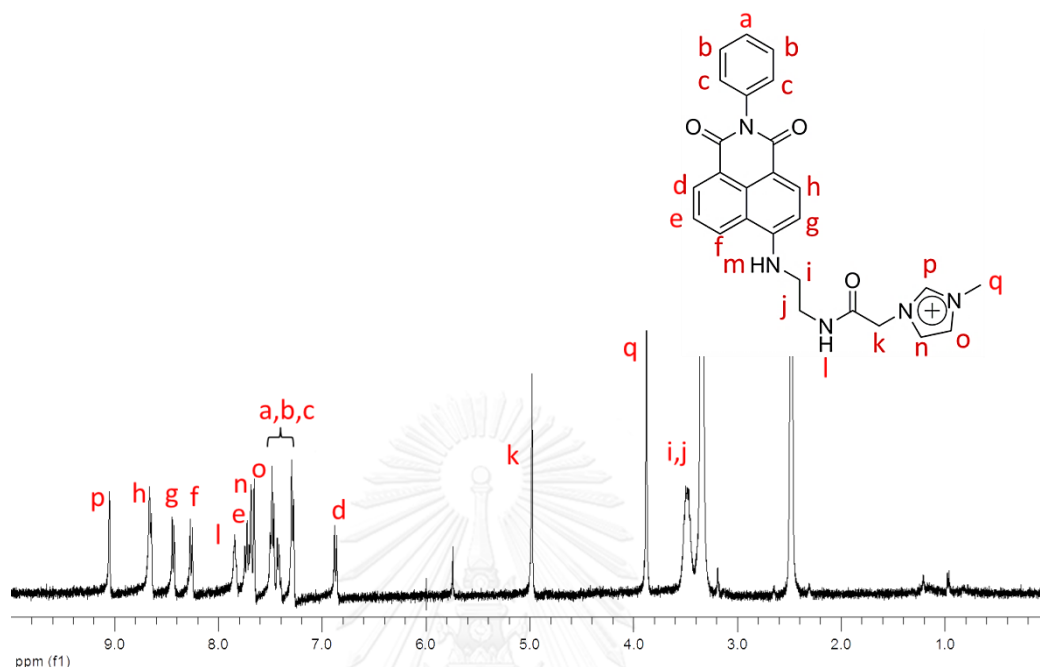


Figure 4.12 The $^1\text{H-NMR}$ spectrum of sensor ANI in d_6 -DMSO at 400 MHz

4.3 Qualitative discrimination of biogenic amines by using sensor HB

4.3.1 Complexation studies of sensor HB and biogenic amines

The formation of sensor **HB** and histamine and histidine is carried out in the 5×10^{-4} M phosphate buffer solution at pH 7.4. Upon the excitation at 320 nm, the complexation of sensor **HB** and HM or HD showed the red shift of emission band from 393 nm to 420 nm corresponding to the emission band of free **HB** and its complex, respectively. To optimize the time of complexation in 10% DMSO:phosphate buffer (5×10^{-4} M, pH 7.4), the fluorescence responses of sensor **HB** in the presence of excess histidine were measured under varying time. It was found that the reaction time over 20 min affected slightly on the fluorescent responses. However, the reaction time of 30 min gave a higher fluorescent intensity. This suggested that the reaction time of 30 min is proper for the formation of sensor **HB** and HD as shown in the Figure 4.13. As a previous report by Kielland, sensor **HB** was highly selective with histidine and histamine

due to the imidazole moiety. They claimed that the imidazole group would activate the stable intermediate which was replaced by aliphatic amine to form the stable product as shown in Figure 4.4 [39].

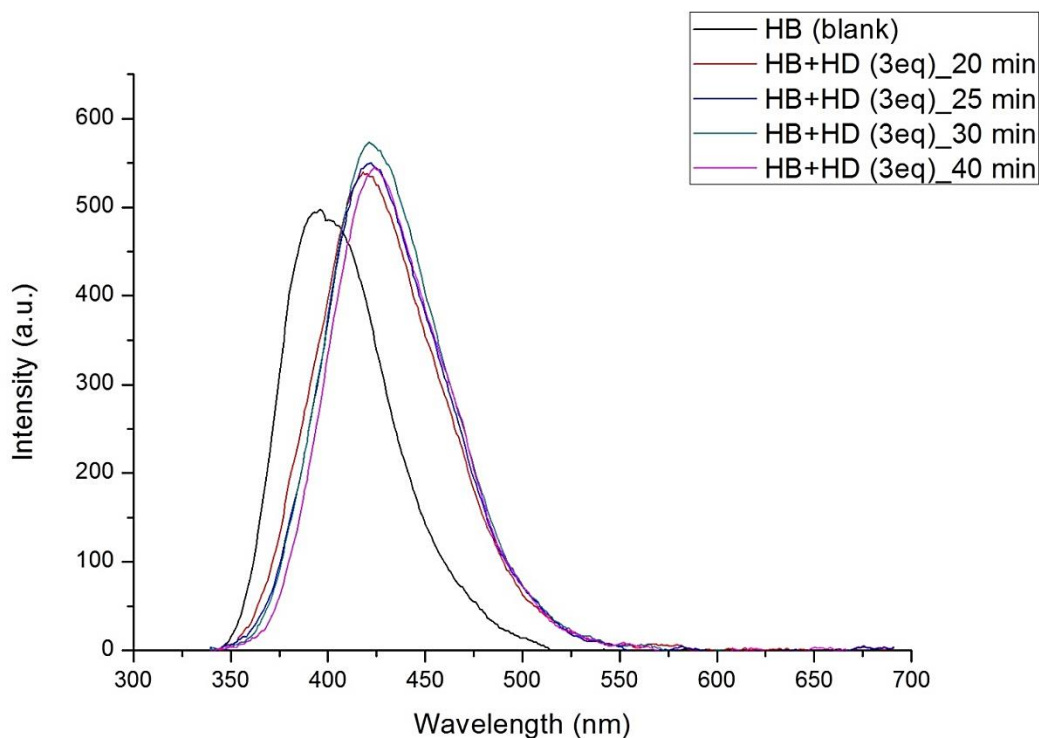


Figure 4.13 The fluorescence spectra of sensor **HB** (1×10^{-5} M) and the **HB** complex with excess HD in 10% DMSO:phosphate buffer (5×10^{-4} M, pH 7.4) with vary time ($\lambda_{\text{ex}} = 320$ nm)

To verify the concentration of HD to react with sensor **HB**, the fluorescence responses of sensor **HB** upon the increment of HD were investigated in Figure 4.14. The emission bands of sensor **HB** in the presence of HD were gradually red-shifted at 420 nm with a concomitant of fluorescence enhancement. However, the highest fluorescence intensity of sensor **HB** was observed at the concentration of 5×10^{-5} M HD. Thus, it is indicative of the optimum concentration of HD at 5 equiv of sensor **HB** for the complete complexation of **HB**⊂HD.

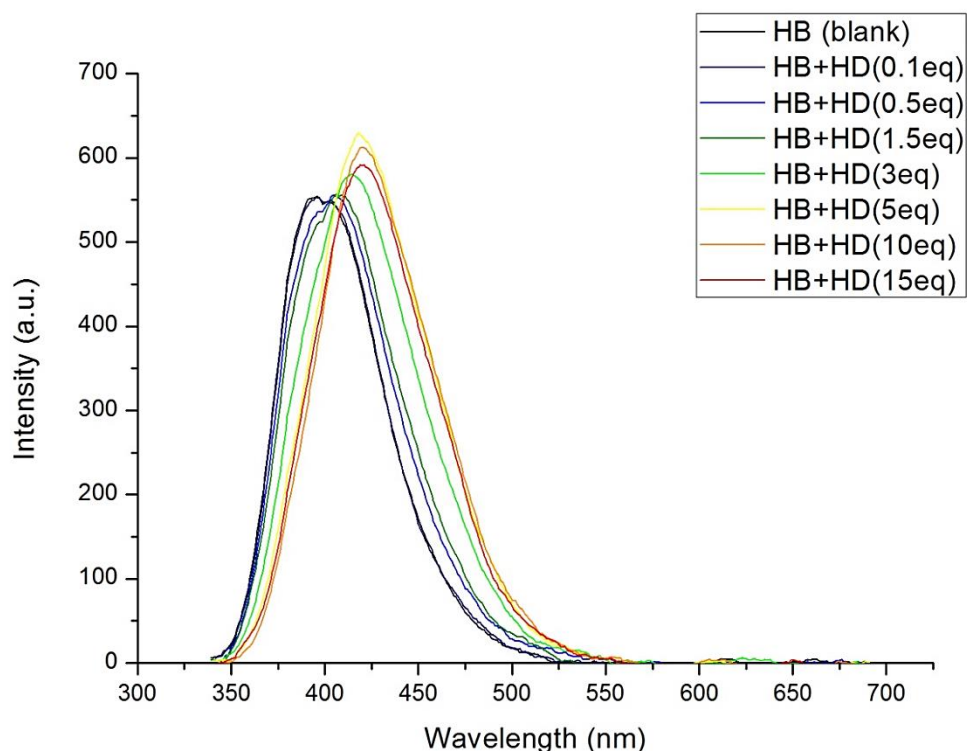


Figure 4.14 The fluorescence spectra of sensor **HB** (1×10^{-5} M) in 10% DMSO:phosphate buffer (5×10^{-4} M, pH 7.4) with varying amount of HD ($\lambda_{\text{ex}} = 320$ nm)

4.3.2 Kinetic study of sensor **HB** and biogenic amines

The kinetic study of biogenic amines was investigated by fluorescence technique. Upon the excitation at 320 nm, the emission bands at 390 nm and 420 nm were assigned as I_0 and I , respectively. The normalized fluorescence intensities (I/I_0) of **HB** and **HB** were plotted against time as shown in Figure 4.15. The I/I_0 values of **HB** were constant after the reaction time of 15-20 min while those of **HB** were constant after reaction time of 10 min. This revealed that the complete reaction of sensor **HB** and HM was faster than that of sensor **HB** and HD.

According to the complexation between sensor **HB** and histidine or histamine, the complexation mechanism of sensor **HB** involved with the imidazole and aliphatic amine groups of biogenic amines as shown in Figure 4.4. However, the formation of histidine complex was slower than histamine complex possibly caused by the steric hindrance of carboxylic group toward the primary amine for the complexed formation.

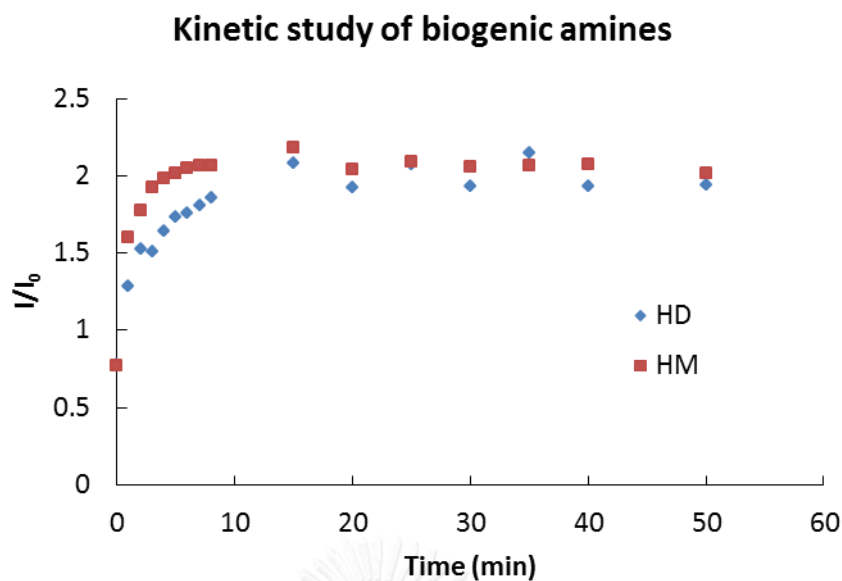


Figure 4.15 The kinetic profiles of complexation of sensor **HB** (1×10^{-5} M) and HD or HM in 10% DMSO:phosphate buffer (5×10^{-4} M, pH 7.4) with varying time ($\lambda_{\text{ex}} = 320$ nm)

4.3.3 Discrimination of biogenic amines by using imidazolium sensor

Considerably, the different structure of complexes **HB**⊂**HD** and **HB**⊂**HM** is the additional carboxylic group as shown in Figure 4.17. Sensor **ANI** composed of imidazolium moiety, was designed for binding with carboxylic group on the side chain of the histidine base. In our expectation, the binding between **HB**⊂**HD** and sensor **ANI** by hydrogen bonding and electrostatic interactions will establish the FRET-on emission band. This approach will not be occurred in the case of Histamine complex. This result might give a benefit of a specific detection of histidine. To study the complexation affinity of **HB**⊂**HD** and sensor **ANI**, upon adding various amount of sensor **ANI** into the **HB**⊂**HD** solution, the emission bands at 425 nm were gradually decreased with the concomitant increasing of emission bands at 550 nm corresponding to emission band of sensor **ANI** as shown in Figure 4.16.

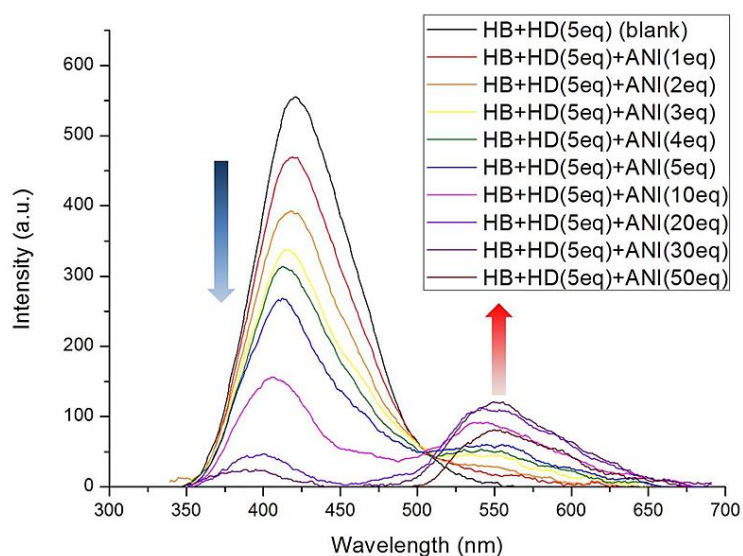


Figure 4.16 The fluorescence spectra of **HB**+**HD** complex (1×10^{-5} M) in 10% DMSO:phosphate buffer (5×10^{-4} M, pH 7.4) with varying amount of sensor **ANI** ($\lambda_{\text{ex}} = 320$ nm)

To confirm that the emission band at 550 nm was occurred by the energy transfer from the complex of **HB**+**HD** to sensor **ANI**, the fluorescence responses of sensor **HB** with varying amount of sensor **ANI** were examined. Figure 4.19 showed the fluorescence quenching at 425 nm of sensor **HB** and the fluorescence enhancement at 550 nm of sensor **ANI**. This revealed that sensor **ANI** is the competitive fluorophore of sensor **HB**. Since, the absorption band of sensor **ANI** is very broad, thus, it would overlap with the absorption band of sensor **HB** as shown in Figure 4.18. This is rationalization that the fluorescence spectra of sensor **ANI** at 550 nm were gradually increased upon the increment of sensor **ANI**. Therefore, the discrimination of HD and HM from this concept is unsuccessful.

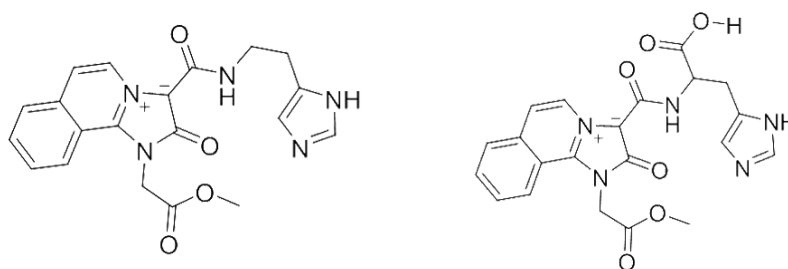


Figure 4.17 The structure of **HB**+**HM** (left) and **HB**+**HD** (right)

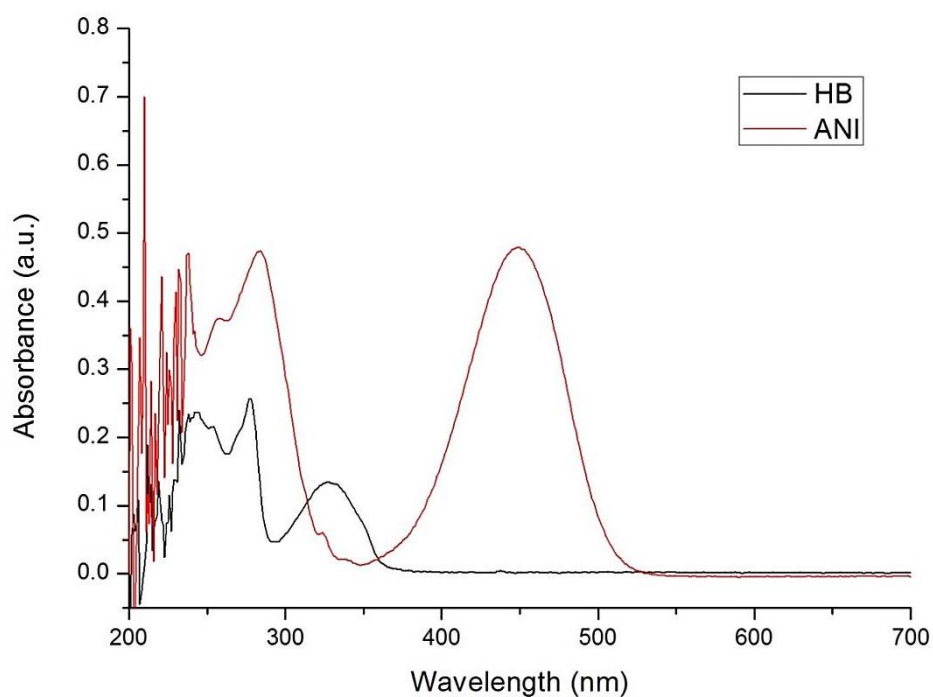


Figure 4.18 The UV-visible spectra of sensors **HB** and **ANI** (1×10^{-5} M) in 10% DMSO:phosphate buffer (5×10^{-4} M, pH 7.4)

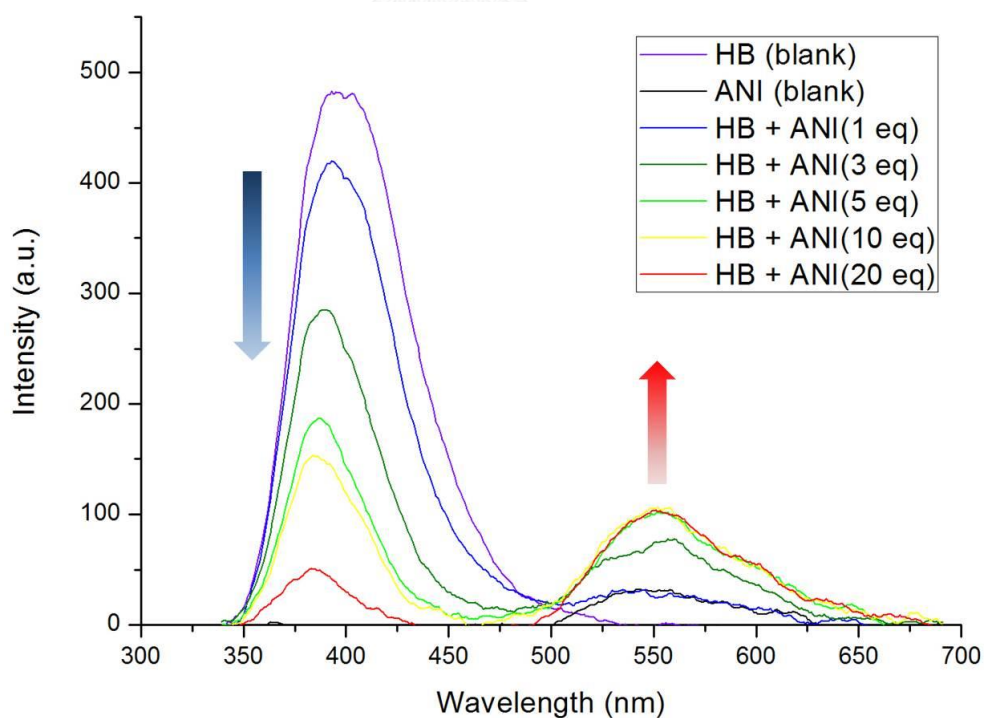


Figure 4.19 The fluorescence spectra of sensor **HB** (1×10^{-5} M) in 10% DMSO:phosphate buffer (5×10^{-4} M, pH 7.4) with varying amount of sensor **ANI** ($\lambda_{\text{ex}} = 320$ nm)

4.3.4 Discrimination of biogenic amines by using sensor HB with Cu²⁺ ion

In our further attempt, we designed the discrimination system by displacement of HB-metal complex by histidine and histamine. Firstly, the selectivity of sensor HB against various metal ions was investigated. The fluorescence spectra of sensor HB with various metal ions (5 equiv) displayed a very slight change as shown in Figure 4.20. We hypothesized that sensor HB did not contain the metal ion binding site.

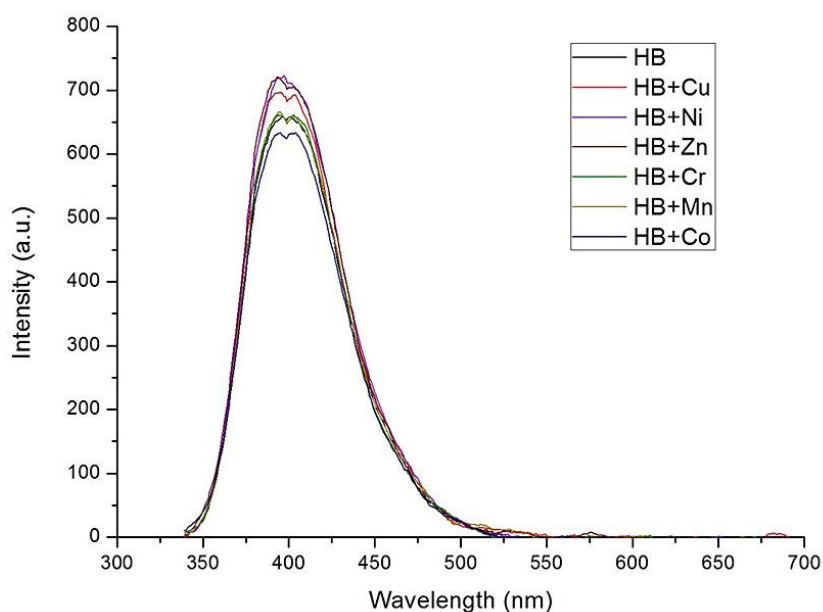


Figure 4.20 The fluorescence spectra of sensor HB (1×10^{-5} M) in 10% DMSO:phosphate buffer (5×10^{-4} M, pH 7.4) with various metals ($\lambda_{\text{ex}} = 320$ nm)

Furthermore, the complex of sensor HB and HD or HM was firstly prepared because we proposed that the carboxylic acid and imidazole group of complex HB-HD might form with metal cation and a consequent fluorescence change would be observed. Interestingly, the emission band at 425 nm of HB-HD complex showed a large quenching upon the addition of Cu²⁺ ion while that of HB-HM complex remained unchanged with various metal ions as shown in Figure 4.21 and 4.22, respectively. This phenomenon can be explained that the HB-HD complex preferred to strongly coordinate with the Cu²⁺ ion by using carboxylic acid and imidazole groups. Otherwise, HB-HM complex consisted of only one binding site of imidazole unit.

Thus, it did not show the fluorescent change in the presence of Cu^{2+} . Moreover, Cu^{2+} ion would quench the fluorescence signal by photoinduced electron transfer (PET) process due to d^9 transition metal effect. This aspect offers the effectively preliminary discrimination of histidine and histamine.

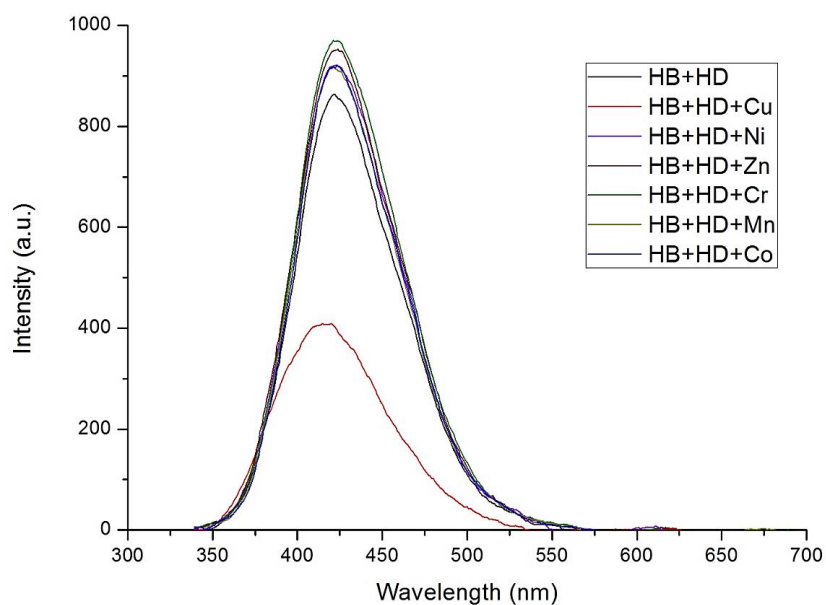


Figure 4.21 The fluorescence spectra of $\text{HB} \subset \text{HD}$ complex (1×10^{-5} M) in 10% DMSO:phosphate buffer (5×10^{-4} M, pH 7.4) with various metal cations ($\lambda_{\text{ex}} = 320$ nm)

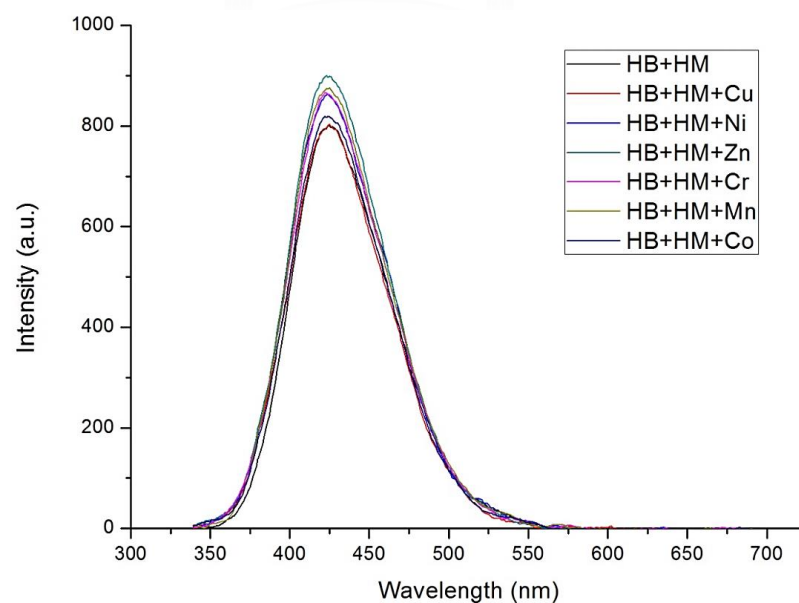


Figure 4.22 The fluorescence spectra of $\text{HB} \subset \text{HM}$ complex (1×10^{-5} M) in 10% DMSO:phosphate buffer (5×10^{-4} M, pH 7.4) with various metal cations ($\lambda_{\text{ex}} = 320$ nm)

Moreover, the binding mode of the complex of **HBC**HD and Cu^{2+} was studied by computational simulation as shown in Figure 4.23.

According to Figure 4.23 and Table 4.1, the **CuL₂** has two conformations including **CuL₂(1)** and **CuL₂(2)**, respectively. **CuL₂(1)** has a distorted tetrahedral geometry between Cu^{2+} ion and two ligands as shown in Figure 4.23a. Moreover, both of them are oriented in the same direction which is called *cis*-conformation. **CuL₂(1)** has C_2 point group and $\Delta E_{\text{complex}}$ is -270.18 kcal/mol. On the other hand, **CuL₂(2)** also has a distorted tetrahedral geometry between Cu^{2+} ion and two ligands as shown in Figure 4.23b. In addition, the direction of two ligands is orthogonal together which is called *ortho*-conformation. **CuL₂(2)** has C_1 point group and $\Delta E_{\text{complex}}$ is -267.96 kcal/mol. Considerably, the $\Delta E_{\text{complex}}$ of **CuL₂(1)** is slightly lower than **CuL₂(2)** because of hydrogen bonding between carboxylate group and the proton of C2 of imidazole moiety. However, the $\Delta E_{\text{complex}}$ of two conformations are not quite different. Therefore, both of them are the possible conformation of **HBC**HD complex.

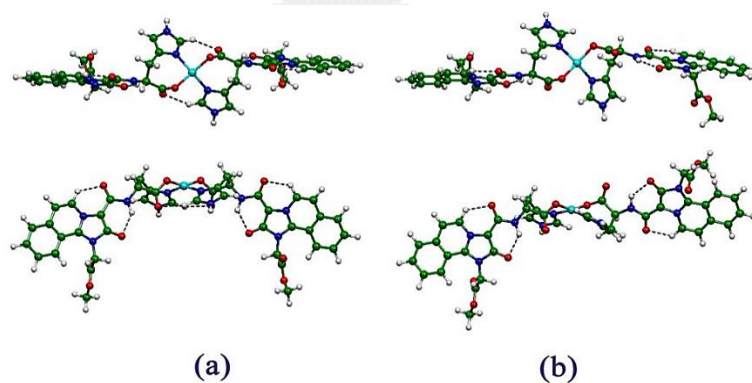


Figure 4.23 The CPCM(DMSO)/CAMB3LYP/6-31G(d,p) optimized structures of (a) **CuL₂(1)** and (b) **CuL₂(2)** isomers. Top and bottom are top and side views of molecules, respectively

Table 4.1 Complexation energies for copper complexes with ligand (L) and relative energies for **CuL₂(1)** and **CuL₂(2)** isomers

Complex/isomers	ΔE_{rel}^a	Structural type	Point group	$\Delta E_{\text{complex}}^a$
1:2 species:				
CuL₂(1)	0.00	Distorted tetrahedral	C ₂	-270.18
CuL₂(2)	2.22	Distorted tetrahedral	C ₁	-267.96

^a In kcal/mol.

As a result of the fluorescence quenching regarding to the preliminary results, only **HB**CHD enabled to bind with Cu²⁺ ion. To prove the discrimination of biogenic amines, the mixture solution of HD and HM was measured by fluorescence technique. It was found that the fluorescent quenching was observed in the system containing HD and Cu²⁺ ion. In contrast, the mixture of HD, HM and Cu²⁺ ion cannot affect the fluorescence change because the competitive reaction between sensor **HB** with HD and HM in the solution was occurred. Regarding to the kinetic studies of sensor **HB** and HD and HM, the HM gave faster reaction time to form **HB**CHM than HD did. We proposed that the dominant **HB**CHM complex was found in the solution. Hence, the fluorescence responses of sensor **HB** in the presence of the mixture HD and HM and Cu²⁺ performed an analog response with the system of **HB**CHM complex.

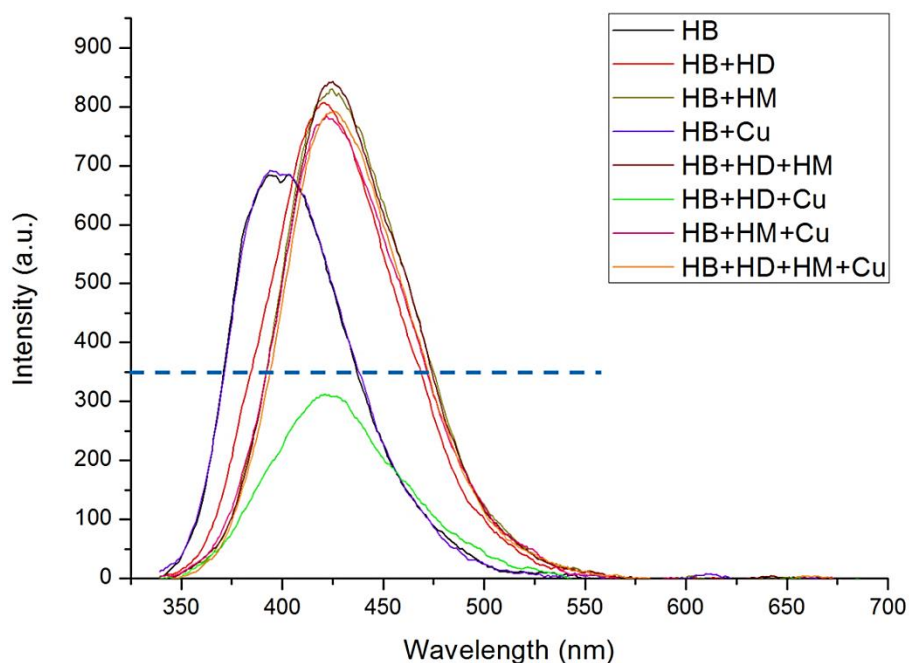
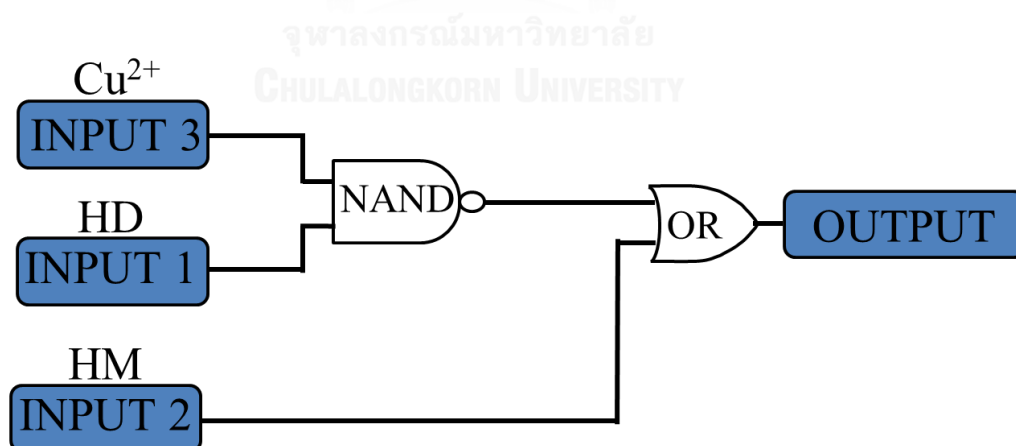


Figure 4.24 The fluorescence spectra of HB (1×10^{-5} M) complexes with 5 equiv HD, 5 equiv HM and 5 equiv Cu^{2+} ion in 10% DMSO:phosphate buffer (5×10^{-4} M, pH 7.4, $\lambda_{\text{ex}} = 320$ nm)

In addition, we applied the fluorescence responses into the logic gates system. In the solution system, the addition of HD, HM and Cu^{2+} ion would effect on the fluorescence responses. We assigned each guest as input 1, input 2 and input 3, respectively. The fluorescence response at 421 nm was assigned as output 1. The combination of dual gates including NAND and OR gates was used to read outputs. We designed the schematic system of logic gates as shown in Scheme 4.1. Following the fluorescence spectra, the intensity threshold of logic gates system was selected at 350 a.u. assigned as blue dot line. Moreover, the fluorescence intensities were defined regarding to above and below the threshold as 1 and 0, respectively. The truth table was created regarding to the fluorescence responses upon adding the stimuli of guest. According to fluorescence response as output upon the stimuli of guest, the construction of logic gate included the NAND and OR which were assigned as a following; (i) NAND designed as the combination of input 1 (HD) and input 3 (Cu^{2+}) which indicated the selectivity of Cu^{2+} ion and $\text{HB} \rightleftharpoons \text{HD}$ complex, (ii) OR designed as

the presence of input 2 (HM) combined with the result of which dominated the influence of HM against the fluorescence response. The results showed that the output 1 has to relate to the combination of NAND and OR gates for analysis of all inputs. According to the truth table in Table 4.2, the first row, no input of any guest causes the appearance of emission band at 421 nm of free sensor **HB**. For the second row, the presence of Cu^{2+} ion in the system causes the appearance of emission band of sensor **HB**. Both cases showed output = 1 because the system has the free sensor **HB** which displays the emission band over the limited threshold of intensity at 350 a.u. On the fifth row, input only HD causes a strong emission band at 421 nm due to the emission of **HB**⊂HD complex. Considering at the sixth row, the combination of HD and Cu^{2+} ion from input 1 and input 3 in the system causes the quenching of the emission band at 421 nm because Cu^{2+} ion was bound with **HB**⊂HD complex. All of the remaining rows, the solution contained HM which effected to the strong fluorescent intensity at 421 nm. Thus, output showed “1” due to the dominant **HB**⊂HM complex in the solution. Interestingly, the logic gate system showed output of “0” upon the input of HD and Cu^{2+} in the sensor **HB** solution. This result corresponds to the fluorescence quenching of the spectrum as mentioned above.



Scheme 4.1 Schematic logic gate system for the complexes of sensor **HB** with HD, HM, Cu^{2+} ion including Input 1 (HD), Input 2 (HM), Input 3 (Cu^{2+}) and Output ($\lambda = 421 \text{ nm}$)

Table 4.2 The logic gates truth table for Output ($\lambda = 421 \text{ nm}$)


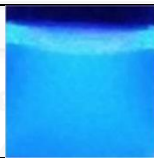
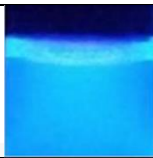
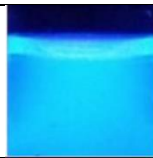



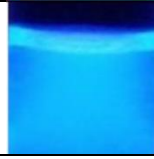
Input 1 (HD)	Input 2 (HM)	Input 3 (Cu ²⁺)	NAND Input 1+3	OR Input 2 + NAND	Output (421 nm)
0	0	0	1	1	1
0	0	1	1	1	1
0	1	0	1	1	1
0	1	1	1	1	1
1	0	0	1	1	1
1	0	1	0	0	0
1	1	0	1	1	1
1	1	1	0	1	1



4.3.1.5 Naked-eye fluorescence discrimination of sensor **HB** against biogenic amines

The naked-eye detection is a promising technique for detecting the highly selective fluorescence sensors by visual change. The fluorescence response of **HB** complexes has a different aspect with sensor **HB**. **HB** complexes give the light blue fluorescence. On the other hand, sensor **HB** gives the dark blue fluorescence in the presence or absence of Cu^{2+} ion in the solution. In addition, the blue brightness of fluorescence in the case of **HB**–HD complex was decreased slightly upon adding Cu^{2+} ion in the solution as shown in Table 4.3. Considering, the feather of naked-eye detection of sensor **HB** in the presence of HD and HM exhibited the similar results in case of the absence and presence of Cu^{2+} . This possibly implied that the solution consisted of dominant **HB**–HM complex which was not influenced by Cu^{2+} . These results were consistent with the fluorescence responses.

Table 4.3 Naked-eye fluorescence of sensor **HB** with HD and HM with Cu^{2+} ion

	HB	HB + HD	HB + HM	HB + HD + HM
Without Cu^{2+}				
With Cu^{2+}				

4.4 Fluorescence studies of imidazole derivatives

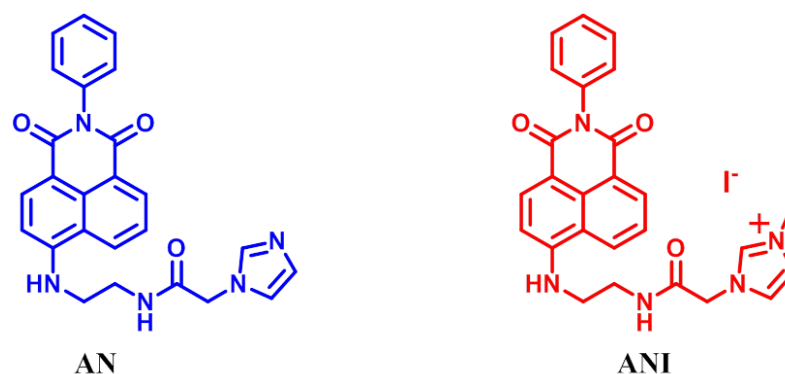


Figure 4.25 The structure of imidazole derivatives including sensor **AN** (left) and sensor **ANI** (right)

4.4.1 Fluorescence studies of sensor AN

4.4.1.1 Selectivity of sensor AN against various metal ions

We studied the selectivity of sensor **AN** against various metal ions including Cr^{3+} , Mn^{2+} , Co^{2+} , Ni^{2+} , Cu^{2+} , Zn^{2+} , Cd^{2+} , Ag^+ , and Au^{3+} which were examined in 10% DMSO/HEPES buffer pH 7.4. Sensor **AN** composed of imidazole group which was expected to form with metal ions. The fluorescence intensities of sensor **AN** were changed upon adding the metal ions as shown in Figure 4.26. Metal ions can partially induce the fluorescence quenching of sensor **AN** due to PET process. Interestingly, fluorescence intensity at 550 nm of sensor **AN** showed a large quenching in the presence of Cu^{2+} ion. For other metal ions, the quenching effect was decreased in the order of Cu^{2+} , Au^{3+} , Zn^{2+} \sim Ag^+ , Ni^{2+} , Co^{2+} , Mn^{2+} = Cd^{2+} , Cr^{3+} . We concluded that sensor **AN** has high selectivity with Cu^{2+} ion. Therefore, we have also focused on studying the binding ability of sensor **AN** toward Cu^{2+} ion.

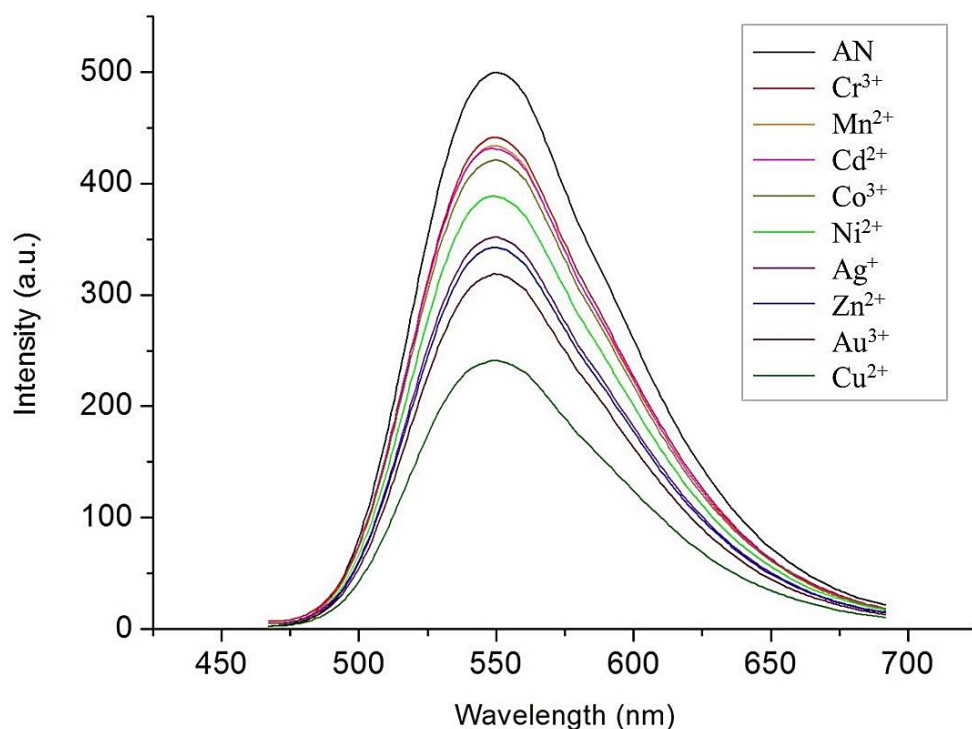


Figure 4.26 Fluorescence spectra of sensor **AN** (10 μM) upon addition of Cr^{3+} , Mn^{2+} , Co^{2+} , Ni^{2+} , Cu^{2+} , Zn^{2+} , Cd^{2+} , Ag^{+} , and Au^{3+} solutions (10 equiv) in 10% DMSO/HEPES buffer pH 7.4 ($\lambda_{\text{ex}} = 448 \text{ nm}$)

4.4.1.2 Job's plot analysis between sensor **AN** and Cu^{2+} ion

The stoichiometry between sensor **AN** and Cu^{2+} ion was investigated by Job's plot analysis as shown in Figure 4.27. The plot of $(I_0 - I)(1-x)$ versus a mole fraction of Cu^{2+} ion showed the highest point of the graph at 0.5 mole of Cu^{2+} ion indicating that the binding mode of sensor **AN** and Cu^{2+} ion is 1:1 stoichiometry.

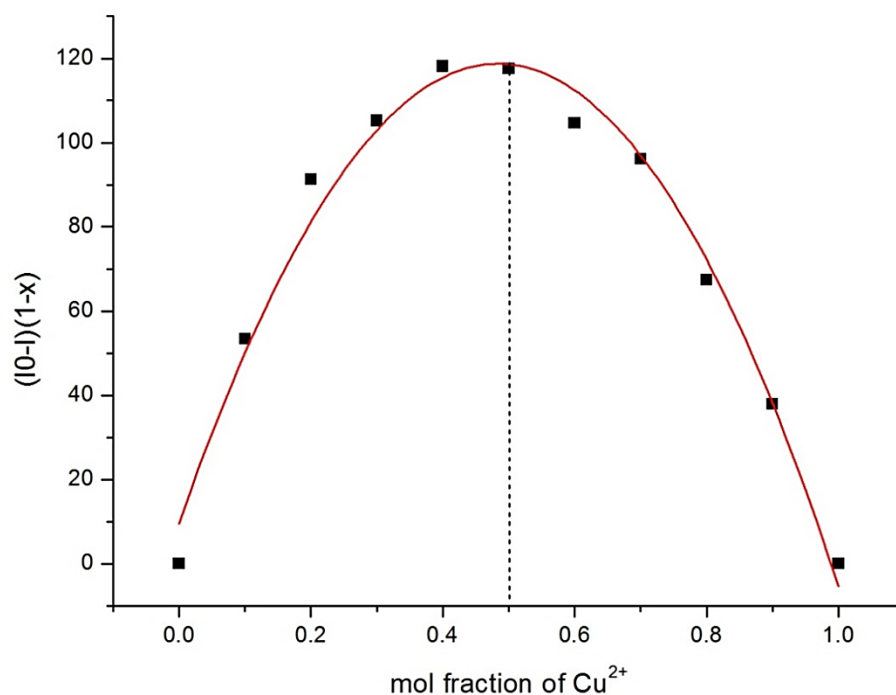


Figure 4.27 Job's plot for sensor **AN** and Cu^{2+} complex with the total concentration of $10 \mu\text{M}$

4.4.1.3 Binding constant determination of sensor **AN** and Cu^{2+} ion

The binding constant of sensor **AN** and Cu^{2+} ion was investigated by fluorescence titration method. The fluorescence spectra between sensor **AN** with the various amounts of Cu^{2+} ion was shown in Figure 4.28. The fluorescence intensity of sensor **AN** was gradually decreased upon the increment of Cu^{2+} ion from 0 to 3.5 equiv. Moreover, the $\log K_s$ value of sensor **AN** complex with Cu^{2+} ion calculated by equation 4.1 was 5.130.

$$I = \frac{I_0 + I_{lim} K_s [G]^n}{1 + K_s [G]^n} \quad 4.1$$

I_0 = initial intensity

I = intensity of a particular concentration of guest

I_{lim} = limited intensity

K_s = binding constant of the sensor with the guest

$[G]$ = concentration of guest

n = number of guest in the complex

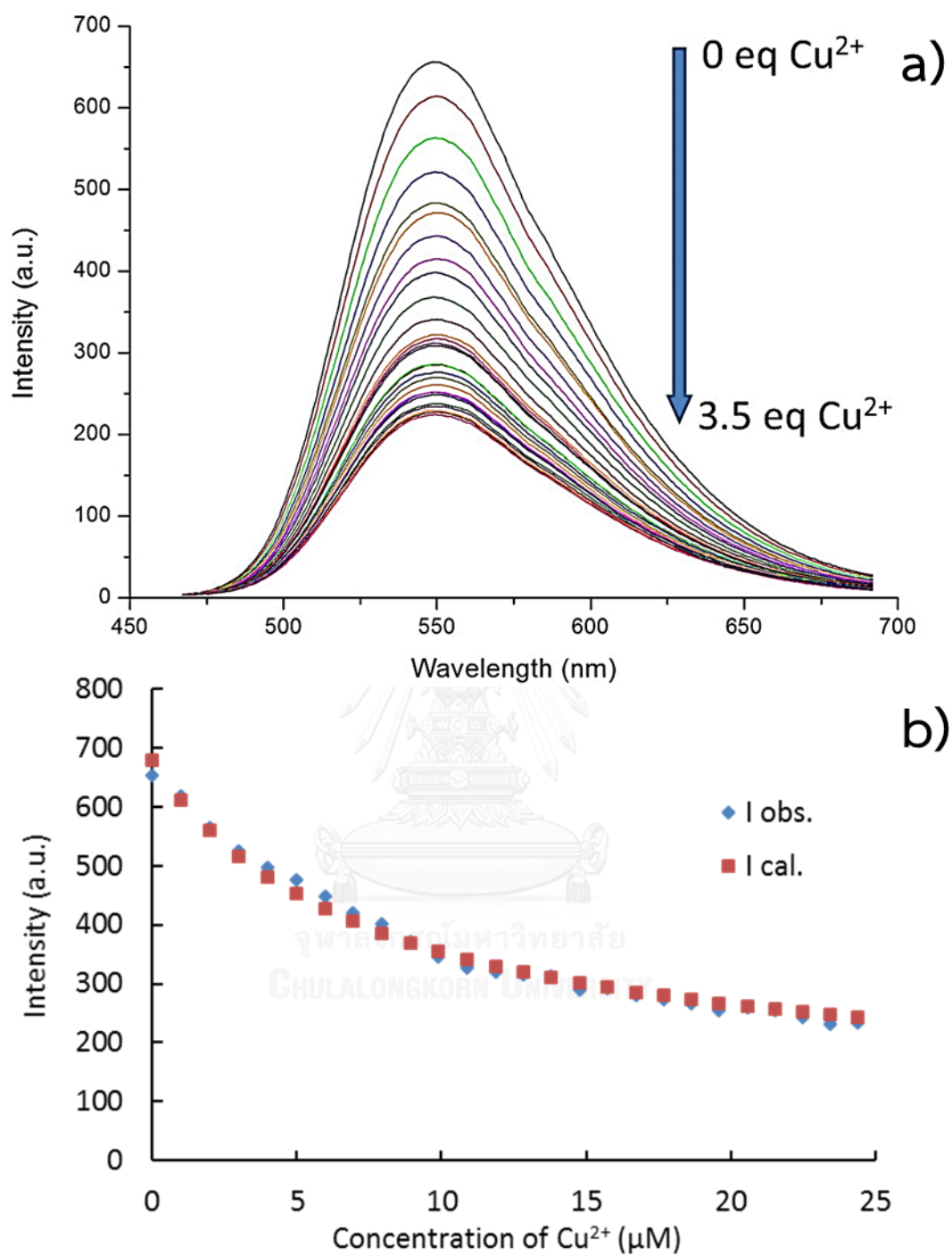


Figure 4.28 a) Fluorescence spectral titration of sensor AN (10 μM) in the presence of different amounts of Cu^{2+} ion (0 – 3.5 equiv) in 10% DMSO/HEPES buffer pH 7.4. b) Fluorescence titration curves in the presence of Cu^{2+} ion

4.4.2 Fluorescence studies of sensor ANI

4.4.2.1 Selectivity of sensor ANI against various amino acids

We studied the selectivity of sensor **ANI** against various amino acids in 10% DMSO/phosphate buffer pH 7.4. We hypothesized that sensor **ANI** which has imidazolium moiety can bind with carboxyl group of amino acids due to the charge attraction of two components. At phosphate buffer pH 7.4, amino acids are mostly formed a zwitterion which are composed of carboxylate anion and ammonium cation. Imidazolium group consists of the positive charge on the imidazole ring. Hydrogen at C-2 position is a strong acidic proton which can bind with carboxylate via hydrogen bonding. The result showed that fluorescence spectrum of sensor **ANI** did not significantly changed in a presence of various amino acids as shown in Figure 4.29. Nevertheless, imidazolium moiety of sensor **ANI** has a weak interaction with carboxylate anion due to their molecular geometry. Therefore, sensor **ANI** is unable to be a sensor for amino acids.

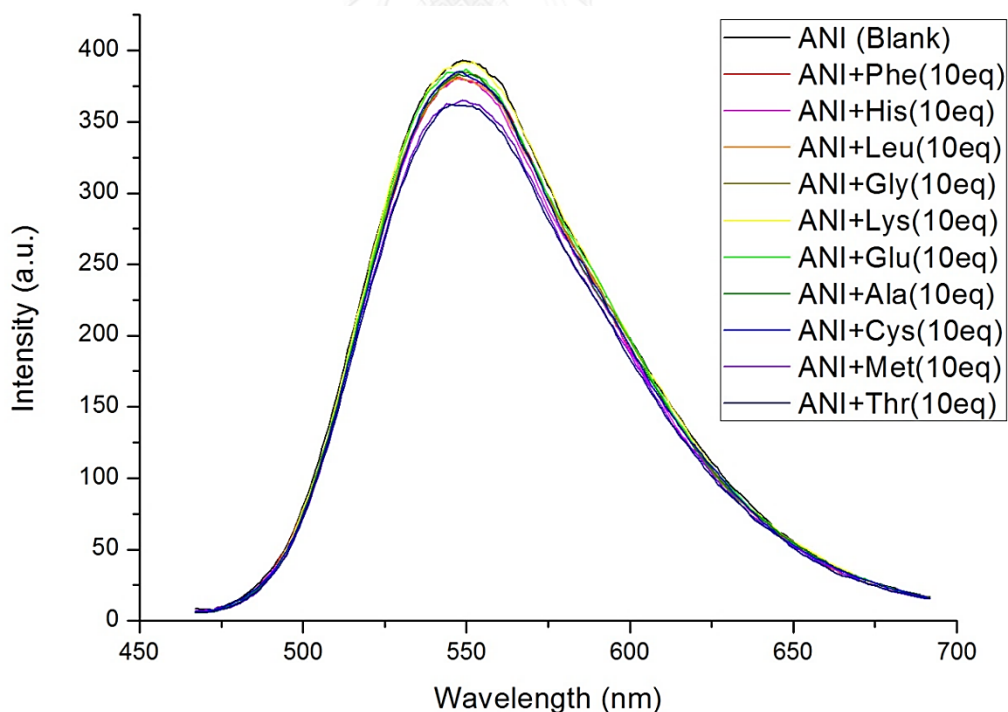


Figure 4.29 Fluorescence spectra of sensor **ANI** (10 μ M) upon addition of various amino acids including Phe, His, Leu, Gly, Lys, Glu, Ala, Cys, Met and Thr solutions (10 equiv) in 10% DMSO/phosphate buffer pH 7.4 ($\lambda_{\text{ex}} = 448$ nm)

4.4.2.2 Selectivity of sensor ANI against various nucleotides

We studied the selectivity of sensor **ANI** against various nucleotides in 10% DMSO/HEPES buffer pH 7.4. We hypothesized that sensor **ANI** can bound with nucleotides which are composed of phosphate group. The result showed that fluorescence spectra of sensor **ANI** were not significantly changed in a presence of various nucleotides as shown in Figure 4.30. The imidazolium acidic proton cannot strongly bind with phosphate group due to their molecular geometry. Therefore, the sensor **ANI** cannot offer a promising detection of nucleotide.

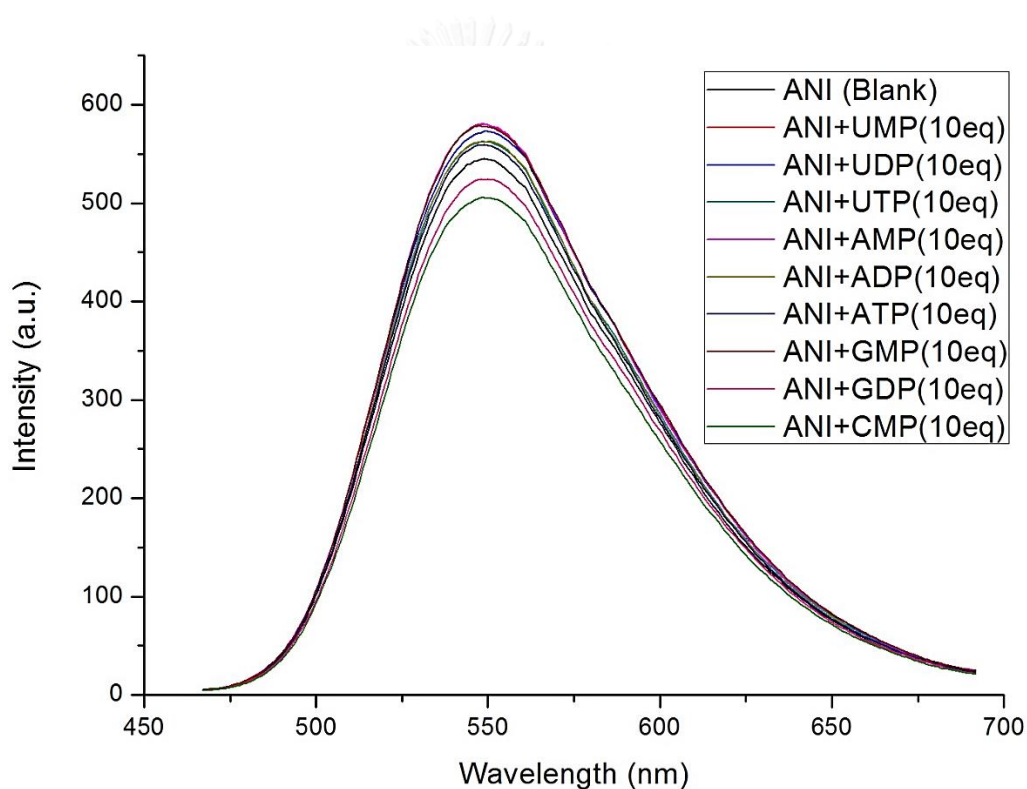


Figure 4.30 Fluorescence spectra of sensor **ANI** (10 μ M) upon the addition of various nucleotides including UMP, UDP, UTP, AMP, ADP, ATP, GMP, GDP and CMP solutions (10 equiv) in 10% DMSO/HEPES buffer pH 7.4 ($\lambda_{\text{ex}} = 448$ nm)

4.4.2.3 Selectivity of sensor ANI against various anions

We studied the sensing properties of sensor **ANI** against various anions including F^- , Cl^- , Br^- , I^- , CN^- , OH^- , PO_4^{3-} , AcO^- and BzO^- in 100% DMSO solution. We hypothesized that the acidic proton and imidazolium cation of sensor **ANI** can interact with anions under the hydrogen bonding interaction. The fluorescence spectra of sensor **ANI** were largely quenched in the presence of F^- anion via PET process as shown in Figure 4.31. For the other anions, the fluorescence spectra remained unchanged or slightly changed. Following hard-soft acid-base (HSAB) theory, the acidic proton of sensor **ANI** was defined as hard acid and the F^- anion was defined as hard base. Thus, the interaction between proton and F^- anion was stronger than the other anions. We concluded that sensor **ANI** offered high selectivity with F^- anion.

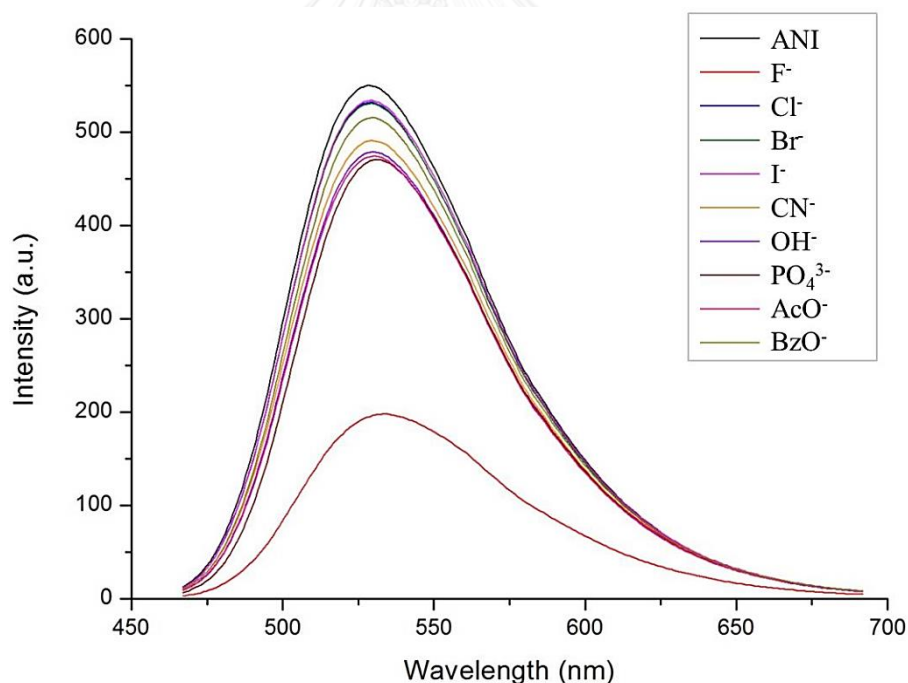


Figure 4.31 Fluorescence spectra of sensor **ANI** (10 μ M) upon the addition of various anions including F^- , Cl^- , Br^- , I^- , CN^- , OH^- , PO_4^{3-} , AcO^- and BzO^- solutions (10 equiv) in 100% DMSO solution ($\lambda_{ex} = 448$ nm)

Moreover, we can confirm that sensor **ANI** has high selectivity with F^- anion due to the positive charge where located on imidazolium ring. Sensor **AN** has the core structure as same as sensor **ANI** but it does not have the positive charge on imidazole ring. We studied the selectivity of sensor **AN** against various anions. No changes of fluorescent responses were observed in the presence of anions as shown in Figure 4.32. It suggested that sensor **AN** is unable to bind with any anions. This result insisted that the positive charge and strong acid proton on C2 plays a crucial role for anion binding affinity, especially F^- anion.

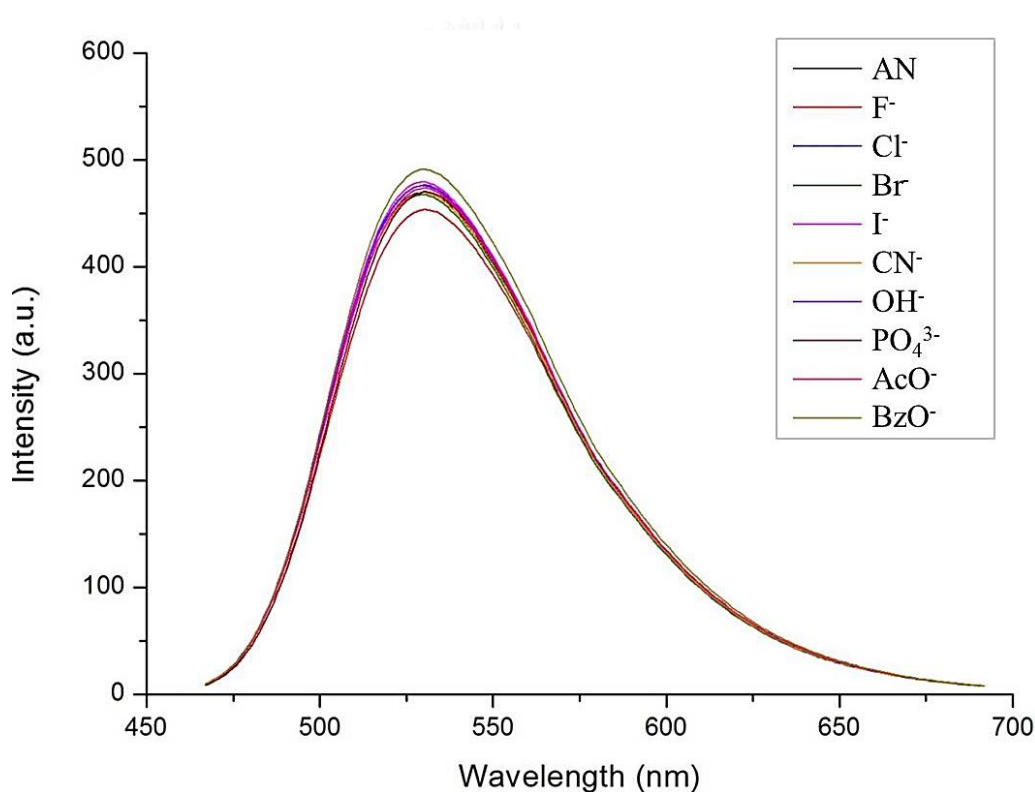


Figure 4.32 Fluorescence spectra of sensor **AN** (10 μ M) upon the addition of various anions including F^- , Cl^- , Br^- , I^- , CN^- , OH^- , PO_4^{3-} , AcO^- and BzO^- solutions (10 equiv) in 100% DMSO solution ($\lambda_{ex} = 448$ nm)

Considerably, the normalized fluorescence intensities (I/I_0) of sensors **ANI** and **AN** were shown in the Figure 4.33. The black bar and the red bar, defined as I/I_0 of

sensors **ANI** and **AN**, respectively, exhibited the small difference of black and red bars in case of F^- anion implied that sensor **ANI** preferentially bound with F^- anion.

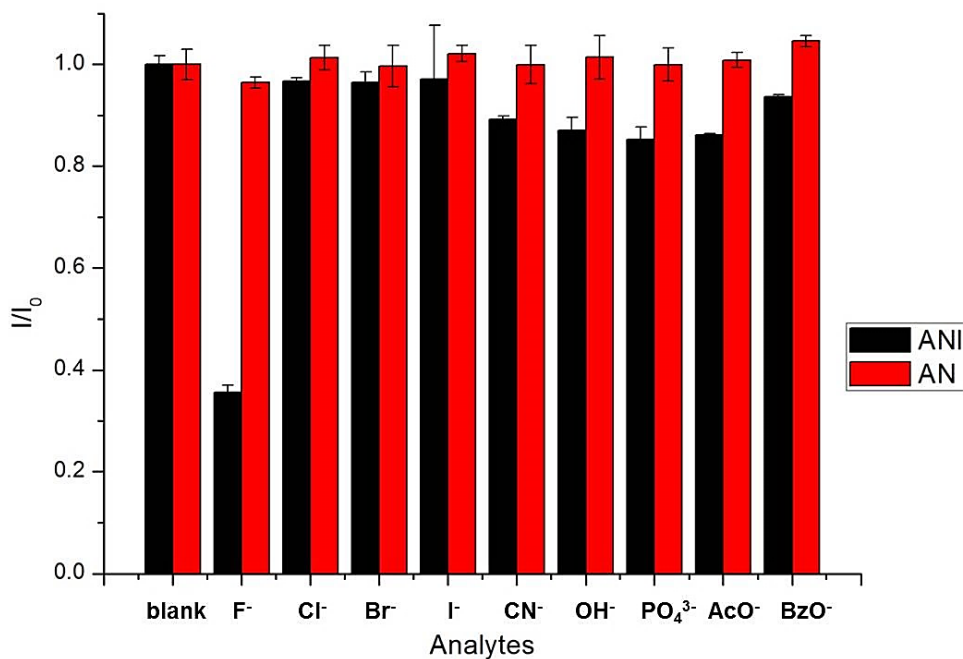


Figure 4.33 Comparison of the selectivity between sensors **ANI** (10 μ M) and **AN** (10 μ M) with various anions including F^- , Cl^- , Br^- , I^- , CN^- , OH^- , PO_4^{3-} , AcO^- and BzO^- solutions (10 equiv) in 100% DMSO solution ($\lambda_{ex} = 448$ nm)

- **Job's plot analysis between sensor ANI and F^- ion**

The stoichiometry between sensor **ANI** and F^- anion was investigated by Job's plot analysis as shown in Figure 4.34. The plot of $(I_0 - I)(1-x)$ versus mole fraction of F^- anion showed the highest point of the graph at 0.5 mole of F^- anion. Therefore, the binding mode of sensor **ANI** and F^- anion is 1:1 stoichiometry.

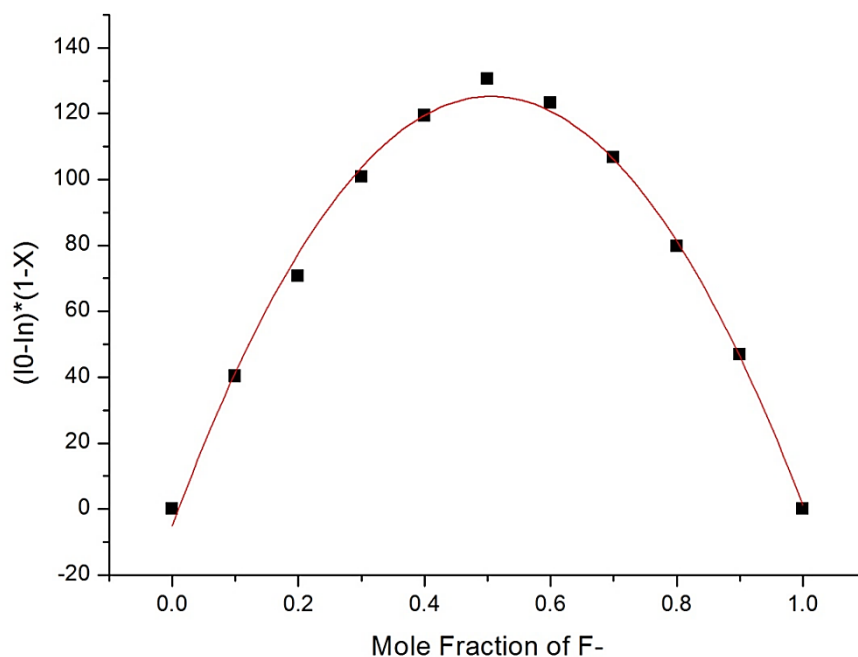


Figure 4.34 Job's plot for sensor ANI and F⁻ complex with the total concentration of 10 μM

- **Binding constant determination of sensor ANI and F⁻ ion**

The binding constant of sensor ANI and F⁻ anion was investigated by fluorescence titration method. The fluorescence spectra between sensors ANI with the various amounts of F⁻ anion were shown in Figure 4.35. The fluorescence intensity of sensor ANI was gradually decreased upon the increment of F⁻ anion from 0 to 1000 equiv. Moreover, the log K_s value of sensor ANI with F⁻ anion calculated by equation 4.1 was 3.05.

$$I = \frac{I_0 + I_{lim} K_s [G]^n}{1 + K_s [G]^n} \quad 4.1$$

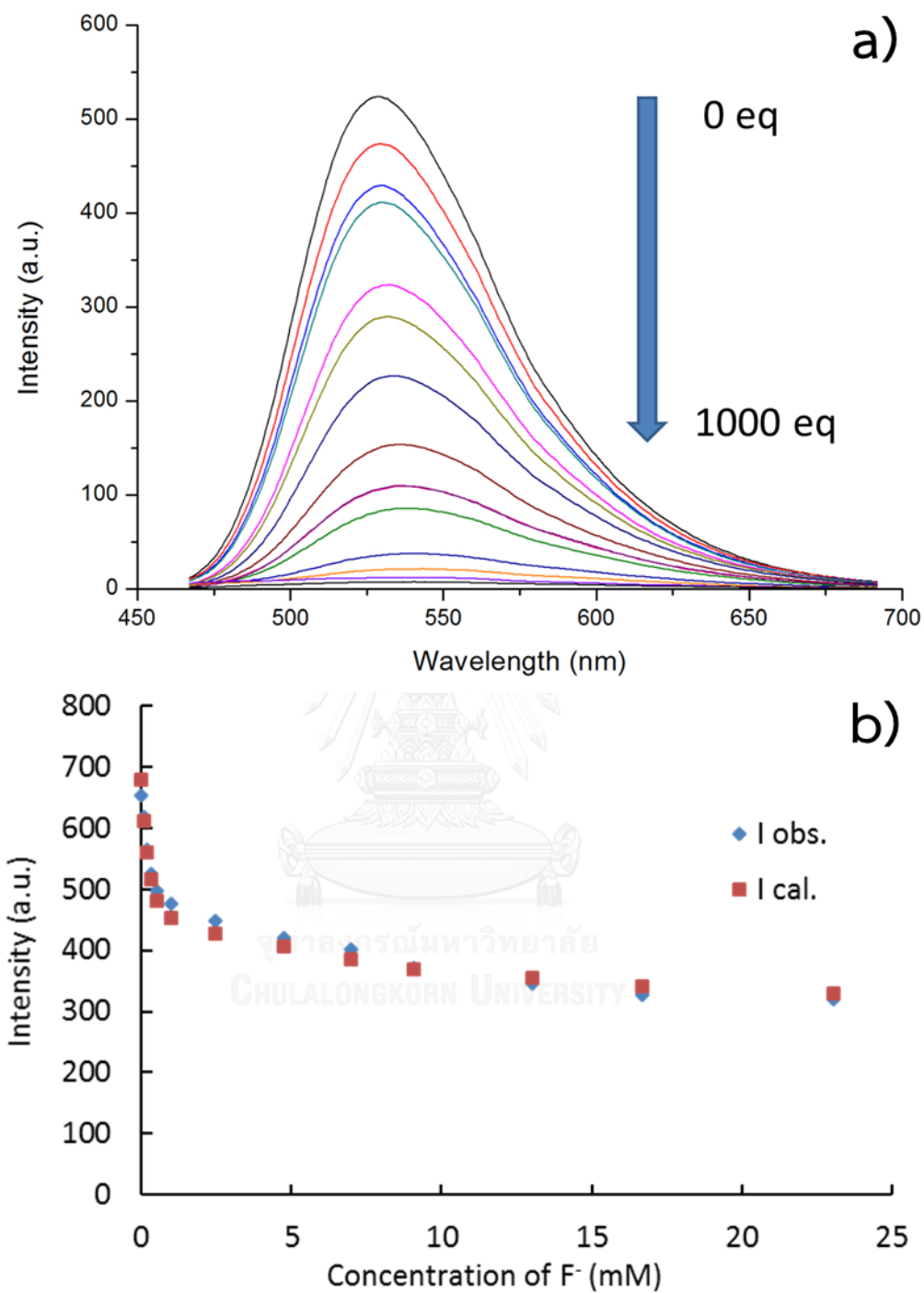


Figure 4.35 a) Fluorescence spectral titration of sensor ANI (10 μM) in the presence of different amounts of F^- ion (0 – 1000 equiv) in 100% DMSO solution. b) Fluorescent titration curves of sensor ANI in the presence of F^- ion

- LOD/LOQ determination of sensor ANI

The limit of detection (LOD) and limit of quantification (LOQ) were determined by method validation using equations 4.3 and 4.4. Firstly, we measured the sensor ANI solution 10 times to set an average baseline. Then, the calibration curve of $(I_0-I)/I_0$ versus concentration of F^- is plotted and the slope is 366.23 with the linear regression of 0.9815. From equations 4.2 and 4.3, LOD and LOQ of sensor ANI toward F^- anion are 0.18 mM and 0.60 mM, respectively.

$$LOD = \frac{3SD}{slope} \quad 4.2$$

$$LOQ = \frac{10SD}{slope} \quad 4.3$$

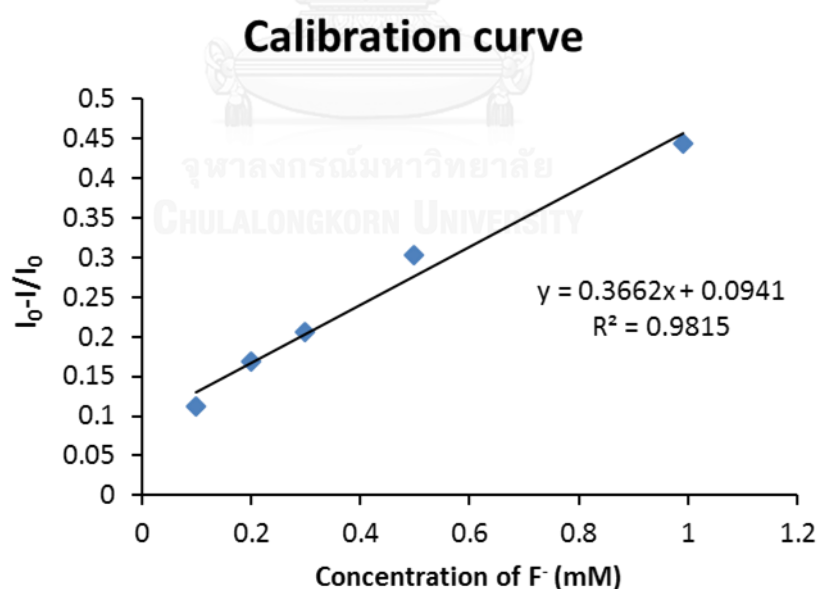


Figure 4.36 Calibration curve of the intensity of sensor ANI and various concentration of F^- anion

- **NMR titration of sensor ANI against F⁻ ion**

To prove the interaction between sensor **ANI** and F⁻ anion, NMR titration was examined in *d*₆-DMSO. The solution of sensor **ANI** was added with varying concentration of F⁻ anion between 0 to 4.0 equiv. The NMR spectra were shown in Figure 4.37. At 0 equivalent of F⁻ anion, the acidic proton on C2 and amide proton of sensor **ANI** was observed at 9.05 ppm and 7.84 ppm, respectively. At 0.5 equivalent of F⁻ anion, all peaks of NMR spectrum were broad and low resolution. The acidic proton on C2 was gradually downfield shifted at 9.10 ppm due to the hydrogen bonding with F⁻. At 1.0 equivalent of F⁻ anion, the acidic proton of C2 at 9.10 ppm was splitted to be two peaks of 9.15 and 9.05 and the amide proton at 7.84 ppm was splitted to be at 8.15 and 7.90 ppm. The splitting of the peaks was occurred in equilibrium between complexes and free receptors. At 2.0 equivalent of F⁻ anion, the acidic proton on C2 was downfield shifted from free sensor at 9.05 ppm to 9.80 ppm of the expected complex. At 4.0 equivalent of F⁻ anion, the color of solution of sensor **ANI** turned from yellow to red solution and NMR spectrum was totally changed due to the excess amount of F⁻ anion. The amide acidic proton was settled on 9.20 ppm. Interestingly, we found the new triplet peak at 16 ppm corresponding to H₂F⁺ proton. Finally, these confirmed that the acidic proton of C2 was interacted with F⁻ anion observing from the downfield shift and the amide proton was further deprotonated upon adding excess F⁻ anion.

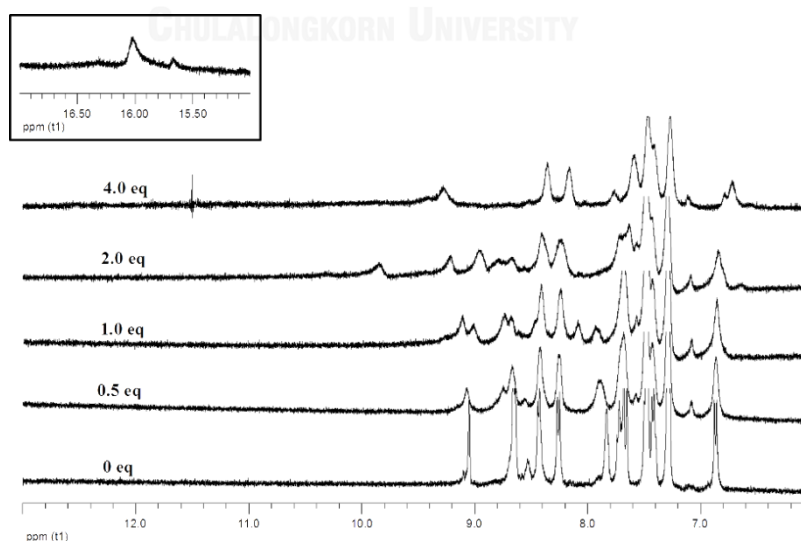


Figure 4.37 NMR titration spectra of sensor **ANI** (100 mM) upon addition of various concentration of F⁻ anion including 0 equiv, 0.5 equiv, 1.0 equiv, 2.0 equiv and 4.0 equiv

- **Colorimetric detection of sensor ANI against various anions**

We applied sensor **ANI** for the use of the colorimetric assay of anion determination. We hypothesized that the color of sensor **ANI** would be changed under the complexation. Firstly, sensor **ANI** was titrated with various anions in the concentration range from 0 - 900 equivalent. Interestingly, the color of sensor **ANI** was changed in the presence of F^- or OH^- . In the case of F^- anion, the color of sensor **ANI** was gradually changed from green to purple at the concentration of F^- anion over 200 equivalents. This phenomenon can be explained that the deprotonation of the acidic proton of sensor **ANI** by F^- anion was occurred to give the unstable intermediate species. Similarly, the case of OH^- anion induced the gradually color change from green to pale at the concentration of OH^- anion over 600 equivalents. All of other anions did not show the color change of sensor **ANI** as shown in Figure 4.38. Definitely, sensor **ANI** can be served as naked-eye detection for F^- anion at 200 equivalents (631.02 ppm) and OH^- anion at 600 equivalents (1556.88 ppm). Taking a part of visual detection of anions, sensor **ANI** offers an effectively promising selectivity for F^- without the interference of OH^- in the range of 2×10^{-3} - 5×10^{-3} M.

	Blank	10 eq	50 eq	100 eq	200 eq	300 eq	400 eq	500 eq	600 eq	700 eq	800 eq	900 eq
F^-	Green	Green	Green	Green	Green	Green	Green	Green	Green	Green	Green	Green
Cl^-	Green	Green	Green	Green	Green	Green	Green	Green	Green	Green	Green	Green
Br^-	Green	Green	Green	Green	Green	Green	Green	Green	Green	Green	Green	Green
I^-	Green	Green	Green	Green	Green	Green	Green	Green	Green	Green	Green	Green
CN^-	Green	Green	Green	Green	Green	Green	Green	Green	Green	Green	Green	Green
OH^-	Green	Green	Green	Green	Green	Green	Green	Green	Green	Green	Green	Green
PO_4^{3-}	Green	Green	Green	Green	Green	Green	Green	Green	Green	Green	Green	Green
BzO^-	Green	Green	Green	Green	Green	Green	Green	Green	Green	Green	Green	Green
AcO^-	Green	Green	Green	Green	Green	Green	Green	Green	Green	Green	Green	Green

Figure 4.38 Colorimetric assay of sensor **ANI** (1×10^{-5} M) responses upon addition of vary concentration (0-900 equiv) of various anions including F^- , Cl^- , Br^- , I^- , CN^- , OH^- , PO_4^{3-} , AcO^- and BzO^-

- **Fluorometric detection of sensor ANI against various anions**

Not only colorimetric assay has been studied but we have also examined the fluorometric assay for F^- anion determination because the sensor **ANI** performed a strong fluorescent intensity. Firstly, sensor **ANI** was added by various anions in concentration range from 0 - 900 equivalents and then the mixture solution were exposed under UV lamp at 265 nm in the black box. The results showed that the green brightness of luminescence sensor **ANI** was gradually quenched upon the addition of F^- anion at 200 equivalences. PET process was occurred when the complex of $ANI \cdot F^-$ was formed. This was explained that electron from F^- anion might interrupted the fluorescence relaxation process. Therefore, sensor **ANI** can be used for fluorometric assay of F^- anion determination in the range of 200-900 equivalents. Interestingly, the other anions did not exhibit the change of brightness of sensor **ANI** except OH^- anion as shown in Figure 4.39. The brightness of sensor **ANI** was largely decreased after adding 600 equivalent of OH^- anion. The excess OH^- anion can deprotonate sensor **ANI** giving the unstable complex. This result was consistent with the color changes.

	Blank	10 eq	50 eq	100 eq	200 eq	300 eq	400 eq	500 eq	600 eq	700 eq	800 eq	900 eq
F^-												
Cl^-												
Br^-												
I^-												
CN^-												
OH^-												
PO_4^{3-}												
BzO^-												
AcO^-												

Figure 4.39 Fluorometric assay of sensor **ANI** (1×10^{-5} M) responses upon addition of vary concentration (0-900 equiv) of various anions including F^- , Cl^- , Br^- , I^- , CN^- , OH^- , PO_4^{3-} , AcO^- and BzO^- ($\lambda_{exc} = 265$ nm)

CHAPTER V

CONCLUSION

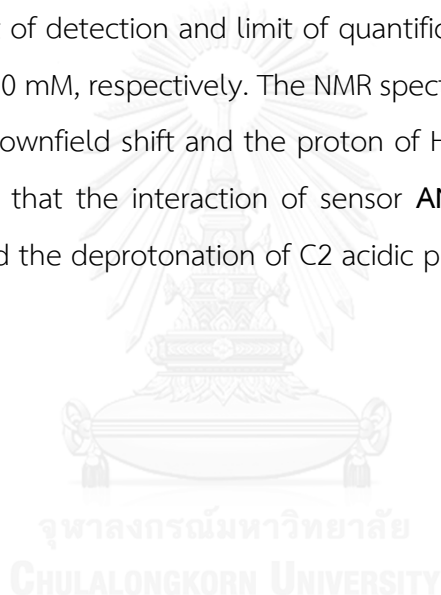
5.1 Conclusion

Following to the objective of this work, our aim is to discriminate the biogenic amines which have the similar structure of histidine and histamine by using fluorescence spectroscopy methods. We have designed and synthesized the fluorescence based imidazole unit sensors such as **AN** and **ANI**. Sensors **AN** and **ANI** were synthesized from the same pathways.

We utilized the combination of two sensors **HB** and **ANI** for discrimination of histidine and histamine via FRET mechanism. This combination cannot discriminate histidine and histamine because the absorption band of **ANI** would interfere to the excitation wavelength of sensor **HB**. Next, we studied the complexation ability of sensor **HB** toward HD and HM. Following the kinetic study, the complex formation of **HB**CHM was faster than that of **HB**CHD because the steric effect of carboxyl group hindered the primary amine to form the product. Moreover, we studied the binding affinities of **HB**, **HB**CHM, and **HB**CHD against various metal ions including Cu^{2+} , Zn^{2+} , Ni^{2+} , Cr^{3+} , Mn^{2+} , and Co^{2+} ions. The fluorescence spectrum of **HB**CHD was quenched in the presence of 5 equivalent of Cu^{2+} ion while that of **HB**CHM remained unchanged in the presence of Cu^{2+} . Thus, we successfully discriminated histidine and histamine compounds by using the combination of two elements of **HB** and Cu^{2+} in system. This system can detect Cu^{2+} under naked-eye detection. In addition, we confirmed the possible two structures of **HB**CHD with Cu^{2+} complex by computer simulation technique. Moreover, we miniaturized the fluorescence response of sensor **HB** toward histidine, histamine and Cu^{2+} into the logic gates schematic pattern by the combination of Boolean operation including NAND and OR gates. This logic gate was designed following to the priority of analytes.

We have studied the binding behavior of sensor **AN** against various metal ion including Cr^{3+} , Mn^{2+} , Co^{2+} , Ni^{2+} , Cu^{2+} , Zn^{2+} , Cd^{2+} , Ag^+ , and Au^{3+} ions. The fluorescence spectra of **AN** displayed a large quenching upon the addition of excess Cu^{2+} ion. The formation of sensor **AN** and Cu^{2+} showed the binding mode of 1:1 stoichiometry and log K value of complex is 5.130.

Finally, we have examined the selectivity of sensor **ANI** against various analytes including amino acids, nucleotides and anions. Interestingly, the fluorescence spectra of sensor **ANI** showed a large decrease in the presence of F^- ions. The sensor **ANI** forms complex with F^- ion with stoichiometry of 1:1 ratio of **ANI**: F^- . The log K value of this complex is 3.05. Limit of detection and limit of quantification values of **ANI** toward F^- were 0.18 mM and 0.60 mM, respectively. The NMR spectrum of sensor **ANI** and excess F^- ion exhibited the downfield shift and the proton of H_2F^+ was observed at 16 ppm. This result confirmed that the interaction of sensor **ANI** and F^- passed through the hydrogen bonding and the deprotonation of C2 acidic proton based sensor **ANI**.



REFERENCES

- [1] Lehn, J.-M. From Molecular to Supramolecular Chemistry. in Supramolecular Chemistry, pp. 1-9: Wiley-VCH Verlag GmbH & Co. KGaA, 2006.
- [2] Rotello, V.M. Core Concepts in Supramolecular Chemistry and Nanochemistry By Jonathan W. Steed (Durham University, U.K.), David R. Turner (Monash University, Australia), and Karl J. Wallace (University of Southern Mississippi). John Wiley & Sons, Ltd: Chichester. 2007. xii + 308 pp. \$50. ISBN 978-0-470-85867-7. Journal of the American Chemical Society 129(46) (2007): 14524-14524.
- [3] Ariga, K. and Kunitake, T. Supramolecular Chemistry - Fundamentals and Applications: Advanced Textbook. Springer Berlin Heidelberg, 2006.
- [4] Steed, J.W. and Atwood, J.L. Supramolecular Chemistry. Wiley, 2013.
- [5] James, T.D. Saccharide-Selective Boronic Acid Based Photoinduced Electron Transfer (PET) Fluorescent Sensors. in Schrader, T. (ed.) Creative Chemical Sensor Systems, pp. 107-152. Berlin, Heidelberg: Springer Berlin Heidelberg, 2007.
- [6] Lakowicz, J.R. Principles of Fluorescence Spectroscopy. Springer US, 2013.
- [7] Valeur, B. and Berberan-Santos, M.N. Molecular Fluorescence: Principles and Applications. Wiley, 2012.
- [8] Anslyn, E.V. Supramolecular analytical chemistry. J Org Chem 72(3) (2007): 687-99.
- [9] Beer, P.D. Transition-metal receptor systems for the selective recognition and sensing of anionic guest species. Accounts of Chemical Research 31(2) (1998): 71-80.
- [10] Ellis, A.B. and Walt, D.R. Guest editorial. Chem Rev 100(7) (2000): 2477-8.
- [11] de Silva, A.P., et al. Signaling Recognition Events with Fluorescent Sensors and Switches. Chem Rev 97(5) (1997): 1515-1566.

- [12] Prodi, L., Bolletta, F., Montalti, M., and Zaccheroni, N. Luminescent chemosensors for transition metal ions. Coordination Chemistry Reviews 205(1) (2000): 59-83.
- [13] Bargossi, C., Fiorini, M.C., Montalti, M., Prodi, L., and Zaccheroni, N. Recent developments in transition metal ion detection by luminescent chemosensors. Coordination Chemistry Reviews 208(1) (2000): 17-32.
- [14] Lakowicz, J.R. Principles of Fluorescence Spectroscopy. Springer US, 2007.
- [15] Bett, S. Jablonski diagram [Online]. 2014. Available from: <https://www.quora.com/What-is-the-Jablonski-diagram> [October 19]
- [16] Kim, J.S. and Quang, D.T. Calixarene-derived fluorescent probes. Chem Rev 107(9) (2007): 3780-99.
- [17] Aoki, I., Kawabata, H., Nakashima, K., and Shinkai, S. Fluorescent calix[4]arene which responds to solvent polarity and metal ions. Journal of the Chemical Society, Chemical Communications (24) (1991): 1771.
- [18] Ji, H.F., Dabestani, R., Brown, G.M., and Sachleben, R.A. A new highly selective calix[4]crown-6 fluorescent caesium probe. Chemical Communications (10) (2000): 833-834.
- [19] Ji, H.-F., Brown, G.M., and Dabestani, R. Calix[4]arene-based Cs⁺ selective optical sensor. Chemical Communications (7) (1999): 609-610.
- [20] Martinez-Manez, R. and Sancenon, F. Fluorogenic and chromogenic chemosensors and reagents for anions. Chem Rev 103(11) (2003): 4419-76.
- [21] Bojinov, V. and Georgiev, N. Molecular sensors and molecular logic gates. Journal of the University of Chemical Technology and Metallurgy 46(1) (2011): 3-26.
- [22] Valeur, B. and Leray, I. Design principles of fluorescent molecular sensors for cation recognition. Coordination Chemistry Reviews 205(1) (2000): 3-40.
- [23] Czarnik, A.W. Fluorescent Chemosensors for Ion and Molecule Recognition. ACS Symposium Series. Vol. 538: American Chemical Society, 1993.
- [24] Rettig, W. and Lapouyade, R. Fluorescence Probes Based on Twisted Intramolecular Charge Transfer (TICT) States and Other Adiabatic Photoreactions. in Lakowicz, J.R. (ed.) Topics in Fluorescence Spectroscopy:

- Probe Design and Chemical Sensing, pp. 109-149. Boston, MA: Springer US, 1994.
- [25] Loehr, H.G. and Voegtle, F. Chromo- and fluoroionophores. A new class of dye reagents. Accounts of Chemical Research 18(3) (1985): 65-72.
- [26] Stryer, L. and Haugland, R.P. Energy transfer: a spectroscopic ruler. Proc Natl Acad Sci U S A 58(2) (1967): 719-26.
- [27] Inc., O.A. Fluorescence Resonance Energy Transfer (FRET) Microscopy [Online]. 2012. Available from:
<http://www.olympusmicro.com/primer/techniques/fluorescence/fret/images/fretintrofigure3.jpg> [October 20]
- [28] de Silva, P.A., Gunaratne, N.H.Q., and McCoy, C.P. A molecular photoionic AND gate based on fluorescent signalling. Nature 364(6432) (1993): 42-44.
- [29] Sreejith, S. Molecular logic gates: Recent advances and perspectives. Indian Journal of Chemistry 51A (2011): 47-56.
- [30] Santos, M.H.S. Biogenic amines: Their importance in foods. International Journal of Food Microbiology 29(2-3) (1996): 213-231.
- [31] Donthuan, J., Yunchalard, S., and Srijaranai, S. Vortex-assisted surfactant-enhanced-emulsification liquid-liquid microextraction of biogenic amines in fermented foods before their simultaneous analysis by high-performance liquid chromatography. J Sep Sci 37(21) (2014): 3164-73.
- [32] Yang, Y.X., Mu, C.L., Zhang, J.F., and Zhu, W.Y. Determination of Biogenic Amines in Digesta by High Performance Liquid Chromatography with Precolumn Dansylation. Analytical Letters 47(8) (2014): 1290-1298.
- [33] Chimalakonda, K.C., Pang, E., Weaver, J.L., Howard, K.E., Patel, V., and Boyne, M.T., 2nd. Development and validation of a liquid-chromatography tandem mass spectrometry method to determine in vitro and in vivo histamine release. J Pharm Biomed Anal 102 (2015): 494-9.
- [34] Seto, D., Soh, N., Nakano, K., and Imato, T. An amphiphilic fluorescent probe for the visualization of histamine in living cells. Bioorg Med Chem Lett 20(22) (2010): 6708-11.

- [35] Chow, C.F., et al. Heterobimetallic Ru(II)-Eu(III) complex as chemodosimeter for selective biogenic amine odorants detection in fish sample. Anal Chem 83(1) (2011): 289-96.
- [36] You, Q.H., Lee, A.W., Chan, W.H., Zhu, X.M., and Leung, K.C. A coumarin-based fluorescent probe for recognition of Cu(2+) and fast detection of histidine in hard-to-transfect cells by a sensing ensemble approach. Chem Commun (Camb) 50(47) (2014): 6207-10.
- [37] Lohar, S., et al. Selective fluorescence and naked eye detection of histidine in aqueous medium via hydrogen bonding assisted Schiff base condensation. Tetrahedron Letters 55(1) (2014): 174-176.
- [38] Chaicham, A., Sahasithiwat, S., Tuntulani, T., and Tomapatanaget, B. Highly effective discrimination of catecholamine derivatives via FRET-on/off processes induced by the intermolecular assembly with two fluorescence sensors. Chem Commun (Camb) 49(81) (2013): 9287-9.
- [39] Kielland, N., Vendrell, M., Lavilla, R., and Chang, Y.T. Imaging histamine in live basophils and macrophages with a fluorescent mesoionic acid fluoride. Chem Commun (Camb) 48(59) (2012): 7401-3.
- [40] Arevalo, M.J., Kielland, N., Masdeu, C., Miguel, M., Isambert, N., and Lavilla, R. Multicomponent Access to Functionalized Mesoionic Structures Based on TFAA Activation of Isocyanides: Novel Domino Reactions. European Journal of Organic Chemistry 2009(5) (2009): 617-625.
- [41] Tachapermpon, Y., Piyanuch, P., Prapawattanapol, N., Sukrat, K., Suwatpipat, K., and Wanichacheva, N. Synthesis of Novel Fluorescent Sensors Based on Naphthalimide Fluorophores for the Highly Selective Hg²⁺-Sensing. Journal of Chemistry 2015 (2015): 9.
- [42] Jia, T., Fu, C., Huang, C., Yang, H., and Jia, N. Highly sensitive naphthalimide-based fluorescence polarization probe for detecting cancer cells. ACS Appl Mater Interfaces 7(18) (2015): 10013-21.
- [43] Lee, M., Jo, S., Lee, D., Xu, Z.C., and Yoon, J. A new naphthalimide derivative as a selective fluorescent and colorimetric sensor for fluoride, cyanide and CO₂. Dyes and Pigments 120 (2015): 288-292.

- [44] Roy, B., Bar, A.K., Gole, B., and Mukherjee, P.S. Fluorescent tris-imidazolium sensors for picric acid explosive. J Org Chem 78(3) (2013): 1306-10.
- [45] Czirik, J.B., et al. Aminonaphthalimide-based dipodal imidazolium/triazole receptors for fluorescent sensing of nucleoside polyphosphates. Sensors and Actuators B-Chemical 182 (2013): 280-287.
- [46] Guo, Q.N., Li, Z.Y., Chan, W.H., Lau, K.C., and Crossley, M.J. Appending zinc tetraphenylporphyrin with an amine receptor at beta-pyrrolic carbon for designing a selective histamine chemosensor. Supramolecular Chemistry 22(2) (2010): 122-129.
- [47] Konstantinova, T.N. and Miladinova, P.M. Synthesis and properties of some fluorescent 1,8-naphthalimide derivatives and their copolymers with methyl methacrylate. Journal of Applied Polymer Science 111(4) (2009): 1991-1998.
- [48] Xia, S., et al. The synthesis of 4,7-disubstituted-2H-benzo[b][1,4]-oxazin-3(4H)-ones using Smiles rearrangement and their in vitro evaluation as platelet aggregation inhibitors. Bioorg Med Chem Lett 24(6) (2014): 1479-83.
- [49] Tomapatnaget, B., Tuntulani, T., Wisner, J.A., and Beer, P.D. New interlocked molecules generated from a podand containing urea units and imidazolium salts using an anion template. Tetrahedron Letters 45(4) (2004): 663-666.
- [50] Lis, R., et al. Synthesis and antiarrhythmic activity of novel 3-alkyl-1-[-omega.-[4-[(alkylsulfonyl)amino]phenyl]-.omega.-hydroxyalkyl]-1H-imidazolium salts and related compounds. 2. Journal of Medicinal Chemistry 30(12) (1987): 2303-2309.



APPENDIX

จุฬาลงกรณ์มหาวิทยาลัย
CHULALONGKORN UNIVERSITY

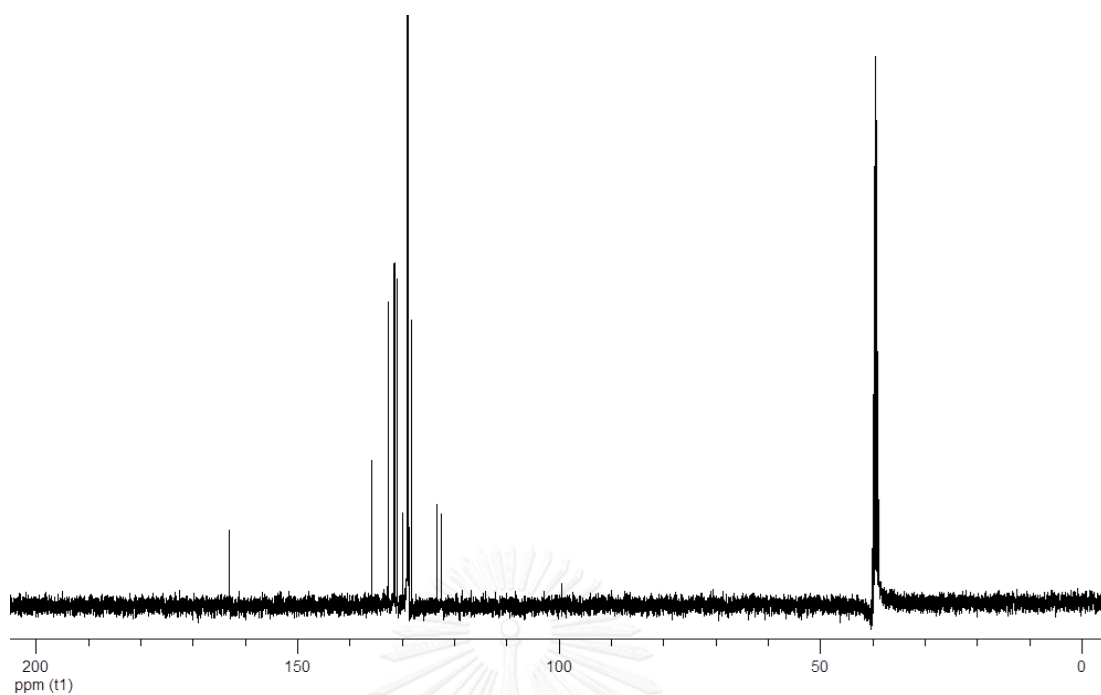


Figure A1 The ^{13}C -NMR spectrum of **1** in d_6 -DMSO at 100 MHz

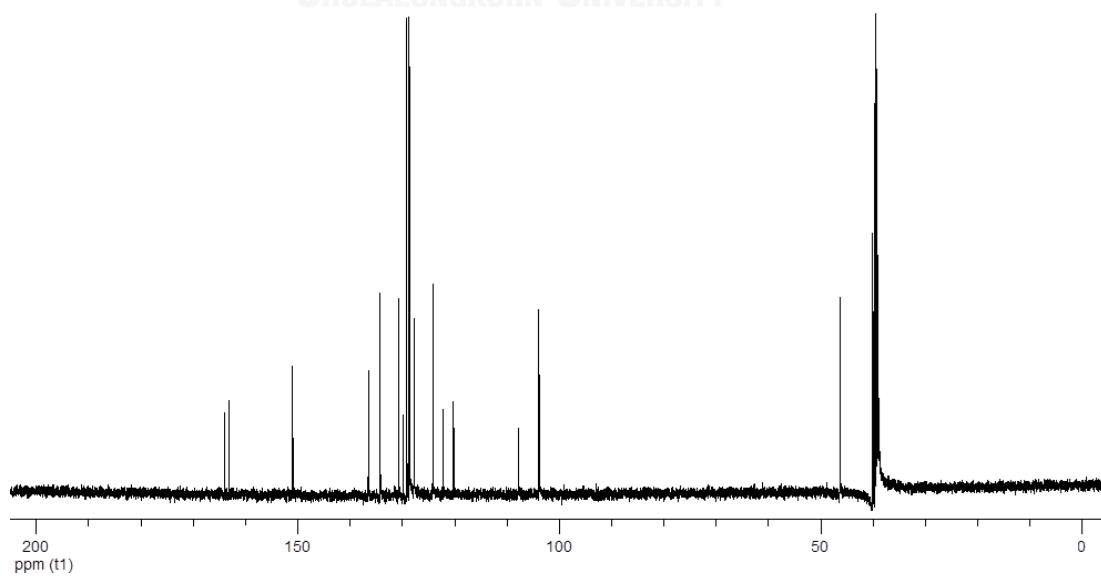


Figure A2 The ^{13}C -NMR spectrum of **2** in d_6 -DMSO at 100 MHz

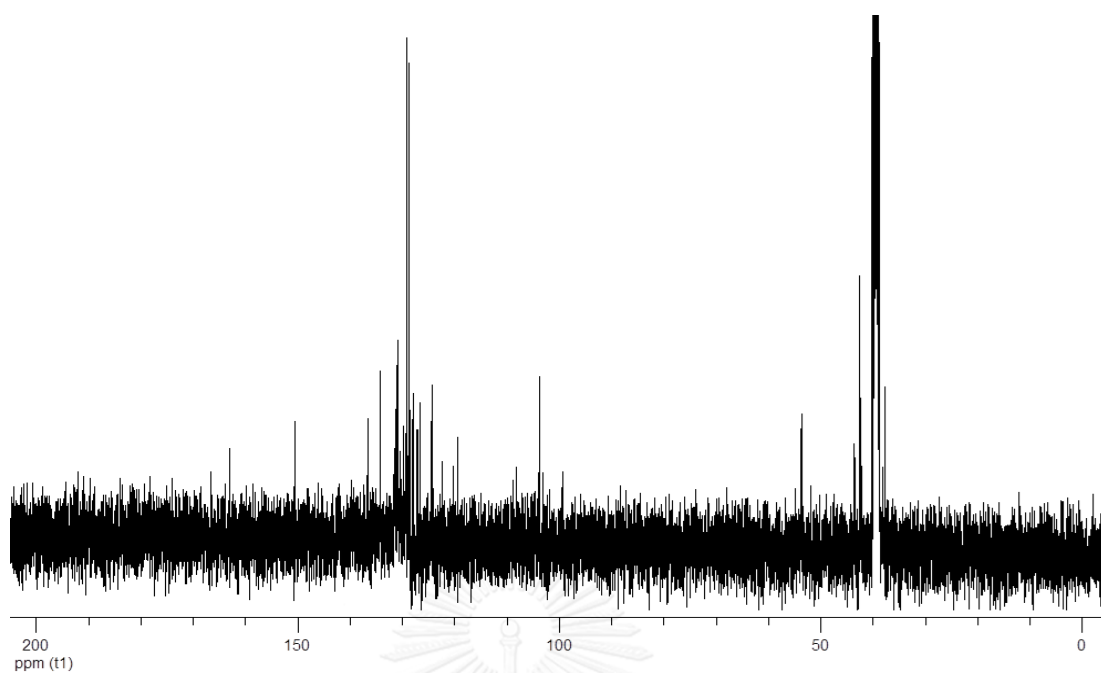


Figure A3 The ^{13}C -NMR spectrum of **3** in d_6 -DMSO at 100 MHz

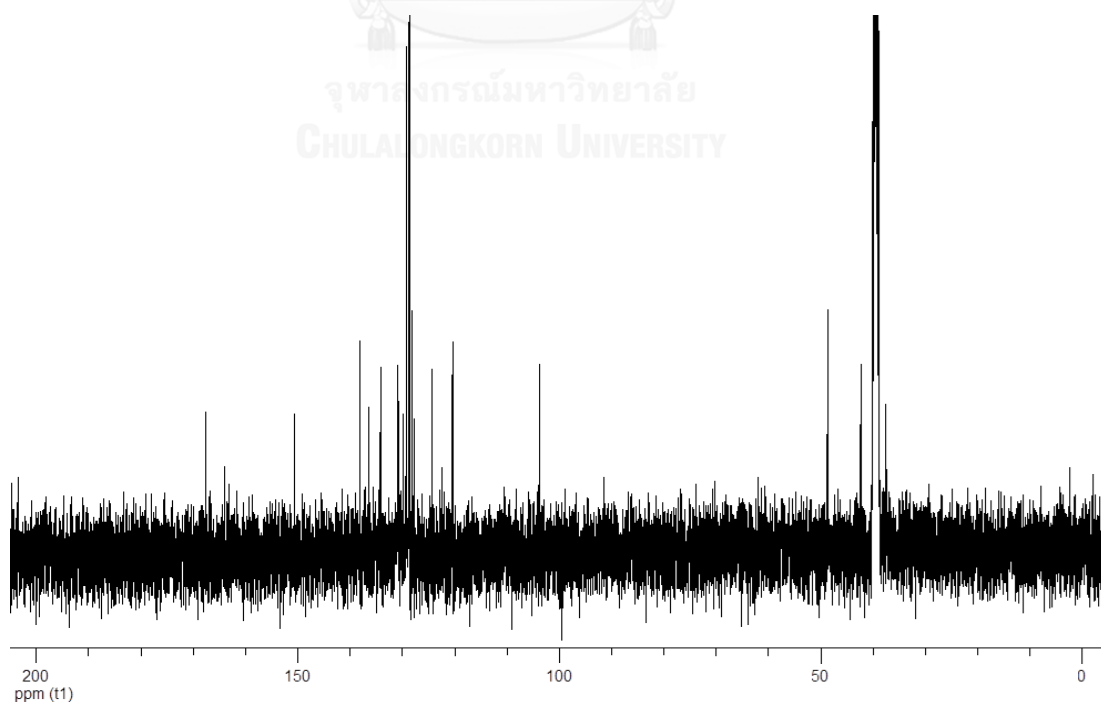


Figure A4 The ^{13}C -NMR spectrum of sensor **AN** in d_6 -DMSO at 100 MHz

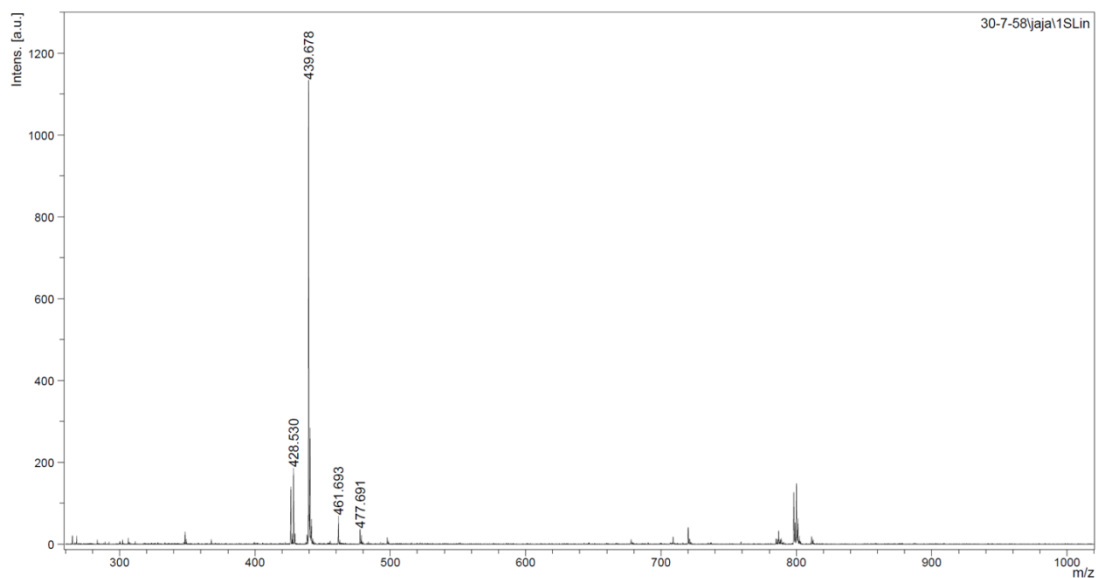


Figure A5 MALDI-TOF mass spectrum of sensor AN shown at 439.678 m/z

Q-ToF MS Report | Frontier Research Center@VISTEC

Analysis Info		Acquisition Date	
Analysis Name	D:\Data\VISTEC Data QTOF\Vinich\PNalaoh\Jaturong\ANel_yellow000001.d	5/29/2016 1:47:57 PM	
Method	DEFAULT.m	Operator	VISTEC_Scientist
Sample Name	BT2T4-6PhC	Instrument	compact 8255754.20068
Comment			

Acquisition Parameter					
Source Type	APCI	Ion Polarity	Positive	Set Nebulizer	2.0 Bar
Focus	Not active	Set Capillary	4500 V	Set Dry Heater	220 °C
Scan Begin	50 m/z	Set End Plate Offset	-500 V	Set Dry Gas	3.5 l/min
Scan End	2500 m/z	Set Charging Voltage	2000 V	Set Divert Valve	Source
		Set Corona	4000 nA	Set APCI Heater	370 °C

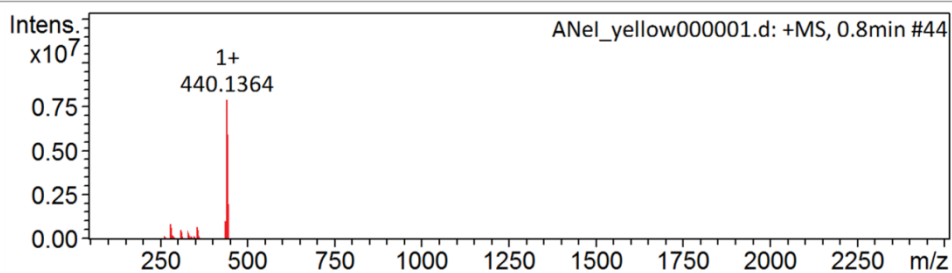


Figure A6 The ESI-High Resolution Mass spectrum of sensor AN

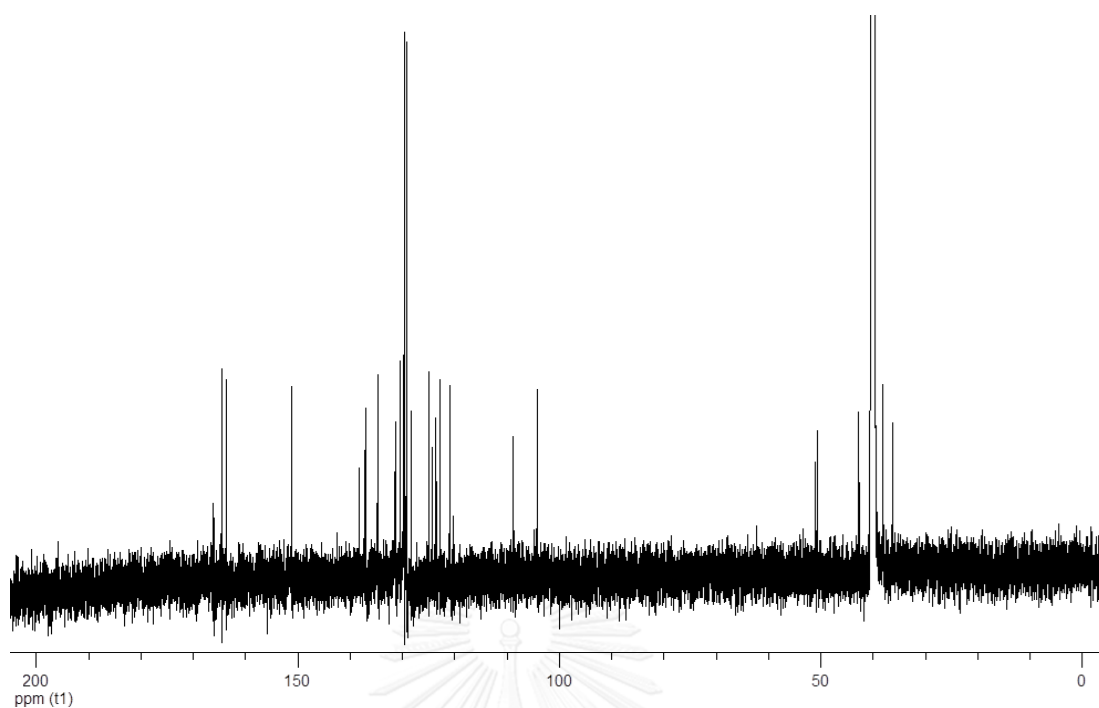


Figure A7 The ^{13}C -NMR spectrum of sensor ANI in d_6 -DMSO at 100 MHz

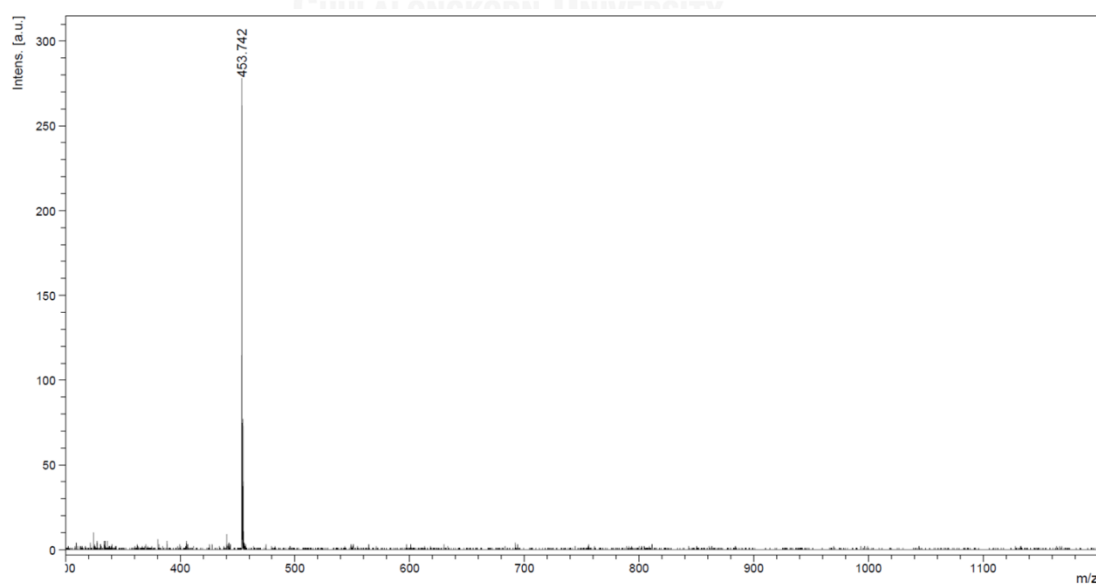


Figure A8 MALDI-TOF mass spectrum of sensor ANI shown at 453.742 m/z

Q-ToF MS Report | Frontier Research Center@VISTEC

Analysis Info

Analysis Name	D:\Data\VISTEC Data QTOF\vinich\PNalaoh\Jaturong\AN_orange000001.d	Acquisition Date	5/29/2016 1:55:41 PM
Method	DEFAULT.m	Operator	VISTEC_Scientist
Sample Name	AN_orange	Instrument	compact 8255754.20068
Comment			

Acquisition Parameter

Source Type	APCI	Ion Polarity	Positive	Set Nebulizer	2.0 Bar
Focus	Not active	Set Capillary	4500 V	Set Dry Heater	220 °C
Scan Begin	50 m/z	Set End Plate Offset	-500 V	Set Dry Gas	3.5 l/min
Scan End	2500 m/z	Set Charging Voltage	2000 V	Set Divert Valve	Source
		Set Corona	4000 nA	Set APCI Heater	370 °C

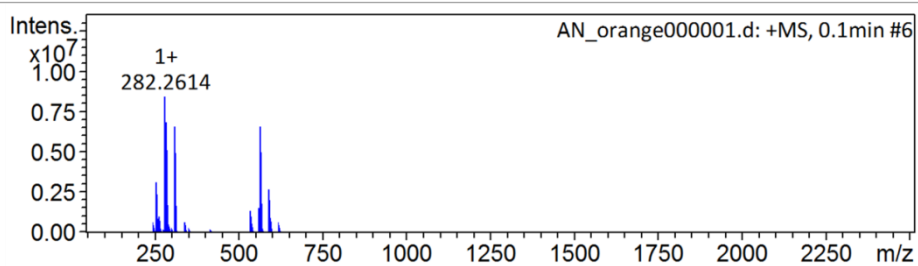


Figure A9 The ESI-High Resolution Mass spectrum of sensor ANI

VITA

Name: Mr. Jaturong Kongwutthivech

Date of birth: May 19, 1991

Nationality: Thai

Address: 2143/11-12 Lat Phrao Road, Saphan Song,
Wang Thong Lang, Bangkok, 10310

Education: 2016 M.Sc. (Chemistry), Chulalongkorn University,
Bangkok, Thailand
2012 B.Sc. (Chemistry), Chulalongkorn University,
Bangkok, Thailand

Conference: Poster presentation “Fluorescence sensor
based on naphthalimide and imidazole unit for
detection of copper ion” at The 41th Congress on
Science and Technology of Thailand (STT41)
at Suranaree University of Technology
in Nakhon Ratchasima, Thailand,
November 6-8, 2015
Poster presentation “Imidazole fluorescent based
on naphthalimide sensor for copper ion” at Pure
and Applied Chemistry International Conference
(PACCON2016) at BITEC in Bangkok, Thailand,
February 9-11, 2016